

THESIS
2
2009



This is to certify that the
dissertation entitled

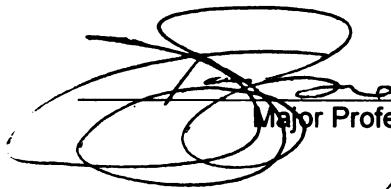
**DEVELOPMENT OF A MICROFLUIDIC BASED
MICROVASCULAR MODEL: TOWARDS A COMPLETE
BLOOD BRAIN BARRIER (BBB) MIMIC**

presented by

LUIZA I. GENES-HERNANDEZ

has been accepted towards fulfillment
of the requirements for the

PhD degree in Chemistry


Major Professor's Signature

12-4-08

Date

**DEVELOPMENT OF A MICROFLUIDIC BASED
MICROVASCULAR MODEL: TOWARDS A COMPLETE BLOOD
BRAIN BARRIER (BBB) MIMIC**

By

Luiza I. Genes-Hernandez

A DISSERTATION

**Submitted to
Michigan State University
in partial fulfillment of the requirements
for the degree of**

DOCTOR OF PHILOSOPHY

Chemistry

2008

ABSTRACT

DEVELOPMENT OF A MICROFLUIDIC BASED MICROVASCULAR MODEL: TOWARDS A COMPLETE BLOOD BRAIN BARRIER (BBB) MIMIC

By

Luiza I. Genes-Hernandez

Multiple sclerosis (MS) is an inflammatory and demyelinating disease of the central nervous system (CNS) that is the most common neurodegenerative condition in young adults, especially women, striking people between the ages of 20 and 40. It is unclear which compounds are most responsible for progressive myelin destruction and remyelination in MS.

Recently, elevated levels of nitrate and nitrite have been measured in cerebral spinal fluid (CSF), urine, and serum of MS patients. The origin of this excess nitric oxide (NO) and its mechanism of action are unknown. Herein, we have constructed a theory that the overabundance of NO metabolites in the CSF is actually blood-borne; in other words, it is possible that the NO levels are high due to overstimulation by red blood cell (RBC)-derived adenosine triphosphate (ATP). Our hypothesis is that MS-RBCs are more deformable, therefore releasing more ATP, which in turn will lead to higher production of NO. One of the biological fates of NO is the ability to cross the blood brain barrier (BBB) into the CNS, where it may result in the breakdown of the myelin sheath, compromise the integrity of the BBB and lead to axonal degeneration. To prove or disprove this hypothesis, the role of RBC-derived ATP and NO derived from brain endothelium has been investigated. In an attempt to make a connection between RBC-derived ATP and the increased levels of NO reported, we were able to demonstrate that

the ATP released from the RBCs obtained from 18 MS patients was more than twice the amount of ATP released from the RBCs of 11 healthy, non-MS controls.

Moreover, in this work we applied the recent developments in microfabrication technology to create a BBB mimic with blood components using lithographically-derived microchips in order to monitor the fate of endothelium-derived NO that is stimulated by mechanically deformed RBCs. We showed that an array of endothelial cells, addressable by an underlying microfluidic network of channels containing RBCs, can be employed as an *in vitro* model of the *in vivo* circulation to monitor cellular communication between different cell types. Results obtained from this array suggest that the ability of iloprost, a stable analogue of prostacyclin, to stimulate NO production in endothelial cells, may be due to its ability to stimulate ATP release from the red cell. These results provide evidence that the described device may serve as a controlled, *in vitro* platform for performing *in vivo*-type measurements.

Moreover, this device was successfully used in a study that attempts to classify the possible role of prolactin releasing peptide (PrRP) (a peptide that stimulate the release of prolactin from the pituitary gland) in regulating the vascular tone by decreasing the endothelium-derived NO production through a decrease in ATP.

~ To my beautiful angel, Sofia ~

ACKNOWLEDGEMENTS

More than anything during this journey, I learned not to take for granted things like family, friends and God. Words alone cannot express the tremendous love, moral support and financial help that my family, especially my parents, surrounded me with all these years. Without their help I could not have been at this point in my life and without my father's guidance I would have never been chosen the path of science.

I also have to thank my teachers that inspired me and helped me to get here. I am deeply thankful to my advisor, Dr. Dana Spence, for challenging me with a difficult project, which if I recall correctly I insisted in taking, and pushing my limits to discover an inner strength that I did not know I had before. I am grateful to him, not only for being a good advisor and teacher, but also a really good person and understanding the challenges I went through outside the lab. When I joined his group in 2004, at Wayne State University, I was not quite sure about what future might hold for me. I always wanted to learn more biology and chemistry, but also not be completely detached from my engineering background. Dr. Spence's enthusiasm about his research and reassurance made everything look really bright and gave me the confidence in approaching a totally different and at the time new for me, field of science. I am really grateful to him for making me take this challenge and I now realize how much I have grown since then, not only as a ready to be independent scientist, but also as a person. And in all honesty, he is the reason why, I now know that I want to pursue an academic career and someday have my own research group.

In these five years I have gained tremendous experience and knowledge and more importantly, beautiful and hopefully ever lasting friendships. I met wonderful people and made amazing friends, and I would like to call them, my Sri Lankan family. I thank you, Wasanthi, Madushi, Ajith, Wathsala for being there for me at times when I needed help and support, both physical and spiritual. I realized that, there is a small world after all, and people are so much alike.

I would also like to acknowledge Nicole, who was like a “ray of sunshine in a cloudy day”. Nicole and I had very fruitful discussions about research and not only. I would like to say that we connected at a very special level and she will always be close to my heart.

I would also take the opportunity to mention Dr. Paul Root, for the coolness that he always exuded while in the lab, and I would like to thank him for sharing his knowledge about cell culturing and nitric oxide biochemistry. There are many people that directly, or indirectly, contributed to me becoming the person and scientist that I am today and I would like to thank them all.

My tremendous love and all my heart go to my little Sofia and my wonderful loving husband, Frank. Both of you are the reasoning of my life and my work, and both of you came into my life at a time when I was completely lost. I love you and I am forever grateful for having you.

TABLE OF CONTENTS

LIST OF TABLES.....	x
----------------------------	----------

LIST OF FIGURES.....	xi
-----------------------------	-----------

CHAPTER 1

1.1	INTRODUCTION.....	1
1.1.1	Red Blood Cell (RBC) Structure and Properties.....	1
1.1.2	RBC-Derived ATP: An Important Factor in Vascular Regulation.....	5
1.1.3	CFTR-Facilitated ATP Transport/Release out of the Cell.....	8
1.1.4	RBC Deformability and Disease Pathogenesis.....	9
1.1.5	Nitric Oxide (NO) and the Blood-Brain Barrier (BBB).....	12
1.2	MICROFLUIDIC TECHNOLOGY.....	17
1.2.1	Short History.....	17
1.2.2	Scaling Effects when Miniaturizing the Chemistry.....	18
1.2.3	Material for Microsystems.....	20
1.2.4	Fabrication of Microfluidic Systems.....	23
1.2.5	Tools for Microfluidic Applications.....	26
1.2.6	Detection Modes in Microfluidic Devices.....	31
1.3	THESIS OBJECTIVE.....	34
	LIST OF REFERENCES.....	36

CHAPTER 2

2.1	MULTIPLE SCLEROSIS: AN AUTOIMMUNE DISEASE?.....	49
2.2	NITRIC OXIDE AS AN ACTIVITY MARKER IN MS.....	51
2.3	RBC DEFORMABILITY IN MS.....	54
2.4	POSSIBLE ROLES OF THE RBC/RBC-DERIVED ATP IN MS.....	55
2.5	EXPERIMENTAL.....	56
2.5.1	Design and Methods.....	57
	<i>Generation of washed RBCs</i>	
	<i>Standard ATP assay</i>	
	<i>Determination of ATP release from RBCs</i>	
2.5.2	Results and Discussion.....	62
	<i>Quantitative Evaluation of the MS RBC ATP release</i>	
2.6	CONSTITUTIVE PRODUCTION OF NITRIC OXIDE IN BRAIN MICROVASCULAR ENDOTHELIAL CELLS.....	62
2.7	EXPERIMENTAL.....	64
2.7.1	Design and Methods.....	65
	<i>Preparation of cells</i>	
	<i>Florescence determination of NO production</i>	
	<i>Control experiment</i>	

2.7.2	Results and Discussion.....	66
	<i>ATP constitutes an in vivo stimulus of NO production in bBMVECs</i>	
	<i>ATP-derived NO production with cells passage</i>	
2.8	CONCLUSIONS.....	70
	LIST OF REFERENCES.....	71

CHAPTER 3

3.1	THE BLOOD BRAIN BARRIER.....	76
3.2	BLOOD BRAIN BARRIER MODELS.....	78
3.3	MICROFLUIDIC TECHNOLOGY FOR THE DEVELOPMENT OF A BLOOD BRAIN BARRIER MIMIC.....	82
3.4	EXPERIMENTAL.....	83
3.4.1	Design and Methods.....	83
	<i>Microchip fabrication</i>	
	<i>Preparation of NO standards</i>	
	<i>Detection of NO</i>	
	<i>Detection of ATP flux through the polycarbonate membrane</i>	
	<i>Fabrication of the microchip-based BBB</i>	
3.4.2	Results and Discussion.....	90
	<i>NO flux through the polycarbonate membrane</i>	
	<i>Cell immobilization on polycarbonate membrane/PDMS channels</i>	
	<i>Detection of ATP flux through the polycarbonate membrane</i>	
3.5	CONCLUSIONS AND OTHER CONSIDERATIONS.....	99
	LIST OF REFERENCES.....	101

CHAPTER 4

4.1	ADDRESSING A VASCULAR ENDOTHELIUM ARRAY WITH BLOOD COMPONENTS USING UNDERLYING MICROFLUIDIC CHANNELS.....	104
4.2	EXPERIMENTAL.....	106
4.2.1	Material and methods.....	106
	<i>Preparation of RBCs</i>	
	<i>Measurement of ATP via chemiluminescence</i>	
	<i>Measurement of bPAEC-derived NO</i>	
	<i>Preparation of glybenclamide solution</i>	
	<i>Preparation of the microfluidic devices</i>	
	<i>Immobilization of the bPAECs on the membrane array</i>	
4.2.2	Results and Discussion.....	111
4.3	CONCLUSIONS.....	119
	LIST OF REFERENCES.....	120

CHAPTER 5

5.1	A PROPOSED MECHANISM FOR THE INVOLVEMENT OF PROLACTIN-RELEASING PEPTIDE (PrRP) IN THE REGULATION OF VASCULAR TONE.....	122
5.2	EXPERIMENTAL.....	125
5.2.1	Materials and Methods.....	125
	<i>Collection of RBCs</i>	
	<i>Measurement of the ATP release</i>	
	<i>Mass spectrometry analysis</i>	
	<i>Fabrication of the microfluidic array</i>	
	<i>Cell immobilization</i>	
	<i>Measurement of Nitric Oxide</i>	
5.2.2	Results and Discussion.....	130
	<i>ATP binding to PrRP</i>	
	<i>Antagonistic effect of PrRP on the ATP release from C-peptide/iloprost treated RBCs</i>	
	LIST OF REFERENCES.....	140

CHAPTER 6

6.1	OVERALL CONCLUSIONS.....	143
6.2	FUTURE DIRECTIONS.....	148
	LIST OF REFERENCES.....	151

LIST OF TABLES

Table 1. Classification of microvalves.....	28
--	-----------

LIST OF FIGURES

Figure 1. a) Healthy RBC with its usual discocyte shape. b) Typical dimensions of a healthy RBC. ¹	2
Figure 2. a) Composition of the membrane of a RBC. b) Image of the spectrin cytoskeleton. ²	4
Figure 3. Proposed mechanism for the effect of RBC-derived ATP on the cells at the luminal and extraluminal side of a blood vessel.	7
Figure 4. Proposed mechanisms for CFTR-facilitated ATP transport/release out of cell. For hypothesis A to occur, CFTR must be expressed in concert with appropriate cofactors or regulators. Hypothesis B and C suggest positive CFTR regulation of a separate and independent ATP transport mechanism and CFTR-facilitated fusion of ATP-filled vesicles, respectively. ³	10
Figure 5. Electrons (e-) are donated by NADPH to the reductase domain of the enzyme (eNOS) and proceed via FAD and FMN redox carriers to the oxygenase domain. There, they interact with the haem iron and BH4 at the active site to catalyze the reaction of oxygen with L-arginine, generating citrulline and NO as products. Electron flow through the reductase domain requires the presence of bound calcium-calmodulin (Ca²⁺/CaM). ⁶¹	14
Figure 6. A) Representation of the steps in the lithographic process. B) Scheme of rapid prototyping.	25

Figure 7. Types of micromixing. **A.** Cyclone micromixer; **B.** Hydrodynamic focusing by compressing a central stream by two outer streams at much larger flow rate; **C.** Multi-lamination flow patterns of a split-and-recombine mixer visualized by a dilution-type experiment; **D.** Staggered herringbone micromixer for the generation of chaotic flows; **E.** Time lapse images of three-electrode mixing at 8 Hz; **F.** Electrokinetic instability micromixing; **G.** Numerical simulation results obtained for two inlet flows pulsed at 180° phase difference; **H.** Photographs showing acoustic microstreaming in a microchamber.⁴30

Figure 8. The two-step bioluminescence reaction between luciferin/luciferase and ATP.....59

Figure 9. Instrumental setup employed to measure the RBC derived ATP release.....61

Figure 10. ATP released from RBCs subjected to shear-induced stress. The average ATP release from the RBCs obtained from healthy controls was 138 +/- 21 nM while the release from the RBCs obtained from people with MS was 375 +/- 51 nM. The error bars are reported as the SEM for 11 controls and 18 MS samples.....63

Figure 11. Effects of ATP (100 μM) and L-NAME (100 μM) on NO production in bBMVEC assessed with DAF-FM DA. L-NAME was used to demonstrate that the increase in DAF-FM DA fluorescence upon stimulation with ATP (100 μM) was the result of NO production (*p ≤ 0.001 vs. control).....67

Figure 12. ATP-derived NO production is decreasing with increasing the passage of the cells. For cell division 3 there is a significant difference between the control (black bars) and the bBMVECs stimulated with 100 μM ATP (grey bars) (*p ≤ 0.001 vs. control).....69

Figure 13. The Blood Brain Barrier. **a)** The BBB is formed by endothelial cells of the level of the cerebral capillaries. These endothelial cells interact with perivascular elements such as basal lamina and closely associated astrocytic end-feet processes, perivascular neurons and pericytes to form a functional BBB. **b)** Cerebral endothelial cells are unique in that they form complex tight junctions (TJ) produced by the interaction of several transmembrane proteins that effectively seal the paracellular pathway. These complex molecular junctions make the brain practically inaccessible for polar molecules, unless they are transferred by transport pathways of the BBB that regulate the microenvironment of the brain.⁴77

Figure 14. Typical *in vitro* model of the BBB. Brain endothelial cells are grown at the bottom of filter inserts together with glial cells grown at the bottom of 6-well plate. Soluble factors secreted from the glial cells induce the BBB phenotype in the brain capillary endothelium.⁴80

Figure 15. Photolithographic procedure for the fabrication of silicon master.
 1) Spin coat 4 mL of SU-8 50 photoresist at 1000 rpm for 20 s;
 2) Pre-bake for 5 min at 95°C to evaporate solvent and densify film;
 3) Post-bake for 5 min at 95°C to cross-link the exposed portions of the photoresist film; 4) UV exposure, 350-450 nm, 50W for 60 s to polymerize and cross-link; 5) Develop with propylene glycol monomethyl ether acetate (PGMEA); 6) Soft-lithography to create microfluidic chip.....84

Figure 16. Detection of ATP flux through a polycarbonate membrane using a flow of luciferin/luciferase mixture hydrodynamically pumped into a spiral-shaped channel of a PDMS device. The set up is enclosed in a light excluding box over a PMT.....87

Figure 17. Proposed design for the microfluidic-based BBB mimic **A.** Assembly of a 3 dimensional fluidic device incorporating microchannels (100 µm diameter) for reagents delivery and a polycarbonate membrane sandwiched in between the PDMS layers. **B.** Micrograph of the channels junction with the polycarbonate membrane (13 mm diameter and 0.2 µm pore size).....89

Figure 18. A. Detailed representation of the microfluidic channels junction with polycarbonate membrane in between. S1 represents the channel under the membrane, where NO (3.8 μM stock solution in PBS) is being hydrodynamically pumped at a flow rate of $1\ \mu\text{L}\ \text{min}^{-1}$. S2 represents the upper channel that poses as the CNS, where DAF-FM (10 μM) is being introduced. B. Micrographs of the upper channel before (1), at (2), and after (3) channels junction showing the formation of the highly fluorescent DAF-FM/NO adduct.....92

Figure 19. Detection of NO flux through the polycarbonate membrane with a pore size of $0.2\ \mu\text{m}$ and at a flow rate of $1\ \mu\text{L}\ \text{min}^{-1}$ as assessed by DAF-FM (10 μM). The control sample is PBS buffer. *, **, and *** represent the statistical significant differences versus control, 100, and 200 nM NO, respectively (* $p \leq 0.001$; ** and *** $p \leq 0.05$). The error bars represent the mean values \pm standard error (n=4).....93

Figure 20. Micrograph of bBMVEC immobilized in a $100\ \mu\text{m}$ PDMS channel. The channel was pre-coated with fibronectin ($100\ \mu\text{g}\ \text{mL}^{-1}$) and incubated for 1 h at 37°C and 5% CO_2 to ensure cell adhesion.....96

Figure 21. Detection of the ATP flux through a polycarbonate membrane with pore size of $1.0\ \mu\text{m}$ and 13 mm diameter as assessed by chemiluminescence in a spiral-shaped channel, as part of a 3D microfluidic device. ATP and luciferin/luciferase flow rates are $3\ \mu\text{L}\ \text{min}^{-1}$ and $1\ \mu\text{L}\ \text{min}^{-1}$, respectively. Control represented by RBCs 7% (0 μM ATP). Iloprost is used as an ATP release stimulant of RBCs. * and ** represent the values statistically different from control and 0.5 μM ATP, respectively (* $p \leq 0.001$, ** $p \leq 0.05$) (n=4).....98

Figure 22. (a) Schematic of experimental set up for chemiluminescence measurements taken to determine the iloprost-stimulated ATP release from RBCs in real time shown in (b).....112

Figure 23. Comparison to the controls of iloprost (1 μM) and RBCs alone as well as the inhibition of ATP release when iloprost-stimulated RBCs were incubated with glybenclamide (250 nM) (* $p \leq 0.005$).....114

Figure 24. Iloprost-derived ATP release from RBCs stimulates NO production in a microfluidic device-containing an endothelium immobilized to a polycarbonate membrane. In (a), the microfluidic device contains a polycarbonate membrane sealed between two PDMS layers that separates a channel containing RBCs (bottom layer) from a layered endothelium (top layer). In (b), fluorescence microscopy images are shown for pre- (images on the top) and post-(images on the bottom) addition of iloprost.....115

Figure 25. The increase in fluorescence intensity due to endothelium-derived NO production when a sample of RBCs incubated with iloprost (23.0 ± 3.5) vs. a sample of RBCs alone (16.5 ± 1.0) is pumped through the channel. The values reported are the average intensity and standard deviation (n=3 wells for each sample). The difference in fluorescence intensity between samples incubated in the presence and absence of iloprost are statistically different ($p \leq 0.005$).....117

Figure 26. Micrographs of a vascular endothelium array with blood components are shown in (a). The wells in columns A and B contain bPAECs cultured on a polycarbonate membrane. Column C contains cell free wells. The rows represent the wells of the array that are addressable by the underlying microchannel network, each delivering a different reagent to the wells as described in the text. The quantitative representation of the data is shown in (b). The difference in fluorescence intensity between samples containing the RBCs in the absence (row 3) and presence (row 4) of iloprost are statistically different from the other rows. There is also a difference in the intensities of rows 3 and 4 (* $p \leq 0.005$).....118

Figure 27. Representation of the mechanism of RBC-mediated regulation of the vascular tone and the possible involvement of prolactin-releasing peptide (PrRP) in scavenging the RBC-derived ATP. ATP binds to the P2y purinergic receptors found on the endothelial cells that line up the luminal side of the blood vessel and through a Ca^{2+} -dependent mechanism triggers the activation of the eNOS, and therefore production of NO. NO activates the guanylate cyclase signaling cascade that ultimately results in vasodilation.....132

Figure 28. PrRP binding to ATP. Filled circles (●) represent the ATP standards (0-1.5 μM) without the peptide. Open triangles (▽), squares (□) and rhomboids (◇) show the decrease in ATP signal after the incubation with PrRP (10 nM) for 0, 30, and 60 min, respectively (n=3). The decrease in chemiluminescence signal suggests that PrRP binds to ATP ($p \leq 0.005$).....133

Figure 29. Effect of PrRP (10nM) on the ATP release from RBCs treated with Zn^{2+} -activated C-peptide. The decrease in chemiluminescence intensity corresponds to a decrease in measured ATP released from the RBCs when PrRP was added to the metal activated C-peptide. Filled bars correspond to the 90 min incubation with PrRP (n=5) and the open bars correspond to 6 hrs incubation (n=8). The results are reported as the average \pm standard error of the mean. The differences in chemiluminescence intensity between the samples incubated in the presence and absence of PrRP are statistically significant (* $p \leq 0.005$).....135

Figure 30. The effect of the PrRP (10 nM) on the measured ATP release from the RBCs treated with iloprost (10 μM) (n=3). All samples contain RBC (final hematocrit 7%). Control sample is represented by RBC 7%. The iloprost-treated RBCs samples incubated with or without PrRP are significantly different (** $p \leq 0.05$).....137

Figure 31. Antagonistic effect of PrRP on the endothelium-derived NO production in the bovine pulmonary artery endothelial cells (bPAECs). Picture I shows micrographs of vascular endothelium array with blood components. The rows a to f represent the wells of the array that are addressable by the underlying microchannel network each delivering a different reagent to the wells as described in the text. The quantitative representation of the normalized data from 4 different experiments is shown in II. The difference in fluorescence intensity between samples containing RBC + C-pep + Zn(II) incubated in the absence (bar C) and presence (bar D) of the PrRP is statistically significant (* $p < 0.05$) There is also significant difference in the intensities of rows (bars E and F), where the RBCs + Iloprost samples were incubated in the absence and the presence of PrRP (** $p < 0.001$), respectively. Errors bars are the mean \pm standard error A: RBC7%; B: RBC + PrRP; C: RBC + C-pep + Zn; D: RBC + C-pep + Zn + PrRP; E: RBC + Ilop; F: RBC + Ilop + PrRP.....138

CHAPTER 1

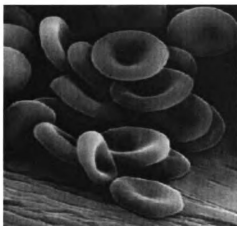
1.1 INTRODUCTION

1.1.1 Red Blood Cell (RBC) Structure and Properties

Red blood cells (RBCs) or erythrocytes (from Greek *erythros* for “red”, *kytos* for “hollow” and *cyte* for “cell”) are the most abundant type of cells in the blood (4 to 5 million cells per μL), making up approximately 45% of the total blood volume. Compared to a typical mammalian cell, the RBC is considered a dead cell because it has no means of reproducing and repairing itself due to the lack of a nucleus and mitochondria. The juvenile RBCs start their journey as reticulocytes in bone marrow. These cells have a lifespan of about 4 days, spending 3 days at the site of their production (bone marrow) and 1 in the peripheral blood. Once matured, the nucleus is extruded and their ability to divide is lost. The RBCs short lifespan of 120 days and their primary function of reversibly transporting oxygen and carbon dioxide by circulating in the vessels throughout the entire body define the RBC cell philosophy of “living in a rush”.

RBCs are smaller than most other human cells and under physiological conditions they have the shape of biconcave disks of 6-8 μm in diameter, 2 μm in thickness at the periphery and 1 μm at the center (Figure 1). This shape (as well as the loss of organelles and nucleus) optimizes the cell for the important function of oxygen exchange with the surroundings.

a)



b)

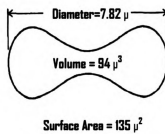
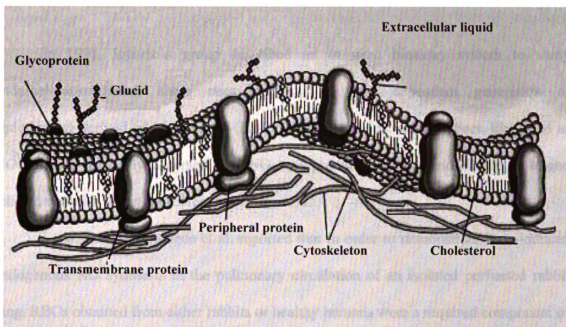


Figure 1. a) Healthy RBC with its usual discocyte shape. b) Typical dimensions of a healthy RBC.¹

This function is carried out by hemoglobin (Hb), the most abundant protein (> 90%) present in RBC. As shown in Figure 2, the RBC is composed of a lipid membrane with an underlying two-dimensional (10 nm in thickness) elastic network of spectrin.⁵ The cytoskeleton is anchored to the lipid bilayer through proteins spanning the membrane. The triangular structure of the spectrin network is presented in Figure 2. This particular geometry, as well as the intrinsic elastic properties of the spectrin, gives remarkable deformability to the RBC. This deformability is key property of the RBCs in their motion through the complex network of the microcirculation. Their deformability is mainly determined by the membrane surface area to volume ratio, cellular morphology, mechanical properties of the cell membrane, and the viscosity of the cellular components.⁶

The RBCs, with a mean diameter of 5 μm , are often subjected to a randomly varying shear stress in the cardiac chamber and larger vessels. In addition, they must also alter their shape to pass through the 3- to 4- μm diameter capillaries of the microcirculation as oxygen carriers. The ability of RBCs to deform and maintain the oxygen-carrying capability under a randomly varying shear flow is of great interest from the standpoint of rheological and functional behavior of RBCs in the cardiovascular system.⁷ The deformability of the RBC under shear stress has been studied extensively during the last 30 years. The increased shear stress was suggested to be a major stimulus for nitric oxide (NO), a small gaseous free radical that is released from the endothelium.^{8,9} NO is an important signaling molecule and it is involved in many physiological and pathological processes within the mammalian body, both beneficial and detrimental.

a)



b)

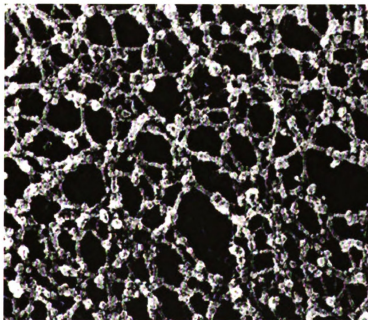


Figure 2. a) Composition of the membrane of a RBC. b) Image of the spectrin cytoskeleton.²

1.1.2 RBC-Derived ATP: An Important Factor in Vascular Regulation

In 1991, Ignarro's group described an *in vitro* bioassay system to study endothelium-mediated, shear stress-induced, or flow dependent generation of endothelium-derived relaxing factor (EDRF), which had just recently been identified as NO.⁹ It was generally accepted that NO was produced by the endothelial cells and relaxed vascular smooth muscles.¹⁰

Later, in 1995, Sprague et al. reported that in order to demonstrate flow-induced endogenous NO synthesis in the pulmonary circulation of an isolated perfused rabbit lung, RBCs obtained from either rabbits or healthy humans were a required component of the perfusate.¹¹ To strengthen their claim, they showed that in the absence of the RBCs, flow-induced increases in shear stress did not stimulate NO synthesis. Moreover, they concluded that an additional key factor must be existing in the rabbit pulmonary circulation that relates RBCs to the vasorelaxation. Therefore, they proposed that the property of these RBCs responsible for the stimulation of NO synthesis was their ability to release adenosine triphosphate (ATP) in response to mechanical deformation.¹²

This hypothesis was based on multiple findings, the first of which being that ATP is an *in vivo* stimulus of endothelial NO production.^{13,14} Secondly, ATP is of particular interest because it is present in millimolar concentrations in the RBCs^{15,16} and it is released in response to physiological stimuli, such as hypoxia and hypercapnia.^{17,18} Additionally, when RBCs are traversing the resistant vessels *in vivo*, they become deformed.¹⁹ Another factor they considered was that ATP reduces vascular resistance in isolated lungs. Moreover, the latter action of ATP was prevented by the NO synthesis

inhibitor N^G-nitro-L-arginine methyl ester (L-NAME).²⁰ It has been shown that as their deformability increases, erythrocytes of rabbits and humans can release increased amounts of ATP. This RBC-derived ATP can then act on the endothelial cells to stimulate endogenous NO synthesis and enable RBCs to participate in local regulation of vascular caliber.^{11,12,18,21-24}

Depending on the type of purinergic receptor to which ATP binds, it can induce antagonistic effects on the vasculature. For example, ATP binding to the P2X receptor found on the vascular smooth muscle cells results in contraction of the cells,²⁵ whereas ATP binding to the P2Y receptor found primarily on the endothelium, results in NO synthesis and/or vasodilation.^{13,14} Thus, ATP applied to the luminal side of a vessel, that released from the RBCs within the circulation, would be expected to produce endothelium-dependent relaxation through an interaction with the endothelial P2Y purinergic receptor (Figure 3).

All these findings suggest that RBCs may be an important determinant in the stimulation of NO production in the circulatory system. Therefore, as RBCs are traversing the circulatory system they are increasingly deformed by increments in the velocity of blood flow through a vessel and/or by reduction in vascular caliber. Moreover, RBCs release ATP which stimulates endothelial synthesis of NO, resulting in relaxation of the vascular smooth muscle and thereby, an increase in vascular caliber.²⁶

On the other hand, failure of this mechanism for deformation-induced ATP release has been associated with primary pulmonary hypertension (PPH), cystic fibrosis (CF) and alveolar hypoxia. It has been shown that the RBCs of CF patients do not release ATP in response to mechanical deformation and CF patients often develop pulmonary

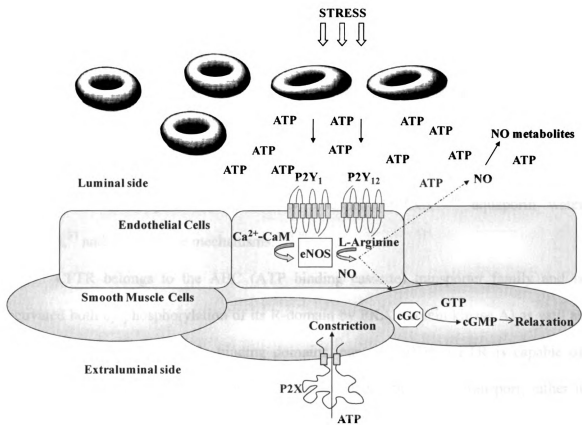


Figure 3. Proposed mechanism for the effect of RBC-derived ATP on the cells at the luminal and extraluminal side of a blood vessel.

hypertension.²⁶ As a result of these findings, it has been suggested that the cystic fibrosis transmembrane regulator (CFTR) is a component of the pathway that links mechanical deformation of the RBC to the release of ATP.

1.1.3 CFTR-Facilitated ATP Transport/Release out of the Cell

CFTR is cAMP-activated chloride channel expressed in epithelial cells that is responsible for transepithelial salt and water transport.²⁷⁻²⁹ Mutations in this protein are responsible for the hallmark defective chloride secretion observed in CF. CFTR regulates other transporters, including Cl⁻/(HCO³⁻) exchangers,³⁰ epithelial sodium channel (ENaC),³¹⁻³³ outwardly rectifying chloride channel (ORCC),³⁴⁻³⁶ aquaporin water channels,³⁷ and ATP release mechanisms.^{3,38,39}

CFTR belongs to the ABC (ATP binding cassette) transporter family and is activated both by phosphorylation of its R-domain by PKA (protein kinase A) as well as ATP binding at its nucleotide binding domains, namely NBD1. CFTR is capable of hydrolyzing ATP, although this activity is not coupled with the ion transport; rather it may serve to initiate or modulate conformational changes that underlie channel opening or closing.

There exists a vast body of work that shows that cAMP-stimulated ATP release is dependent on CFTR, that expression of CFTR is associated with ATP conductance, and that there are multiple interpretations of the ATP transport phenomenon.^{36,38,40-43} In these previous studies, the precise route of the ATP through the membrane was not defined; however, ATP transfer across the membrane occurred only in the presence of CFTR and *mdr* (multidrug resistance gene). It is clear that if CFTR can facilitate ATP release, CFTR

itself must be modulated by regulators or stimuli in a concerted manner or CFTR itself must modulate an ATP release pathway that is expressed universally (Figure 4).³

1.1.4 RBC Deformability and Disease Pathogenesis

Abnormal RBC deformability has been also associated with such diseases as diabetes and multiple sclerosis.^{44,45} For example, it has been shown that deformability is decreased in RBCs of patients with type I and type II diabetes. In addition, the whole blood of patients with MS was found to be more viscoelastic when compared with the whole blood of healthy patients.⁴⁶⁻⁴⁸

Interestingly, it is known that the RBCs of MS patients have abnormally high levels of glutathione (GSH), the most abundant non-enzymatic antioxidant present in a cell. In 1979 Szeinberg *et al* showed that the activity of glutathione peroxidase (GSH-Px) in erythrocytes of patients with MS was significantly lower than in a control group of 30 patients with various neurological disorders.⁴⁹ Therefore, they were confirming a similar finding of a decrease in activity of GSH-Px in erythrocytes of a group of MS patients in Denmark.⁵⁰

In the next two decades, an important body of work was published in regard to the abnormal activity of this enzyme in MS RBCs.^{49,51-55} Glutathione peroxidase catalyses the reaction between the reduced monomeric glutathione (GSH) and hydrogen peroxide with the formation of the glutathione disulfide (GS-SG). Glutathione reductase then reduces the oxidized glutathione to complete the cycle. If the activity of the GSH-Px is reduced, an increase in the ratio of GSH/GSSG will result, thus altering the redox status

in the cell. The levels of GSH have been linked with the deformability characteristics of the RBCs. That is, low levels of GSH are found in diabetic red cells, which are known to be less deformable than the RBCs from healthy patients.^{56,57} Moreover, recent studies in our group involving diabetic RBCs have shown that a weakened oxidant defense system in RBCs will lead to lower levels of ATP release.⁵⁸ We demonstrated that RBCs-derived ATP is affected by oxidant insults and that the recovery from this insult is independent of the pentose phosphate pathway, the pathway that maintains the concentrations of GSH. Moreover, in this study we showed that erythrocytes from individuals with type II diabetes released 50% less ATP than the erythrocytes from healthy, non-diabetic patients. As a consequence of decreased levels of ATP release from RBCs, less endothelium-derived NO may be available for the regulation of the vascular caliber. Our group also reported that there is a direct relationship between the ability of the extracellular ATP to stimulate NO in endothelial cells and diabetic complications.⁵⁸

If, in the case of MS patients, the RBCs are more deformable and the increase in deformability results in an increase of ATP release, then an increase in the NO production would be expected. Indeed, it is recognized that there exist higher than normal levels of NO metabolites, nitrate and nitrite, in the cerebral spinal fluid (CSF) and serum of patients with MS.^{44,59} Taken collectively, we have constructed a theory that perhaps explains the overabundance of NO metabolites in the CSF is actually blood-borne; in other words, it is possible that the NO levels are increased due to overstimulation by RBC-derived ATP.

Our hypothesis is that MS-RBCs are more deformable, therefore releasing more ATP, which in turn will lead to increased production of NO. However, a molecular level

understanding of the mechanisms by which RBC deformability properties relate to the occurrence of MS is lacking. To prove or disprove this hypothesis, the role of RBC-derived ATP and NO derived from brain endothelium must be investigated.

1.1.5 Nitric Oxide (NO) and the Blood-Brain Barrier (BBB)

During the past decade NO has emerged as an important mediator of physiological and pathophysiological processes. Elevated NO biosynthesis has been associated with nonspecific immune-mediated cellular cytotoxicity and the pathogenesis of chronic, inflammatory autoimmune diseases including rheumatoid arthritis, insulin-dependent diabetes, inflammatory bowel disease, and MS. Recent evidence suggests, however, that NO is also immunoregulatory and suppresses the function of activated proinflammatory macrophages and T lymphocytes involved in these diseases.⁶⁰

NO is a small gaseous radical that is biosynthesized from the guanidino nitrogen atom of L-arginine within the active site of NO synthases (NOS), which in mammals are encoded by three genes corresponding to neuronal (nNOS), inducible (iNOS), and endothelial (eNOS) isoforms.⁶¹ These isoforms have been classified on the basis of their constitutive (eNOS and nNOS) versus inducible (iNOS) expression, and their calcium-dependence (eNOS and nNOS) or calcium-independence (iNOS). They share an overall amino acid sequence homology of approximately 55%, and there is strong sequence conservation in the regions of the proteins that are important in the catalysis.⁶²

The NOS isoforms carry out a five-electron reduction process utilizing oxygen, and cofactors such as reduced NADPH, tetrahydrobiopterin (BH₄), flavin adenine

dinucleotide (FAD), flavin mononucleotide (FMN) and iron protoporphyrin IX (heme) participate in the formation of NO (Figure 5). L-Arginine in the presence of NADPH and O₂ is oxidized to N-hydroxyarginine, which is reoxidized to citrulline producing NO.⁶³

Although NO has many biological fates, one possible scenario is that it crosses the blood brain barrier (BBB) into the central nervous system (CNS), where it may result in a breakdown of the myelin sheath, compromise the integrity of the BBB, and lead to axonal degeneration.⁶⁴ The BBB is comprised of the endothelial cells that line the capillaries of the brain. The distinguishing features of the brain capillary endothelium include the presence of tight intercellular junctions.⁶⁵ The existence of these junctions between the endothelial cells forms a very selective filter for the blood-borne molecules.^{66,67} Therefore, the passive diffusion of the compounds across the BBB is dependent upon their physicochemical properties, such as lipid solubility, molecular weight, electrical charge, or extent of ionization.

Bradbury *et al* showed that lipid soluble substances penetrated the cerebral endothelial plasma membranes readily and also equilibrated easily between blood and brain tissue.⁶⁸ However, water soluble molecules, such as amino acids, nucleosides, and hexoses, and macromolecules are transported in the brain by means of selective carrier mechanisms or specific transporters.⁶⁵

The importance of the barrier arises from the fact that it restricts the movement of specific substances, such as infectious organisms from the circulatory system, to the brain tissue and extracellular fluid. In the CNS, the endothelial cell membrane is further surrounded by the end feet of the astrocytes outside the capillary wall, which influences and conserves the barrier function of the cerebral endothelial cells.

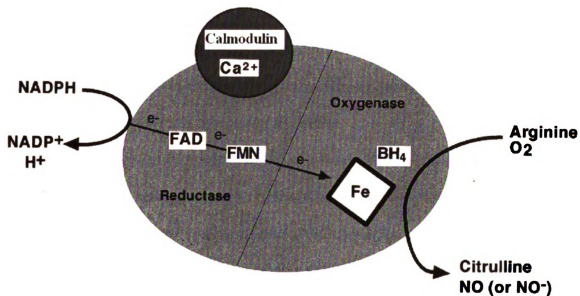


Figure 5. Electrons (e^-) are donated by NADPH to the reductase domain of the enzyme (eNOS) and proceed via FAD and FMN redox carriers to the oxygenase domain. There they interact with the haem iron and BH $_4$ at the active site to catalyze the reaction of oxygen with L-arginine, generating citrulline and NO as products. Electron flow through the reductase domain requires the presence of bound calcium-calmodulin (Ca $^{2+}$ /CaM).⁶¹

It is well established that there are many pathophysiological conditions that disrupt the integrity of the BBB and can lead to the increased permeation of substances across the BBB.⁶⁹ For example bacterial meningitis and MS are two of the conditions that can alter the BBB and allow normally excluded substances to enter into the cerebrospinal and interstitial fluids. Moreover, when inflammation occurs (as in MS or encephalitis) a massive leucocyte migration into the brain takes place.^{70,71} Cytokines (signaling proteins and glycoproteins used in cellular communication), secreted in the early steps of inflammation, are found to increase the permeability of the barrier, therefore permitting compounds to enter the brain by opening the BBB.⁷²

Other inflammatory mediators, such as eicosanoids (e.g. prostaglandins), adhesion molecules, and free radicals can play an important role in the permeability of the BBB.⁷³ Of the free radicals, reactive oxygen species (ROS) can cause extensive damage to the membrane lipids in the CNS by peroxidating the fatty acids, thus destroying the myelin and cell membranes.^{74,75}

One of the free radicals that can damage the BBB is NO. Endothelial cells of the BBB are known to possess the inducible form of NOS. When produced in excessive amounts, usually as part of a biochemical cascade stimulated by injury or inflammatory conditions, NO production may no longer be beneficial for the cells; instead, the large quantities of NO become neurotoxic.⁷⁶

As mentioned above, elevated levels of nitrate and nitrite have been reported in cerebral spinal fluid (CSF), urine and serum of MS patients.⁴⁴ Particularly, nitrate and nitrite levels were significantly higher in CSF compared to serum,⁷⁷ which could be the consequence of BBB dysfunction mediated by NO.⁷⁸ Although nitrate and nitrite are

elevated in CSF, there is no significant correlation between their levels and clinical activity,⁷⁷ possibly because the origin of this excess NO and its mechanism of action are unknown.

It is well established that endothelial cells can produce NO in small amounts and, when released, are able to control the local blood flow through the activation of the guanylate cyclase signaling cascade that ultimately results in vasodilation. It has also been previously shown that the mechanism by which NO is released into the circulatory system involves ATP, and that this ATP is released from erythrocytes that are subjected to mechanical deformation.^{12,79} Moreover, it was reported that as the deformability increases, erythrocytes of rabbits and humans can release higher amounts of ATP.^{12,80} Collectively, these findings involving the ability of RBCs to produce ATP and the increased deformability of RBCs from MS patients suggest a possible mechanism for the increased levels of NO found in the CSF of MS patients.

However, a molecular level understanding of the mechanisms by which the RBCs deformability properties relate to the occurrence of MS is lacking. To gain insight into these mechanisms, it would be ideal to employ an *in vitro* model that mimics an *in vivo* system. A possible approach to developing such a system would be a microfabricated fluidic approach.

In this work we propose to create a system that would allow mechanically deformed RBCs to release ATP, stimulate the endothelium-derived NO and that would allow one to monitor the fate of that NO in a dynamic fashion.

1.2 MICROFLUIDIC TECHNOLOGY

1.2.1 Short History

The history of analytical miniaturized devices starts with the remarkable work of Terry in 1979.⁸¹ Even though, at the time he was not acknowledged for his work, the gas chromatograph fabricated on silicon, he was presenting, was able to separate a simple mixture of compounds in a matter of seconds. Terry was bold enough to take the existing microfabrication technology used in microelectronics and successfully apply it to study basic scientific phenomena that occur at small dimensions. The device required only small quantities of reagents, had a relatively short analysis time and showed efficiency in separation that were better than larger counterparts. One of the other earliest examples of reported silicon micromachined devices was a colorimetric acid-base titration system, which employed a solid state pH-sensitive sensor to determine the acid or base concentration of a solution.⁸²

In the early 1980's, Michael Widmer proposed the concept of "miniaturized total chemical analysis systems" or μ TAS, in which silicon chip analyzers incorporated sample pretreatment, separation, and detection.⁸³ The complete analysis (sampling, sample transport, any necessary chemical reactions, separations, detection) were incorporated into a flow system. Due to inclusion of sample pretreatment, the detector no longer needs to be as selective as a sensor, because interfering compounds are eliminated, masked or separated from compound of interest.

At the beginning, the analytical performance of these devices was more desirable than their reduced size. However, miniaturization was the route to shorter analysis time and also versatility. The central technology for a number of miniaturized systems was the microfluidic technology, where liquids and gases were manipulated in channels with cross sectional dimensions on the order of 10-100 μm .

1.2.2 Scaling Effects when Miniaturizing the Chemistry

As the dimensions of a system change, the relative performance of a system and the operational success of miniaturized chemical separation, reaction and detection devices can be predicted by the scaling laws. During the last two decades, microfluidics, micrometer-scale total analysis systems (μTAS) or so called “lab-on-a-chip” devices have required consideration of scaling laws and dimensionless parameters for downscaling purposes.⁸³

There exist two main approaches to be considered when miniaturizing a device: the dimensionless-parameter approach and the similarity approach. In the dimensionless approach, parameters such as volume, column length, linear flow rate, retention time and pressure drop can be assumed to be constant over the entire system. The Reynolds number (Re), used to characterize laminar and turbulent regimes is a particularly useful dimensionless parameter.

$$Re = v \cdot \rho \cdot d / \eta \quad (1)$$

where v represents the average velocity, ρ the fluid density, η is the dynamic viscosity and d is the characteristic length, such as the diameter of the capillary. Because the

Reynolds number (Re) is proportional with the characteristic length d , for miniaturized systems, a small volume will be obtained, indicating laminar flow.

On the other hand, the approach that considers proportionality provides helpful information related to the behavior of a simple flow system when miniaturized. If miniaturization is assumed as a downscaling process in three dimensions (represented by a typical length, d) the behavior of the physical variables of interest can be predicted.⁸⁴ In a system, where the timescale is the same for the miniaturized system as for the full-scale system, the parameters that would change are: linear flow rate that in a tube would decrease by a factor of d , volumetric flow rate by a factor of d^3 , and the Reynolds number by d^2 .

In miniaturized systems, diffusion has a more dominant role in mass flow and becomes more important when molecular diffusion, heat diffusion or flow characteristics dictate the separation efficiency of the system. Additionally, in a diffusion-controlled system, the time is regarded as a surface and is proportional with d^2 . This system is in accordance with the band-broadening theory in chromatography and electrophoresis. So, if a system is downscaled by 1/10, the time variables decrease by 1/100, pressure increases by a factor of 100, and voltage requirements remain constant, but the essential chemistry and separation behavior retain the same quality.⁸⁵

Miniaturization can exploit the particle Brownian motion to efficiently mix solutions. In small structures, the mixing by diffusion is enhanced greatly because the time a molecule needs to travel a distance d decreases as $1/d^2$. Because of the low Reynolds numbers, therefore no turbulence in the micrometer regime, much effort is focused on improving the mixing capabilities. By using herringbone mixers, Stroock *et*

*al.*⁸⁶ demonstrated that the mixing process can be enhanced by chaotic advection. Also, Song *et al* showed that by using a two-phase flow, mixing in droplets was possible.⁸⁷

1.2.3 Materials for Microsystems

Microfabrication revolutionized the modern science and technology. Although microfabrication has its basis in microelectronics applications in other areas rapidly emerged. These include systems for microanalysis,⁸⁸⁻⁹¹ micro-volume reactors,^{92,93} combinatorial synthesis,⁹⁴ microelectromechanical systems (MEMS),^{95,96} and optical components.⁹⁷

One particularly exciting use for microanalytical devices is in the separation and analysis of chemical and biological substances. In addition, microstructures used in MEMS have evolved to integrate electronics with monitoring, actuating, and controlling tools for use in engineering. Most of the devices categorized as MEMS are fabricated from silicon using standard microlithographic techniques (silicon bulk micromachining and polysilicon surface micromachining).⁹⁸

Microsystems can be built on various substrates with a range of materials, from crystalline silicon to amorphous silicon, glass, quartz, metals, and organic polymers. Each of these materials possess their advantages and disadvantages depending on the type of application.

Silicon processing itself can be carried out using thin films of organic photoresists for etch patterning and this technique is very well developed. Moreover, two and three dimensional shapes can be reproduced with high precision.⁹⁸ Because similar techniques

used in electronic integrated circuits are applied, silicon microdevices can be batch fabricated. Also, due to the electronics industry, silicon is a readily available material. Chemically, one of the most attractive features of silicon and silicon dioxide is the chemical and thermal stability.

However, there are also some disadvantages that limit the spectrum of utilization of these materials. Crystalline silicon is relatively expensive, brittle, and opaque in the UV/visible regions. In contrast to glass or plastic, silicon will conduct current limiting its usefulness for electrokinetic devices. Because of these drawbacks and also complicated surface chemistry, alternative materials to silicon have been used to fabricate microsystems. Such materials are glass, quartz and some rigid organic polymers (e.g., epoxy, polyurethane, polyimide, polystyrene, and polymethylmethacrylate).^{99,100}

These materials have properties that make them useful for fabrication of microsystems. More specifically, they are transparent in the visible and UV regions, therefore they can be adapted to optical detection in microanalytical systems. Also, the surface properties of these substrates (e.g., wetting, adhesion, adsorption, reactivity) can be modified using a variety of surface chemistries. Microstructures of these materials can be replicated inexpensively by molding or embossing.⁹⁹⁻¹⁰⁴

Two of the most actively developed polymers for microfluidics and other applications are poly(dimethylsiloxane) (PDMS) and poly(methylmethacrylate) (PMMA).¹⁰⁵⁻¹⁰⁷ Elastomeric materials, such as PDMS, gained popularity mostly because of their optical properties. However aside the fact that PDMS is optically transparent to ~ 300 nm,¹⁰⁸ it can deform reversibly and repeatedly without permanent distortion,¹⁰⁹ it can

be molded for feature sizes of 0.1 to 10 μm ,¹¹⁰ it is durable and chemically inert, non-toxic, commercially available and inexpensive.

When selecting the material for a device, one of the most important features is its surface chemistry. PDMS, for example, is highly hydrophobic material, comprised of repeating units of $-\text{O}-\text{Si}(\text{CH}_3)_2-$. This hydrophobicity makes the channels less wettable with aqueous solutions and is prone to adsorption of hydrophobic species. However, by exposing the PDMS to plasma oxidation, its surface will be rendered more hydrophilic by the formation of silanol groups ($\text{Si}-\text{OH}$) at the expense of methyl groups ($\text{Si}-\text{CH}_3$).¹¹¹⁻¹¹³ These polar groups can then condense with appropriate polar groups on a different surface, and by bringing the two surfaces in conformal contact will result in the formation of covalent bonds that represent the basis of irreversible sealing. For PDMS and glass, for example, these bonds are $\text{Si}-\text{O}-\text{Si}$ after the loss of water.

There are also other parameters of the material that have a critical role in the success of the application of microfluidic devices. Such parameters include autofluorescence (for devices with optical detection), permeability (when using living cells), chemical resistance (when using non-aqueous solutions) and analyte adsorption.¹¹⁴

Heat dissipation, characterized by the thermal conductivity, in a substrate material is especially important when considering electroosmotic pumping, which is the most common method to propagate flow in microfluidic systems. In this case, a device or channels made of/in fused quartz will withstand higher localized heating compared to any plastic, and the efficiency of the separation will not be compromised. Moreover, the electroosmotic flow (EOF) in channels made of different polymer materials is highly variable due to the wide range of different charge and charge densities. The

electroosmotic flow is generated by the surface charge on the microchannel walls in combination with an electric field along the microchannel.

All of these parameters have been extensively evaluated and characterized for the wide range of applications of the microfluidic devices such as: miniaturized analytical systems, biomedical devices, tools for chemistry, biochemistry and medical applications.

1.2.4 Fabrication of Microfluidic Systems

One of the most commonly used techniques for the fabrication of microfluidic systems is photolithography.^{115,116} Here, a substrate, most often made of silicon, is spin-coated with a thin layer of photoresist (photosensitive polymer) and exposed to a UV light source through a photomask. The photoresist, exposed to UV light through a quartz plate covered with patterned microstructures, becomes either more (positive resist) or less (negative resist) soluble in a developing solution. Therefore, the pattern of the photomask is transferred on the film of photoresist. Finally, the substrate holding the desired pattern can serve as a master to make PDMS stamps.

Spin coating involves the acceleration of the coating material, which is deposited in the center of the substrate that is being rotated. The process of the film forming is driven by two independent parameters, namely viscosity (η) and rotational speed (ω). Other variable process parameters involved are the solid content and the speed time. Generally, the rotational speeds for spin coating are reported to be between 1500 and 8000 rpm, this giving a resist film uniformity ± 5 nm from substrate to substrate with a typical thickness of 0.8-3 μm .¹¹⁷

The photoresist processing consists of six steps illustrated in Figure 6 A) such as dehydration or chemical clean and priming, resist coating, soft baking, exposure, development, and post-development inspection.¹¹⁸ The dehydration/chemical cleaning step is performed to eliminate any moisture or any traces of contaminants (organic, ionic or metallic) adsorbed by the substrate surface and it is followed by the deposition of a silicon dioxide (SiO₂) which serves as a barrier layer. The next step is the spin coating of the resist onto the wafer surface. Depending on the type of application and/or the thickness desired, the speed can be calculated according to the formula:

$$z = k P^2/w^{1/2} \quad (2)$$

where z is the film thickness; k is a constant; P is the percentage of solids; and w is the rotational speed.

A soft baking step is performed usually between 90-95°C using either a convection oven, IR source, or hot plate. This step is important for the evaporation of solvent on the spun-on resist, to improve the adhesion of the resist to the wafer, and anneal the shear stresses induced during the spin coating. After spin coating and baking, the wafer must be exposed to UV light that will produce the pattern image on the resist. Depending on the type of resist used, the irradiated regions on the resist will become more or less soluble in the developer, therefore, giving a positive image or a negative image of the mask on the wafer. The development process involves chemical reactions where the unexposed parts of the resist get dissolved in the developer.¹¹⁸

A widely used technique for microfabrication is soft lithography. This technique belongs to a class of non-photolithographic techniques that are based on printing of self-assembled monolayers (SAMS)¹¹⁹ and molding of organic polymers. Soft lithographic

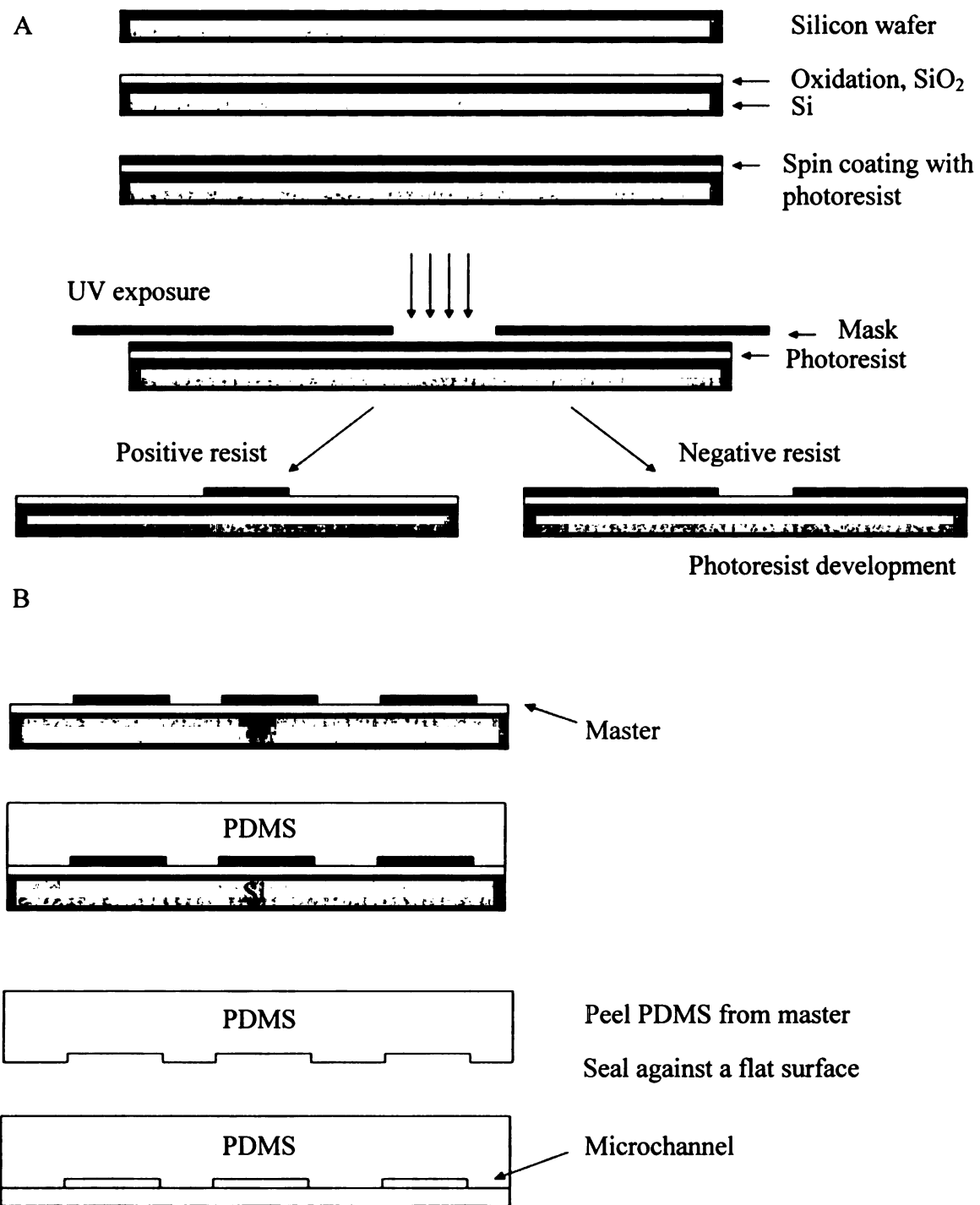


Figure 6. A) Representation of the steps in the lithographic process. B) Scheme of rapid prototyping.

techniques include microcontact printing,¹²⁰ micromolding in capillaries,¹²¹ microtransfer molding, replica molding,^{104,110} embossing,¹⁰² and injection molding. Replica molding is the easiest, more economic, and more amenable technique for analytical or biological applications. Here, microstructures are directly formed by casting and curing a UV curable polymer against an elastomeric mold. Feature sizes ranging from millimeters to approximately 3 nm can be replicated with high fidelity.

Another way of creating pattern structures on the submicrometer scale is the micro contact printing technique (μ CP).¹²² Using this technique, SEMS can be patterned in a simple way, allowing the fabrication of multi-array biosensors.

There are several other methods for microfabrication that are gaining more and more popularity, for example: embossing (or imprinting),¹⁰² injection molding,¹⁰¹ laser ablation,¹²³ electrochemical micromachining (EMM),¹²⁴ and ultrasonic machining.¹²⁵

1.2.5 Tools for Microfluidic Applications

Microfluidic devices can be used for a wide range of applications, from obtaining molecular diffusion coefficients,^{126,127} to measurements of the fluid viscosity,¹²⁸ to chemical binding coefficients,^{129,130} and enzyme reaction kinetics.¹³¹⁻¹³³

Other applications of microfluidic devices include capillary electrophoresis,¹³⁴ isoelectric focusing,^{130,135} immunoassays,¹³⁶⁻¹³⁹ flow cytometry,¹⁴⁰ sample injection of proteins for analysis via mass spectrometry,¹⁴¹⁻¹⁴³ PCR amplification,¹⁴⁴⁻¹⁴⁷ DNA analysis,¹⁴⁸⁻¹⁵⁰ cell manipulation,¹⁵¹ cell separation,¹⁵² cell patterning,^{153,154} and chemical gradient formation.^{155,156}

Many of these applications have utility for clinical diagnostics.^{157,158} Because of the small size of the channels, from micro- to nanometers, the amount of reagents and analytes is quite small, hence, microfluidic devices present a significant advantage to conduct biomedical research and to create clinically useful technologies. One of the long term goals in the field of microfluidics is to create integrated portable clinical diagnostic devices for home and bedside use, thereby eliminating time consuming laboratory analysis procedures.

In an effort to achieve this goal, recent microfluidic devices have undergone the transition from simple to highly integrated systems. Individual microfluidic components such as sample preparation, analysis and detection can be integrated on a single chip. Higher level of integration has been enabled by components such as microvalves,¹⁵⁹ micropumps,¹⁶⁰ flow sensors and other physical sensors, flow selectors, micromixers,⁴ microreactors, extractors, droplet generator, filters, traps, and sieves.

One of the most important components for the fabrication of a fully integrated microfluidic system, such as lab-on-a chip or μ TAS,^{83,84,161-163} were considered to be the microvalves and micropumps. Valves and pumps provide direct control of the flow and therefore are essential elements of a system that handles fluids at small scale.

Microvalves are essential components in many devices for portable chemical analysis, drug delivery, mixing, dosing and they can be roughly classified in two groups: passive valves (work without an actuator) and active valves (work with an actuator) that use mechanical, non-mechanical and external moving parts as shown in Table 1. Microvalves have a number of advantages over traditional valves. For example, because of their small size they do not require excessive power consumption, they have no

Categories			
Active	Mechanical	Magnetic	External magnetic fields Integrated magnetic inductors
		Electric	Electrostatic Electrokinetic
		Piezoelectric	
	Non-mechanical	Thermal	Bimetallic Thermopneumatic Shape memory alloy
		Bistable	
		Electrochemical Phase change	Hydrogel Sol-gel Paraffin
External	Rheological	Electro-rheological Ferrofluids	
	Modular	Built-in Rotary Membrane In-line	
	Pneumatic		
Passive	Mechanical	Check valve	Flap Membrane Ball In-line mobile structure Diffuser Abrupt
	Non-mechanical	Capillary	Liquid triggered Burst Hydrophobic valve

Table 1. Classification of microvalves.

leakage and result in minimal dead volume. Some of their ideal characteristics are their infinite differential pressure capability, insensitivity to particular contamination, zero response time, potential for linear operation and ability to operate with liquids and gases.¹⁶⁴

For achieving flow rates controllable over a certain range (0.25 to 10 $\mu\text{L min}^{-1}$) and with as little pulsation of possible, micropumps were the best choice. Current micropumps are roughly divided into two groups namely, reciprocating micropumps and continuous flow micropumps. Reciprocating micropumps use the oscillatory or the rotational movement of the mechanical parts to displace the fluid, while continuous flow micropumps rely on the direct transformation of nonmechanical or mechanical energy into a continuous fluid movement.¹⁶⁰

Beside microvalves and micropumps, micromixers are another important component in a microfluidic system. Rapid mixing is essential in many of the microfluidic systems used in biochemical analysis, drug delivery and sequencing or synthesis of nucleic acids. Due to low Re numbers, in microfluidic devices the mixing of different flowing streams rely only on molecular diffusion. However, if the application requires fast mixing and analysis, the mixing can be induced by using input of energy from the exterior, termed active mixing. Some examples of external energy inputs are ultrasound,¹⁶⁵ acoustic, bubble-induced vibrations,^{166,167} electrokinetic instabilities,¹⁶⁸ periodic variation of flow rate,^{169,170} electrowetting-merging of droplets,¹⁷¹ piezoelectric vibrating membranes,¹⁷² magneto-hydrodynamic action,¹⁷³ small impellers, integrated microvalves/pumps¹⁷⁴ (Figure 7).

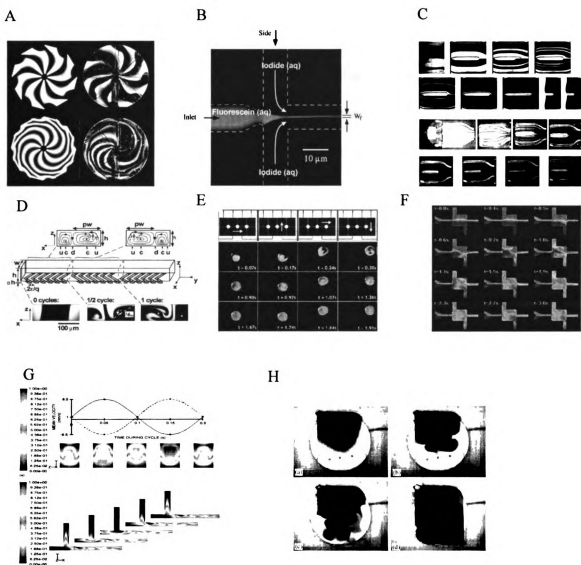


Figure 7. Types of micromixing. **A.** Cyclone micromixer ; **B.** Hydrodynamic focusing by compressing a central stream by two outer streams at much larger flow rate ; **C.** Multi-lamination flow patterns of a split-and-recombine mixer visualized by a dilution-type experiment ; **D.** Staggered herringbone micromixer for the generation of chaotic flows ; **E.** Time lapse images of three-electrode mixing at 8 Hz ; **F.** Electrokinetic instability micromixing ; **G.** Numerical simulation results obtained for two inlet flows pulsed at 180° phase difference ; **H.** Photographs showing acoustic microstreaming in a microchamber ⁴

1.2.6 Detection Modes in Microfluidic Devices

In order to quantitatively and qualitatively characterize an analyte of interest, the microsystem must be equipped with a high performance detection scheme. Reduction of the size of the microchannels makes the diffusion a very fast process and therefore, separation techniques on microchips, such as chromatography, electrophoresis, electrochromatography and separations in immunochemical assays are more advantageous than the conventional systems.¹⁷⁵ There are three major types of detection that should be mentioned: optical detection, electrochemical and mass spectrometry. Optical detection typically comprises fluorescence, absorbance, chemiluminescence, and refractive index.

Fluorescence detection is the most common detection mode for microchip devices because of its versatility and also sensitivity (picomolar detection limits). The most sensitive ($< 10^{13}$ M) small volume detection method present to date is the laser-induced fluorescence (LIF).¹⁷⁸ In fact, single molecule detection has been demonstrated in a capillary using LIF.¹⁷⁹ LIF typically requires off-chip derivatization of the sample which increases the time of the total analysis. However, because the detection of native fluorescence has disadvantages, such as weak signal and high background fluorescence (poor sensitivity), LIF has been considered a more attractive choice. Fluorescence detection is used not only for single point detection but also to image a large area, such as monitoring of the fluid flow. For applications involving parallel analysis (monitoring multiple channels), laser scanning techniques can be utilized.¹⁸⁰ Also, organic light

emitting diodes (LEDs)¹⁸¹ and fiber optics were considered successful ways of integrated detection methods for on-chip analysis.

For microseparations, and particularly for capillary electrophoresis, the most common method of detection used is absorbance, and this is because most organic compounds can be detected at 195-210 nm. However, due to the small internal diameter of the microchannels, the path length dependency of absorbance detection makes the detection of solutes with poor absorptivity very difficult.¹⁸² Other optical detection modes include chemiluminescence, where no external light source is needed and background signal is minimal, and refractive index detection, which is useful for compounds with poor absorbance/fluorescence (270 nM LOD for unlabelled proteins).¹⁸³

Another very sensitive and selective method of detection that has been widely used in microdevices is electrochemical detection (EC). Electrochemical detection has the advantage of low cost, relatively easy operation and no need for labeling, required in LIF. There are three types of electrochemical detection: potentiometry (ion selective electrode, measures voltage), amperometry (measures current), and conductivity (measures voltage/current). Potentiometric detectors are based on classical ion selective microelectrodes (ISE) and have the ability to detect very small quantities of organic and inorganic ions in small probe volumes. The first example of potentiometric detection on chip was reported by Manz *et al.*¹⁸⁴ This study described a micromachined ISE chip for Ba⁺ sensing.

The mechanism for amperometry relies on the electron transfer to/from electroactive analyte at solid electrode (DC voltage applied) and the resultant current is proportional with the analyte concentration. When amperometric detection is applied for

conventional CE, there are some issues that have to be overcome. For example, the electrophoretic current is usually up to 10^6 larger than the detector current, thus the detector has to be decoupled from the high voltage. That was accomplished by using a fine crack in the capillary as a decoupler. Therefore, electroosmotic flow (EOF) generation stops at crack and the pressure from EOF pushes the analyte to the electrode. For the on chip integration there have been different attempts to align the electrodes with the decoupler. Mathies *et al.*¹⁸⁵ reported a device where the decoupling from high potential was accomplished by placing the working electrode (10 μm wide) 30 μm beyond the end of the separation channel in 1 mm wide exit channel. They used the device for the detection of neurotransmitters with very good limits of detection (LOD); for example, dopamine (66 attomol in 18 pL), epinephrine (6.5 μM) and catechol (12 μM). However, there are major drawbacks of these amperometric techniques, one of them being the strong adsorption of the analyte reaction intermediates to the surface of the electrodes (carbon electrodes). Some researchers got around this problem by utilizing for example, dual-electrode detectors with two gold working electrodes configured in series¹⁸⁶ or pulsed amperometric detection (PAD) which utilizes a continuous three-step potential waveform.¹⁸⁷

Mass spectrometry has also been used as a detection mode for both glass^{188,189} and PDMS devices.¹⁹⁰ Although mass spectrometry can provide more chemical information than any other types of detectors, it is less sensitive than LIF, very expensive and cannot yet be integrated in a portable chip. However, many groups tried and succeeded to interface microfluidic devices with mass spectrometry, especially electrospray ionization time-of-flight mass spectrometry (ESI-TOF MS)¹⁹¹⁻¹⁹⁴ for the detection of large

biomolecules with high sensitivity. CE-MS detection on chip has been studied extensively by many researchers.^{195,196}

On chip micromachined ionization sources that resemble electrospray emitter tips have been reported by a number of groups.¹⁹⁷⁻²⁰¹ Arscott *et al.* reported a planar on-chip nib-like structure using the epoxy-based negative photoresist SU-8 as part of a microfabricated ionization source that functions in nanoelectrospray conditions.²⁰²

With the progress in microfabrication technologies and detection methods, researchers can basically choose any detection method that is suitable for their applications. μ -TAS and lab on-a-chip systems will continue to develop and possibly integrate multiple detection schemes for multiple analytes in same device, for different types of applications, for example rapid, on-site diagnostic.

1.3 THESIS OBJECTIVE

In this work we propose to apply the recent developments in microfabrication technology to create an *in vitro* model that will closely mimic an *in vivo* system. Because a molecular level understanding of the mechanisms by which RBCs deformability properties relate to the occurrence of MS is lacking, to gain insight into these mechanisms would be ideal to employ such a model system.

More specifically, this work describes the development of a complete blood brain barrier (BBB) mimic using lithographically-derived microchips in order to monitor the fate of endothelium-derived NO that is stimulated by mechanically deformed RBCs. The microchip-based BBB mimic was developed by addressing an array of cell reservoirs,

which pose as the central nervous system (CNS), with a network of underlying channels that represent the circulatory system. The cells were cultured on a polycarbonate membrane, integrated in the device that separates the “so called” CNS from the “so called” blood stream. The diameters of the patterned channels in the fabricated chips will ultimately approximate those of brain capillaries *in vivo*.

This approach was used to monitor ATP-stimulated NO levels in the cells cultured on the polycarbonate membrane. Importantly, using chip technology, we were able to investigate the flux of NO across the BBB brought about by changes in ATP concentrations, both in the form of ATP standards and RBC-derived ATP. As the detection scheme, fluorescence microscopy was employed to enable the qualitative and quantitative identification of endothelium derived-NO after it diffuses through the membrane of the microchip device.

LIST OF REFERENCES

- (1) Evans, E.; Fung, Y. C. *Microvasc Res* **1972**, *4*, 335-347.
- (2) Hartwig, J. H.; DeSisto, M. *J Cell Biol* **1991**, *112*, 407-425.
- (3) Schwiebert, E. M.; Benos, D. J.; Egan, M. E.; Stutts, M. J.; Guggino, W. B. *Physiol Rev* **1999**, *79*, S145-166.
- (4) Hessel, V.; Loewe, H.; Schoenfeld, F. *Chem. Eng. Sci.* **2005**, *60*, 2479-2501.
- (5) Mohandas, N.; Evans, E. *Annu. Rev. Biophys. Biomol. Struct. FIELD Full Journal Title: Annual Review of Biophysics and Biomolecular Structure* **1994**, *23*, 787-818.
- (6) Linderkamp, O.; Meiselman, H. J. *Blood* **1982**, *59*, 1121-1127.
- (7) Watanabe, N.; Kataoka, H.; Yasuda, T.; Takatani, S. *Biophys. J.* **2006**, *91*, 1984-1998.
- (8) Rubanyi, G. M.; Romero, J. C.; Vanhoutte, P. M. *Am J Physiol* **1986**, *250*, H1145-1149.
- (9) Buga, G. M.; Gold, M. E.; Fukuto, J. M.; Ignarro, L. J. *Hypertension* **1991**, *17*, 187-193.
- (10) Furchgott, R. F.; Zawadzki, J. V. *Nature* **1980**, *288*, 373-376.
- (11) Sprague, R. S.; Stephenson, A. H.; Dimmitt, R. A.; Weintraub, N. A.; Branch, C. A.; McMurdo, L.; Lonigro, A. J. *American Journal of Physiology* **1995**, *269*, H1941-H1948.
- (12) Sprague, R. S.; Ellsworth, M. L.; Stephenson, A. H.; Lonigro, A. J. *American Journal of Physiology* **1996**, *271*, H2717-H2722.
- (13) Busse, R.; Ogilvie, A.; Pohl, U. *Am J Physiol* **1988**, *254*, H828-832.
- (14) Bogle, R. G.; Coade, S. B.; Moncada, S.; Pearson, J. D.; Mann, G. E. *Biochem Biophys Res Commun* **1991**, *180*, 926-932.

- (15) Dean, B. M.; Perrett, D. *Biochim Biophys Acta* **1976**, *437*, 1-5.
- (16) Miseta, A.; Bogner, P.; Berenyi, E.; Kellermayer, M.; Galambos, C.; Wheatley, D. N.; Cameron, I. L. *Biochim Biophys Acta* **1993**, *1175*, 133-139.
- (17) Bergfeld, G. R.; Forrester, T. *Cardiovasc. Res.* **1992**, *26*, 40-47.
- (18) Ellsworth, M. L.; Forrester, T.; Ellis, C. G.; Dietrich, H. H. *American Journal of Physiology* **1995**, *269*, H2155-H2161.
- (19) Goldsmith, H. L. *J Gen Physiol* **1968**, *52*, 5Suppl-28s.
- (20) Hassessian, H.; Burnstock, G. *Br J Pharmacol* **1995**, *114*, 846-850.
- (21) Collins, D. M.; McCullough, W. T.; Ellsworth, M. L. *Microvascular research* **1998**, *56*, 43-53.
- (22) Dietrich, H. H.; Ellsworth, M. L.; Sprague, R. S.; Dacey, R. G., Jr. *American Journal of Physiology* **2000**, *278*, H1294-H1298.
- (23) Dietrich, H. H.; Kajita, Y.; Dacey, R. G., Jr. *The American journal of physiology* **1996**, *271*, H1109-1116.
- (24) McCullough, W. T.; Collins, D. M.; Ellsworth, M. L. *American Journal of Physiology* **1997**, *272*, H1886-H1891.
- (25) Houston, D. A.; Burnstock, G.; Vanhoutte, P. M. *J Pharmacol Exp Ther* **1987**, *241*, 501-506.
- (26) Sprague, R. S.; Stephenson, A. H.; Ellsworth, M. L.; Keller, C.; Lonigro, A. J. *Exp Biol Med (Maywood)* **2001**, *226*, 434-439.
- (27) Quinton, P. M. *Nature* **1983**, *301*, 421-422.
- (28) Anderson, M. P.; Gregory, R. J.; Thompson, S.; Souza, D. W.; Paul, S.; Mulligan, R. C.; Smith, A. E.; Welsh, M. J. *Science* **1991**, *253*, 202-205.
- (29) Bear, C. E.; Li, C. H.; Kartner, N.; Bridges, R. J.; Jensen, T. J.; Ramjeesingh, M.; Riordan, J. R. *Cell* **1992**, *68*, 809-818.
- (30) Lee, M. G.; Wigley, W. C.; Zeng, W.; Noel, L. E.; Marino, C. R.; Thomas, P. J.; Muallem, S. *J Biol Chem* **1999**, *274*, 3414-3421.

- (31) Knowles, M. R.; Stutts, M. J.; Spock, A.; Fischer, N.; Gatzky, J. T.; Boucher, R. C. *Science (Washington, D. C., 1883-)* **1983**, *221*, 1067-1070.
- (32) Stutts, M. J.; Canessa, C. M.; Olsen, J. C.; Hamrick, M.; Cohn, J. A.; Rossier, B. C.; Boucher, R. C. *Science* **1995**, *269*, 847-850.
- (33) Boucher, R. C.; Stutts, M. J.; Knowles, M. R.; Cantley, L.; Gatzky, J. T. *J Clin Invest* **1986**, *78*, 1245-1252.
- (34) Gabriel, S. E.; Clarke, L. L.; Boucher, R. C.; Stutts, M. J. *Nature* **1993**, *363*, 263-268.
- (35) Jovov, B.; Ismailov, I. I.; Benos, D. J. *J Biol Chem* **1995**, *270*, 1521-1528.
- (36) Schwiebert, E. M.; Egan, M. E.; Hwang, T. H.; Fulmer, S. B.; Allen, S. S.; Cutting, G. R.; Guggino, W. B. *Cell* **1995**, *81*, 1063-1073.
- (37) Schreiber, R.; Nitschke, R.; Greger, R.; Kunzelmann, K. *J Biol Chem* **1999**, *274*, 11811-11816.
- (38) Reisin, I. L.; Prat, A. G.; Abraham, E. H.; Amara, J. F.; Gregory, R. J.; Ausiello, D. A.; Cantiello, H. F. *J Biol Chem* **1994**, *269*, 20584-20591.
- (39) Sugita, M.; Yue, Y.; Foskett, J. K. *Embo J* **1998**, *17*, 898-908.
- (40) Abraham, E. H.; Okunieff, P.; Scala, S.; Vos, P.; Oosterveld, M. J.; Chen, A. Y.; Shrivastav, B. *Science* **1997**, *275*, 1324-1326.
- (41) Abraham, E. H.; Prat, A. G.; Gerweck, L.; Seneveratne, T.; Arceci, R. J.; Kramer, R.; Guidotti, G.; Cantiello, H. F. *Proc Natl Acad Sci U S A* **1993**, *90*, 312-316.
- (42) Pasyk, E. A.; Foskett, J. K. *J Biol Chem* **1997**, *272*, 7746-7751.
- (43) Prat, A. G.; Reisin, I. L.; Ausiello, D. A.; Cantiello, H. F. *Am J Physiol* **1996**, *270*, C538-545.
- (44) Giovannoni, G.; Heales, S. J. R.; Land, J. M.; Thompson, E. J. *Multiple Sclerosis* **1998**, *4*, 212-216.
- (45) Mazzanti, L.; Faloia, E.; Rabini, R. A.; Staffolani, R.; Kantar, A.; Fiorini, R.; Swoboda, B.; De Pirro, R.; Bertoli, E. *Clin Biochem* **1992**, *25*, 41-46.
- (46) Blair, G. W.; Matchett, R. H. *J Neurol Neurosurg Psychiatry* **1972**, *35*, 730-731.

- (47) Karlov, V. A.; Savin, A. A.; Smertina, L. P.; Redchits, E. G.; Seleznev, A. N.; Svetailo, L. I.; Margosiuk, N. V.; Stulin, I. D.: *USSR*, 1990, pp 47-50.
- (48) Simpson, L. O.; Shand, B. I.; Olds, R. J.; Larking, P. W.; Arnott, M. J. *Pathology* **1987**, *19*, 51-55.
- (49) Szeinberg, A.; Golan, R.; Ben Ezzer, J.; Sarova-Pinhas, I.; Sadeh, M.; Braham, J. *Acta Neurol. Scand.* **1979**, *60*, 265-271.
- (50) Shukla, V. K. S.; Jensen, G. E.; Clausen, J. *Acta Neurol. Scand.* **1977**, *56*, 542-550.
- (51) Zachara, B.; Gromadzinska, J.; Czernicki, J.; Maciejek, Z.; Chmielewski, H. *Klin Wochenschr* **1984**, *62*, 179-182.
- (52) Szeinberg, A.; Golan, R.; Ben-Ezzer, J.; Sarova-Pinhas, I.; Kindler, D. *Acta Neurol Scand* **1981**, *63*, 67-75.
- (53) Polidoro, G.; Di Ilio, C.; Arduini, A.; La Rovere, G.; Federici, G. *Int. J. Biochem.* **1984**, *16*, 505-509.
- (54) Jensen, G. E.; Clausen, J. *J. Neurol. Sci.* **1984**, *63*, 45-53.
- (55) Golan, R.; Szeinberg, A.; Ezzer, J. B.; Sarova-Pinhas, I.; Sadde, M.; Braham, J. *Prog. Clin. Biol. Res.* **1980**, *39*, 467.
- (56) Ghigo, D.; Bosia, A.; Pagani, A.; Pescarmona, G. P.; Pagano, G.; Lenti, G. *Ric Clin Lab* **1983**, *13 Suppl 3*, 375-381.
- (57) Matkovics, B.; Kotorman, M.; Varga, I. S.; Hai, D. Q.; Roman, F.; Novak, Z. *Acta Physiol Hung* **1997**, *85*, 99-106.
- (58) Carroll, J.; Raththagala, M.; Subasinghe, W.; Baguzis, S.; Oblak, T. D. a.; Root, P.; Spence, D. *Mol. BioSyst.* **2006**, *2*, 305-311.
- (59) Giovannoni, G. *Multiple Sclerosis* **1998**, *4*, 27-30.
- (60) Parkinson, J. F.; Mitrobcvic, B.; Merrill, J. E. *Journal of Molecular Medicine (Berlin)* **1997**, *75*, 174-186.
- (61) Alderton, W. K.; Cooper, C. E.; Knowles, R. G. *Biochemical Journal* **2001**, *357*, 593-615.
- (62) Michel, T.; Feron, O. *Journal of Clinical Investigation* **1997**, *100*, 2146-2152.

- (63) Guix, F. X.; Uribesalgo, I.; Coma, M.; Munoz, F. J. *Progress in Neurobiology (Amsterdam, Netherlands)* **2005**, *76*, 126-152.
- (64) Karg, E.; Klivenyi, P.; Nemeth, I.; Bencsik, K.; Pinter, S.; Vecsei, L. *Journal of neurology* **1999**, *246*, 533-539.
- (65) Audus, K. L.; Borchardt, R. T. *Handbook of Experimental Pharmacology* **1991**, *100*, 43-70.
- (66) Brightman, M. W.; Reese, T. S. *J Cell Biol* **1969**, *40*, 648-677.
- (67) Reese, T. S.; Karnovsky, M. J. *J Cell Biol* **1967**, *34*, 207-217.
- (68) Bradbury, M. W. *Circ Res* **1985**, *57*, 213-222.
- (69) Audus, K. L.; Chikhale, P. J.; Miller, D. W.; Thompson, S. E.; Borchardt, R. T. *Adv. Drug Res.* **1992**, *23*, 1-64.
- (70) Andersson, P. B.; Perry, V. H.; Gordon, S. *Neuroscience* **1992**, *48*, 169-186.
- (71) Lassmann, H.; Zimprich, F.; Rossler, K.; Vass, K. *Rev Neurol (Paris)* **1991**, *147*, 763-781.
- (72) de Vries, H. E.; Blom-Roosemalen, M. C. M.; van Oosten, M.; de Boer, A. G.; van Berkel, T. J. C.; Breimer, D. D.; Kuiper, J. *J. Neuroimmunol.* **1996**, *64*, 37-43.
- (73) De Vries, H. E.; Kuiper, J.; De Boer, A. G.; Van Berkel, T. J. C.; Breimer, D. D. *Pharmacol. Rev.* **1997**, *49*, 143-155.
- (74) Griot, C.; Vandeveld, M.; Richard, A.; Peterhans, E.; Stocker, R. *Free Radical Res. Commun.* **1990**, *11*, 181-193.
- (75) Kim, Y. S.; Kim, S. U. *J Neurosci Res* **1991**, *29*, 100-106.
- (76) Thiel, V. E.; Audus, K. L. *Antioxidants & Redox Signaling* **2001**, *3*, 273-278.
- (77) Yuceyar, N.; Taskiran, D.; Sagduyu, A. *Clinical neurology and neurosurgery* **2001**, *103*, 206-211.
- (78) Mayhan, W. G. *Brain research* **1996**, *743*, 70-76.

- (79) Sprague, R. S.; Ellsworth, M. L.; Stephenson, A. H.; Kleinhenz, M. E.; Lonigro, A. J. *American Journal of Physiology* **1998**, *275*, H1726-H1732.
- (80) Fischer, T. M.; Haest, C. W.; Stohr, M.; Kamp, D.; Deuticke, B. *Biochim Biophys Acta* **1978**, *510*, 270-282.
- (81) Terry, S. C.; Angell, J. B. *Theory, Des., Biomed. Appl. Solid State Chem. Sens., Workshop* **1978**, 207-218.
- (82) Van der Schoot, B.; Bergveld, P. *Sens. Actuators* **1985**, *8*, 11-22.
- (83) Manz, A.; Graber, N.; Widmer, H. M. *Sens. Actuators, B* **1990**, *B1*, 244-248.
- (84) Reyes, D. R.; Iossifidis, D.; Auroux, P.-A.; Manz, A. *Analytical Chemistry* **2002**, *74*, 2623-2636.
- (85) Manz, A.; Harrison, D. J.; Verpoorte, E. M. J.; Fettingner, J. C.; Paulus, A.; Luedi, H.; Widmer, H. M. *J. Chromatogr.* **1992**, *593*, 253-258.
- (86) Stroock, A. D.; Dertinger, S. K. W.; Ajdari, A.; Mezit, I.; Stone, H. A.; Whitesides, G. M. *Science (Washington, DC, U. S.)* **2002**, *295*, 647-651.
- (87) Song, H.; Bringer, M. R.; Tice, J. D.; Gerdts, C. J.; Ismagilov, R. F. *Appl. Phys. Lett.* **2003**, *83*, 4664-4666.
- (88) Jacobson, S. C.; Hergenroder, R.; Koutny, L. B.; Warmack, R. J.; Ramsey, J. M. *Anal. Chem.* **1994**, *66*, 1107-1113.
- (89) Manz, A. *Chimia* **1996**, *50*, 140-143.
- (90) Bratten, C. D.; Cobbold, P. H.; Cooper, J. M. *Anal Chem* **1998**, *70*, 1164-1170.
- (91) Clark, R. A.; Hietpas, P. B.; Ewing, A. G. *Anal. Chem.* **1997**, *69*, 259-263.
- (92) Ananchenko, G. S.; Bagryanskaya, E. G.; Tarasov, V. F.; Sagdeev, R. Z.; Paul, H. *Chem. Phys. Lett.* **1996**, *255*, 267-273.
- (93) Song, M. I.; Iwata, K.; Yamada, M.; Yokoyama, K.; Takeuchi, T.; Tamiya, E.; Karube, I. *Anal Chem* **1994**, *66*, 778-781.
- (94) Briceno, G.; Chang, H.; Sun, X.; Schultz, P. G.; Xiang, X. D. *Science (Washington, D. C.)* **1995**, *270*, 273-275.
- (95) Kovaca, G. T. A.; Petersen, K.; Albin, M. *Anal. Chem.* **1996**, *68*, 407A-412A.

- (96) MacDonald, N. C.; Adams, S. G.; Ayon, A. A.; Boehringer, K. F.; Chen, L. Y.; Das, J. H.; Haronian, D.; Hofmann, W.; Huang, X. T.; et al. *Microelectron. Eng.* **1996**, *30*, 563-564.
- (97) Lee, S. S.; Lin, L. Y.; Wu, M. C. *Appl. Phys. Lett.* **1995**, *67*, 2135-2137.
- (98) Sniegowski, J. J. *Tribol. Issues Oppor. MEMS, Proc. NSF/AFOSR/ASME Workshop* **1998**, 325-340.
- (99) Frazier, A. B.; Ahn, C. H.; Allen, M. G. *Sens. Actuators, A* **1994**, *A45*, 47-55.
- (100) Williams, G.; D'Silva, C. *Sens. VI [Proc. Conf. Sens. Their Appl.], 6th* **1993**, 161-166.
- (101) Emmelius, M.; Pawlowski, G.; Vollmann, H. W. *Angew. Chem.* **1989**, *101*, 1475-1502.
- (102) Chou, S. Y.; Krauss, P. R.; Renstrom, P. J. *Science (Washington, D. C.)* **1996**, *272*, 85-87.
- (103) Palmer, E. W.; Hutley, M. C.; Franks, A.; Verrill, J. F.; Gale, B. *Rep. Prog. Phys.* **1975**, *38*, 975-1048.
- (104) Xia, Y.; Kim, E.; Zhao, X.-M.; Rogers, J. A.; Prentiss, M.; Whitesides, G. M. *Science (Washington, D. C.)* **1996**, *273*, 347-349.
- (105) McDonald, J. C.; Duffy, D. C.; Anderson, J. R.; Chiu, D. T.; Wu, H.; Schueller, O. J. A.; Whitesides, G. M. *Electrophoresis* **2000**, *21*, 27-40.
- (106) McDonald, J. C.; Whitesides George, M. *Acc Chem Res* **2002**, *35*, 491-499.
- (107) Becker, H.; Locascio, L. E. *Talanta* **2002**, *56*, 267-287.
- (108) Clarson, S. J.; Semlyen, J. A. *Siloxane Polymers*, 1993.
- (109) Rogers, J. A.; Qin, D.; Schueller, O. J. A.; Whitesides, G. M. *Rev. Sci. Instrum.* **1996**, *67*, 3310-3319.
- (110) Xia, Y.; McClelland, J. J.; Gupta, R.; Qin, D.; Zhao, X. M.; Sohn, L. L.; Celotta, R. J.; Whitesides, G. M. *Adv. Mater. (Weinheim, Ger.)* **1997**, *9*, 147-149.
- (111) Chaudhury, M. K.; Whitesides, G. M. *Langmuir* **1991**, *7*, 1013-1025.
- (112) Chaudhury, M. K.; Whitesides, G. M. *Science (Washington, D. C., 1883-)* **1992**, *255*, 1230-1232.

- (113) Morra, M.; Occhiello, E.; Marola, R.; Garbassi, F.; Humphrey, P.; Johnson, D. *J. Colloid Interface Sci.* **1990**, *137*, 11-24.
- (114) Becker, H.; Gartner, C. *Electrophoresis* **2000**, *21*, 12-26.
- (115) Moreau, W. M. *Opt. Eng.* **1983**, *22*, 181-184.
- (116) Brambley, D.; Martin, B.; Prewett, P. D. *Adv. Mater. Opt. Electron.* **1994**, *4*, 55-74.
- (117) Flack, W. W.; Nguyen, H.-A.; Capsuto, E. S. *Proc. SPIE-Int. Soc. Opt. Eng.* **2003**, *5039*, 1257-1271.
- (118) Wolf, S.; Tauber, R. N. *Silicon Processing for the VLSI ERA, Vol. 1: Process Technology*, 1986.
- (119) Whitesides, G. M.; Mathias, J. P.; Seto, C. T. *Science (Washington, D. C., 1883-)* **1991**, *254*, 1312-1319.
- (120) Kumar, A.; Abbott, N. L.; Biebuyck, H. A.; Kim, E.; Whitesides, G. M. *Acc. Chem. Res.* **1995**, *28*, 219-226.
- (121) Kim, E.; Xia, Y.; Whitesides, G. M. *Nature (London)* **1995**, *376*, 581-584.
- (122) Mrksich, M.; Whitesides, G. M. *Trends Biotechnol.* **1995**, *13*, 228-235.
- (123) Grzybowski, B. A.; Haag, R.; Bowden, N.; Whitesides, G. M. *Anal. Chem.* **1998**, *70*, 4645-4652.
- (124) Schuster, R.; Kirchner, V.; Allongue, P.; Ertl, G. *Science (Washington, D. C.)* **2000**, *289*, 98-101.
- (125) Iwata, F.; Kawaguchi, M.; Aoyama, H.; Sasaki, A. *Thin Solid Films* **1997**, *302*, 122-126.
- (126) Kamholz, A. E.; Weigl, B. H.; Finlayson, B. A.; Yager, P. *Anal Chem* **1999**, *71*, 5340-5347.
- (127) Kamholz, A. E.; Yager, P. *Biophys J* **2001**, *80*, 155-160.
- (128) Forster, F. K.; Galambos, P. C.; Weigl, B. H.; Holl, M. R.; (University of Washington, USA). Application: US, 1999, pp 23 pp.
- (129) Weigl, B. H.; Yager, P. *Sens. Actuators, B* **1997**, *B39*, 452-457.
- (130) Macounova, K.; Cabrera, C. R.; Yager, P. *Anal Chem* **2001**, *73*, 1627-1633.

- (131) Hadd, A. G.; Jacobson, S. C.; Ramsey, J. M. *Anal. Chem.* **1999**, *71*, 5206-5212.
- (132) Hadd, A. G.; Raymond, D. E.; Halliwell, J. W.; Jacobson, S. C.; Ramsey, J. M. *Anal. Chem.* **1997**, *69*, 3407-3412.
- (133) Duffy, D. C.; Gillis, H. L.; Lin, J.; Sheppard, N. F., Jr.; Kellogg, G. J. *Anal. Chem.* **1999**, *71*, 4669-4678.
- (134) Kameoka, J.; Craighead, H. G.; Zhang, H.; Henion, J. *Anal. Chem.* **2001**, *73*, 1935-1941.
- (135) Xu, J.; Lee, C. S.; Locascio, L. E. *Book of Abstracts, 219th ACS National Meeting, San Francisco, CA, March 26-30, 2000* **2000**, ANYL-009.
- (136) Hatch, A.; Kamholz, A. E.; Hawkins, K. R.; Munson, M. S.; Schilling, E. A.; Weigl, B. H.; Yager, P. *Nat. Biotechnol.* **2001**, *19*, 461-465.
- (137) Eteshola, E.; Leckband, D. *Sens. Actuators, B* **2001**, *B72*, 129-133.
- (138) Cheng, S. B.; Skinner, C. D.; Taylor, J.; Attiya, S.; Lee, W. E.; Picelli, G.; Harrison, D. J. *Anal. Chem.* **2001**, *73*, 1472-1479.
- (139) Yang, T.; Jung, S.-y.; Mao, H.; Cremer, P. S. *Anal. Chem.* **2001**, *73*, 165-169.
- (140) Sohn, L. L.; Saleh, O. A.; Facer, G. R.; Beavis, A. J.; Allan, R. S.; Notterman, D. A. *Proc. Natl. Acad. Sci. U. S. A.* **2000**, *97*, 10687-10690.
- (141) Jiang, Y.; Wang, P.-C.; Locascio, L. E.; Lee, C. S. *Anal. Chem.* **2001**, *73*, 2048-2053.
- (142) Gao, J.; Xu, J.; Locascio, L. E.; Lee, C. S. *Anal. Chem.* **2001**, *73*, 2648-2655.
- (143) Figeys, D.; Gygi, S. P.; McKinnon, G.; Aebersold, R. *Anal. Chem.* **1998**, *70*, 3728-3734.
- (144) Northrup, M. A.; White, R. M.; (Regents of the University of California, USA). Application: WO, 1994, pp 51 pp.
- (145) Belgrader, P.; Okuzumi, M.; Pourahmadi, F.; Borkholder, D. A.; Northrup, M. A. *Biosens. Bioelectron.* **2000**, *14*, 849-852.
- (146) Khandurina, J.; McKnight, T. E.; Jacobson, S. C.; Waters, L. C.; Foote, R. S.; Ramsey, J. M. *Anal. Chem.* **2000**, *72*, 2995-3000.
- (147) Lagally, E. T.; Medintz, I.; Mathies, R. A. *Anal. Chem.* **2001**, *73*, 565-570.

- (148) Fan, Z. H.; Mangru, S.; Granzow, R.; Heaney, P.; Ho, W.; Dong, Q.; Kumar, R. *Anal. Chem.* **1999**, *71*, 4851-4859.
- (149) Koutny, L.; Schmalzing, D.; Salas-Solano, O.; El-Difrawy, S.; Adourian, A.; Buonocore, S.; Abbey, K.; McEwan, P.; Matsudaira, P.; Ehrlich, D. *Anal. Chem.* **2000**, *72*, 3388-3391.
- (150) Woolley, A. T.; Mathies, R. A. *Proc Natl Acad Sci U S A* **1994**, *91*, 11348-11352.
- (151) Glasgow, I. K.; Zeringue, H. C.; Beebe, D. J.; Choi, S. J.; Lyman, J. T.; Chan, N. G.; Wheeler, M. B. *IEEE Trans Biomed Eng* **2001**, *48*, 570-578.
- (152) Yang, J.; Huang, Y.; Wang, X.-B.; Becker, F. F.; Gascoyne, P. R. C. *Anal. Chem.* **1999**, *71*, 911-918.
- (153) Chiu, D. T.; Li Jeon, N.; Huang, S.; Kane, R. S.; Wargo, C. J.; Choi, I. S.; Ingber, D. E.; Whitesides, G. M. *Proc. Natl. Acad. Sci. U. S. A.* **2000**, *97*, 2408-2413.
- (154) Folch, A.; Jo, B.-H.; Hurtado, O.; Beebe, D. J.; Toner, M. *J. Biomed. Mater. Res.* **2000**, *52*, 346-353.
- (155) Dertinger, S. K. W.; Chiu, D. T.; Jeon, N. L.; Whitesides, G. M. *Anal. Chem.* **2001**, *73*, 1240-1246.
- (156) Jeon, N. L.; Dertinger, S. K. W.; Chiu, D. T.; Choi, I. S.; Stroock, A. D.; Whitesides, G. M. *Langmuir* **2000**, *16*, 8311-8316.
- (157) Weigl, B. H.; Darling, R. B.; Yager, P.; Kriebel, J.; Mayes, K. *Proc. SPIE-Int. Soc. Opt. Eng.* **1999**, *3606*, 82-89.
- (158) Cunningham, D. D. *Anal. Chim. Acta* **2001**, *429*, 1-18.
- (159) Hesketh, P. J.; Bintoro, J. S.; Luharuka, R. *Sens. Update* **2004**, *13*, 233-302.
- (160) Woias, P. *Sens. Actuators, B* **2005**, *B105*, 28-38.
- (161) Auroux, P.-A.; Iossifidis, D.; Reyes, D. R.; Manz, A. *Analytical Chemistry* **2002**, *74*, 2637-2652.
- (162) Dittrich, P. S.; Tachikawa, K.; Manz, A. *Anal. Chem.* **2006**, *78*, 3887-3907.
- (163) Vilkner, T.; Janasek, D.; Manz, A. *Anal. Chem.* **2004**, *76*, 3373-3386.
- (164) Manz, A.; Becker, H.; Editors *Microsystem Technology in Chemistry and Life Science. [In: Top. Curr. Chem., 1998; 194]*, 1998.

- (165) Yang, Z.; Matsumoto, S.; Goto, H.; Matsumoto, M.; Maeda, R. *Sens. Actuators, A* **2001**, *A93*, 266-272.
- (166) Liu, R. H.; Yang, J.; Pindera, M. Z.; Athavale, M.; Grodzinski, P. *Lab Chip* **2002**, *2*, 151-157.
- (167) Liu, R. H.; Lenigk, R.; Druyor-Sanchez, R. L.; Yang, J.; Grodzinski, P. *Anal. Chem.* **2003**, *75*, 1911-1917.
- (168) Oddy, M. H.; Santiago, J. G.; Mikkelsen, J. C. *Anal. Chem.* **2001**, *73*, 5822-5832.
- (169) Glasgow, I.; Aubry, N. *Lab Chip* **2003**, *3*, 114-120.
- (170) Qian, S.; Bau, H. H. *Anal. Chem.* **2002**, *74*, 3616-3625.
- (171) Paik, P.; Pamula, V. K.; Fair, R. B. *Lab Chip* **2003**, *3*, 253-259.
- (172) Woias, P.; Hauser, K.; Yacoub-George, E. *Micro Total Anal. Syst. 2000, Proc. micro TAS Symp., 4th* **2000**, 277-282.
- (173) West, J.; Karamata, B.; Lillis, B.; Gleeson, J. P.; Alderman, J.; Collins, J. K.; Lane, W.; Mathewson, A.; Berney, H. *Lab Chip* **2002**, *2*, 224-230.
- (174) Voldman, J.; Gray, M. L.; Schmidt, M. A. *J. Microelectromech. Syst.* **2000**, *9*, 295-302.
- (175) Uchiyama, K.; Nakajima, H.; Hobo, T. *Anal. Bioanal. Chem.* **2004**, *379*, 375-382.
- (176) Landers, J. P.; Editor *Handbook of Capillary Electrophoresis, Second Edition*, 1997.
- (177) Timperman, A. T.; Khatib, K.; Sweedler, J. V. *Anal Chem* **1995**, *67*, 139-144.
- (178) Gassmann, E.; Kuo, J. E.; Zare, R. N. *Science (Washington, D. C., 1883-)* **1985**, *230*, 813-814.
- (179) Chen, D. Y.; Dovichi, N. J. *J. Chromatogr., B: Biomed. Appl.* **1994**, *657*, 265-269.
- (180) Kwon, S.; Lee Luke, P. *Opt Lett* **2004**, *29*, 706-708.
- (181) Gu, G.; Shen, Z.; Burrows, P. E.; Forrest, S. R. *Adv. Mater. (Weinheim, Ger.)* **1997**, *9*, 725-728.
- (182) Swinney, K.; Bornhop, D. J. *Electrophoresis* **2000**, *21*, 1239-1250.
- (183) Markov, D.; Begari, D.; Bornhop, D. J. *Anal. Chem.* **2002**, *74*, 5438-5441.

- (184) Tantra, R.; Manz, A. *Anal. Chem.* **2000**, *72*, 2875-2878.
- (185) Woolley, A. T.; Lao, K.; Glazer, A. N.; Mathies, R. A. *Anal. Chem.* **1998**, *70*, 684-688.
- (186) Martin, R. S.; Gawron, A. J.; Lunte, S. M.; Henry, C. S. *Anal. Chem.* **2000**, *72*, 3196-3202.
- (187) Ewing, A. G.; Mesaros, J. M.; Gavin, P. F. *Anal Chem* **1994**, *66*, 527A-537A.
- (188) Dolnik, V.; Liu, S.; Jovanovich, S. *Electrophoresis* **2000**, *21*, 41-54.
- (189) Figeys, D.; Gygi, S. P.; McKinnon, G.; Aebersold, R. *Anal Chem* **1998**, *70*, 3728-3734.
- (190) Chan, J. H.; Timperman, A. T.; Qin, D.; Aebersold, R. *Anal Chem* **1999**, *71*, 4437-4444.
- (191) Ramsey, R. S.; Ramsey, J. M. *Anal. Chem.* **1997**, *69*, 1174-1178.
- (192) Rohner, T. C.; Rossier, J. S.; Girault, H. H. *Anal. Chem.* **2001**, *73*, 5353-5357.
- (193) Tang, K.; Lin, Y.; Matson, D. W.; Kim, T.; Smith, R. D. *Anal Chem* **2001**, *73*, 1658-1663.
- (194) Kameoka, J.; Craighead, H. G.; Zhang, H.; Henion, J. *Anal Chem* **2001**, *73*, 1935-1941.
- (195) Xue, Q.; Dunayevskiy, Y. M.; Foret, F.; Karger, B. L. *Rapid Commun Mass Spectrom* **1997**, *11*, 1253-1256.
- (196) Lazar, I. M.; Ramsey, R. S.; Sundberg, S.; Ramsey, J. M. *Anal. Chem.* **1999**, *71*, 3627-3631.
- (197) Desai, A.; Tai, Y.-C.; Davis, M. T.; Lee, T. D. *Transducers 97, Int. Conf. Solid-State Sens. Actuators* **1997**, *2*, 927-930.
- (198) Lin, L.; Shia, T. K.; Chiu, C. J. *J. Micromech. Microeng.* **2000**, *10*, 395-400.
- (199) Licklider, L.; Wang, X. Q.; Desai, A.; Tai, Y. C.; Lee, T. D. *Anal Chem* **2000**, *72*, 367-375.
- (200) Tang, K.; Lin, Y.; Matson, D. W.; Kim, T.; Smith, R. D. *Anal. Chem.* **2001**, *73*, 1658-1663.

- (201) Schultz, G. A.; Corso, T. N.; Prosser, S. J.; Zhang, S. *Anal. Chem.* **2000**, *72*, 4058-4063.
- (202) Arscott, S.; Le Gac, S.; Druon, C.; Tabourier, P.; Rolando, C. *J. Micromech. Microeng.* **2004**, *14*, 310-316.

CHAPTER 2

2.1 MULTIPLE SCLEROSIS: AN AUTOIMMUNE DISEASE?

Multiple sclerosis (MS) is thought to be an inflammatory and demyelinating disease of the central nervous system (CNS) that is the most common neurodegenerative condition in young adults, especially women, striking people between the ages of 20 and 40 years. Globally, 2 to 3 million individuals have this disease, 400,000 in the US alone.¹ It is five times more prevalent in temperate climates, especially northern Europe or northern United States, with approximately 1 in 1,000 individuals of northern European origin developing MS.²

MS is characterized by a chronic inflammatory process resulting in damage to myelin (the multilayered membrane surrounding the axons) and myelin-producing cells (oligodendrocytes) and eventual neuronal loss. It has been hypothesized that myelin is damaged due to an immune attack of autoantibodies and autoreactive T cells activated against myelin antigens such as myelin basic protein (MBP), proteolipid protein (PLP), and myelin oligodendrocyte glycoprotein (MOG).³ Myelin is very important for nervous system function and when this tissue is disrupted, the nerve conduction slows and leads to neuromotor dysfunction. Moreover, in MS plaque tissue oligodendrocytes are hypertrophied, with swollen nuclei and disrupted plasma and mitochondrial membranes.⁴

Studies on experimental allergic encephalomyelitis (EAE) models, which is a widely used animal model for MS, indicated that inflammatory molecules (cytokines, chemokines, and adhesion molecules) induce the recruitment of leucocytes from the

periphery to the CNS. Thus, the inflammation reaches the CNS through a disrupted blood brain barrier (BBB). The pathological hallmark of the disease is the formation of plaques, areas of white-matter demyelination, or eventual axonal degeneration and loss, leading to long-term disability.⁵

However, there are contradictory reports in the literature about the autoimmune hypothesis of this disease, largely because no autoantigen(s) specific to or causative for MS has ever been identified. Some reports indicate that demyelination may precede inflammation,⁶ while others say that MS is not an autoimmune disease but either a genetically determined disorder characterized by metabolically dependent neurodegeneration⁷ or resulting from a chronic viral infection.⁸⁻¹⁰ Moreover, there are indications that MS is a disease triggered by an environmental factor in genetically susceptible individuals. Dyment *et al.* showed that there is a 70% discordance of MS among monozygotic twins, suggesting that an exogenous factor caused the disease.¹¹

Although there is controversy about what causes the disease, and an established mechanism of its occurrence may not yet exist, it is unanimously accepted that axonal degeneration is the major determinant of irreversible neurological disability in patients with MS. Also, it was agreed that MS is somewhat heterogeneous and it has been classified into several disease types such as relapsing, primary progressive, secondary progressive and progressive relapsing. At onset, approximately 85% of the MS patients show a relapsing remitting course, characterized by attacks of neurological deficits, followed by complete or incomplete recovery. It has also been shown that 40-65% of patients with relapsing disease will experience slow progression (secondary progressive course).¹²

2.2 NITRIC OXIDE AS AN ACTIVITY MARKER IN MS

Although causative factors for MS have not been identified, there exists a large body of evidence for the role of the autoimmunity in the pathogenesis of the disease.^{13,14} Among other molecules produced during the inflammation cascade, nitric oxide (NO) is one of the major molecules associated with the damage of the myelin and oligodendroglia.¹⁵⁻¹⁸

NO is involved in important physiological functions of the CNS, including neurotransmission, learning and memory, and synaptic plasticity. It also has a role in gastrointestinal motility and neuroendocrine regulation.¹⁹⁻²³ It is clear that NO can modulate the induction of the immune response, permeability of the BBB, trafficking of the cells to the CNS, and local response in the inflammatory milieu.⁴ Therefore, NO can have both beneficial and deleterious effects. Because of its short life-time *in vivo*, NO can be rapidly converted to more reactive intermediates such as nitrite and nitrate.¹⁸ Recently, elevated levels of nitrate and nitrite have been measured in cerebral spinal fluid (CSF), blood, urine, and serum of MS patients in relapse.²⁴ The neurotoxicity of excessive concentrations of NO in MS has been previously reported,^{16-18,25} however the origin of this excess and its mechanism of action is yet unknown.

NO is a simple gaseous molecule with a complex chemistry *in vitro* and poorly understood biochemistry *in vivo*. At the site of inflammation, NO can exist not only in the form of a free radical, but also can be converted into a variety of other related compounds formed by the different conditions present in the tissue environment (e.g., redox conditions, pH, oxygen tension).²⁶ These compounds include the nitroxyl (NO⁻) ion,

nitrous acid (HNO_2), the nitrogen dioxide (NO_2) radical, peroxynitrite (ONOO^- ; a product of the combination of superoxide and NO) and peroxynitrous acid (ONOOH). All of these compounds have their own chemistries and biochemistries *in vivo* and they have also been found at the sites of inflammatory lesions in MS.

The high abundance of NO and its metabolites at sites of inflammation may be due to the increased expression of the inducible form of nitric oxide synthase (iNOS). This form of the enzyme produces NO continuously at high rates and does not depend on free calcium. In normal conditions, iNOS is absent in the CNS, although iNOS mRNA and protein become expressed at the inflammatory lesions of animals with EAE.²⁷⁻²⁹ Other findings also showed that iNOS mRNA was expressed in abundance in biopsy samples³⁰ or brains¹⁵ of patients with MS.

In this construct, inhibition of NO production, especially of iNOS, as a method of effective therapy for MS has been extensively investigated for the past 15 years.³¹⁻³⁸ However, results have turned out to be inconclusive given the complexity of NO involvement in the immune regulation.

It has been hypothesized that NO has two major effects on cerebral vessels, both of which may be involved in the pathogenesis of the MS lesions, namely vasodilation and disturbance of the BBB integrity.²⁶ It is also believed that vasodilation by itself can lead to an infiltration of inflammatory cells through the BBB into the CNS. The reasoning behind this hypothesis is that with the increase in vasodilation, a decrease in the blood flow will help leucocytes to bind to the vessel wall and migrate through it. In accordance with this belief, Giovannoni *et al.* reported that nitrite and nitrate concentrations in the CSF of patients with MS were correlated with the breakdown of the BBB, as measured

by the leakage of albumin.²⁴ This NO present in MS lesions could arise from various sources such as nerve terminals,^{39,40} induction of iNOS,⁴¹ or the release of neurotransmitters.^{42,43}

In this work, we hypothesize that another source of NO could contribute to the elevated levels of this radical (and its metabolites) in CSF or other fluids of patients with MS. Specifically, the stimulation of endothelial NOS (eNOS) by RBC-derived ATP may be the source of NO. eNOS produces low (nanomolar) concentrations of NO in a calcium-dependent manner and this NO is known to contribute to the regulation of blood flow by inducing smooth muscle relaxation. However, there exists a fine balance between the effects of the over production of NO and the underproduction of NO *in vivo*. Increased concentrations of RBC-derived ATP may lead to increased levels of NO and ultimately to relaxation of the vessels. This relaxation will slow the blood flow and will allow the adherence of leucocytes to the vessel wall and eventual penetration of the BBB and leakage into the CNS, as previously proposed by Smith *et al.*²⁶

All previous studies, however, hypothesized that NO sources are within the CNS. The NO production in the brain microvascular capillaries is a subject of controversy and no solid evidence about the constitutive production of NO was yet reported. Herein, we show that brain microvascular endothelial cells constitutively produce NO and, moreover, ATP represents an *in vitro* stimulus for eNOS in this cell line.

2.3 RBC DEFORMABILITY IN MS

It has been previously shown that abnormal RBC deformability is associated with diseases such as diabetes and multiple sclerosis.^{44,45} While RBC deformability is decreased in RBCs of patients with type I and type II diabetes, the whole blood of patients with MS was found to be more viscoelastic when compared with the whole blood of healthy patients.⁴⁶⁻⁴⁸

Interestingly, it is known that the RBCs of MS patients have abnormally high levels of glutathione (GSH), the most abundant non-enzymatic antioxidant present in a cell. The levels of GSH have been linked with the deformability characteristics of the RBCs. That is, low levels of GSH are found in diabetic red cells, which are known to be less deformable than the RBCs from healthy patients.^{49,50} Moreover, recent studies in our group involving diabetic RBCs have shown that a weakened oxidant defense system in RBCs will lead to lower levels of ATP release.⁵¹

If, in the case of MS patients, the RBCs are more deformable and the increase deformability results in an increase of ATP release, then an increase in the NO production would be expected. Indeed, it is recognized that there exist higher than normal levels of NO metabolites, nitrate and nitrite, in the cerebral spinal fluid (CSF) and serum of patients with MS.^{24,44}

Taken collectively, we have constructed a theory that explains the overabundance of NO metabolites in the CSF is actually blood-borne. In other words, it is possible that the NO levels are increased due to overstimulation by RBC-derived ATP.

Our hypothesis is that MS-RBCs are more deformable, therefore releasing more ATP, which in turn will lead to increased production of NO. However, a molecular level understanding of the mechanisms by which RBC deformability properties relate to the occurrence of MS is lacking. To prove or disprove this hypothesis, the role of RBC-derived ATP and NO derived from brain endothelium must be investigated.

2.4 POSSIBLE ROLES OF THE RBC/RBC-DERIVED ATP IN MS

RBCs, when traversing microvascular beds, are subjected to mechanical deformation. Previously, it has been reported in the isolated perfused rabbit lung that in order to demonstrate flow-induced endogenous NO synthesis in the pulmonary circulation, RBCs obtained from either rabbits or healthy humans were a required component of the perfusate.⁵² Importantly, it was reported that the property of these RBCs responsible for the stimulation of NO synthesis was their ability to release ATP in response to mechanical deformation.⁵³ These reports suggest a novel mechanism for the control of endothelium-derived NO production.

It is proposed that as the RBC is increasingly deformed by increments in the velocity of blood flow through a vessel and/or by reductions in vascular diameter, it releases ATP that stimulates endothelial synthesis of NO. Indeed, it has been reported that RBC-derived ATP contributes to the control of vascular resistance in both the pulmonary⁵²⁻⁵⁴ and systemic circulation.⁵⁵⁻⁵⁹ The finding that ATP is released from RBCs in response to mechanical deformation, and that the levels of ATP released from RBCs

increase as the RBC deformability increases, suggest that the RBC may be an important determinant of NO production as these cells traverse the intact circulation.

If RBC-derived ATP is a determinant of NO production *in vivo*, and NO plays a major role in MS, it is important to investigate the relationship between MS RBCs, ATP, NO and brain microvascular endothelial cells (BMVEC). The first step towards this goal is to establish that RBCs of MS patients release higher levels of ATP compared to healthy, non-MS controls and that bBMVECs produce NO upon ATP stimulation.

2.5 EXPERIMENTAL

It has been well established that RBCs release ATP in response to mechanical deformation.^{53,54} Deformability measurements of the red cells have been previously performed by different methods based on viscosity,⁶⁰ centrifugal sedimentation,⁶¹ micropipette aspiration,⁶² rheoscopy,⁶³ filtration or nucleopore filtration, or nuclear track microfilters and laser diffraction or ektacytometer.⁶⁴⁻⁶⁶ However, most of these techniques required manual manipulation and thus, they were inaccurate and clinically inapplicable. A more practical method to consider is the filtration-based method, where the RBCs are passed through the pores of a filter under pressure. The pores have uniform size and dimensions similar to those of capillaries (5 μm diameter), in an effort to mimic the *in vivo* conditions. The deformability of the RBCs was determined by the rate of filtered cells.⁶⁷⁻⁶⁹

Previously, our group developed an alternative method for studying ATP release from RBCs as they traverse fused silica microbore tubing with internal diameters

comparable to those of resistance vessels in the intact circulation.^{57,70} Here, this technology will be used to quantitatively determine the ATP release from mechanically deformed RBCs of patients with MS. Our hypothesis is that RBCs obtained from patients with MS are more deformable, therefore releasing more ATP, which in turn will lead to increased levels of NO production.

For a more realistic depiction of the mechanism of endothelium-derived NO production *in vivo*, the RBCs obtained from MS patients were mechanically deformed by hydrodynamically pumping them through microbore capillary tubing. A continuous flow system is employed to create stress on the RBCs once they have entered the microbore tubing.⁷¹

2.5.1 Design and Methods

Generation of washed RBC. MS and control blood samples were kindly provided by Dr. James Garbern, M.D., associate professor in the Department of Neurology at Wayne State University. Blood was centrifuged at 500g at 4°C for 10 min. The plasma and buffy coat (other elements in the blood) were discarded. RBCs were resuspended and washed three times in a physiological salt solution [PSS; in mM, 4.7 KCl, 2.0 CaCl₂, 140.5 NaCl 12 MgSO₄, 21.0 tris(hydroxymethyl)aminomethane, 11.1 dextrose with 5% bovine serum albumin (final pH 7.4)]. For all studies reported here, a hematocrit of 7% was prepared. The value of 7% was found to be optimal for our studies, although higher values 10-20% represent an average over the microcirculation. It is known that when moving from the macrocirculation (arteries) to microcirculation (arteriols and capillaries), the viscosity of

the blood decreases therefore the hematocrit changes with the vessel diameter. Cells were prepared on the day of use.

Standard ATP assay. A mixture of luciferin/luciferase was used to measure the ATP by chemiluminescence⁷¹ conform to the reaction shown in Figure 8. Chemiluminescence intensity is proportional to the ATP concentration. The sensitivity of the assay is enhanced by the addition of 2 mg of D-luciferin (Sigma, St. Louis, MO) to the crude firefly extract (Sigma, St. Louis, MO). Intensities of ATP standards were taken on the day of each experiment by adding authentic ATP to a luciferin/luciferase reaction mixture. The luciferin/luciferase solutions were prepared by diluting the luciferin in 5 mL of distilled, deionized 18 M Ω water (DDW) and adding it to a vial containing 100 mg luciferase. The luciferin/luciferase mixture was prepared on the day of use.

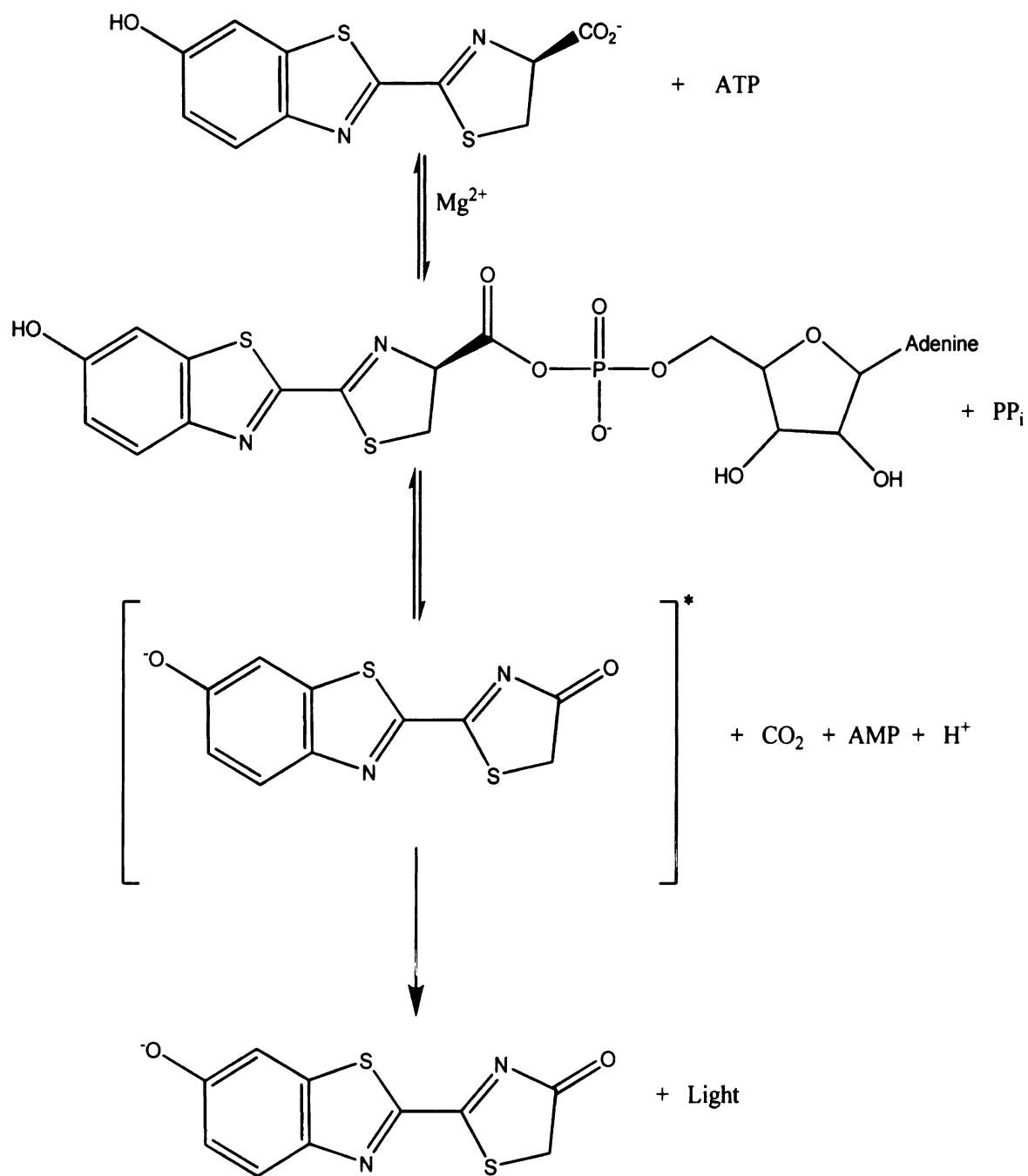


Figure 8. The two-step bioluminescence reaction between luciferin/luciferase and ATP.

Determination of ATP release from RBCs. The amount of ATP release from RBCs was determined, near-real time, by using 50 μm inside diameter fused-silica tubing that was intended to resemble the vessels *in vivo*. The instrumentation employed consisted of a syringe pump (Harvard Apparatus, Boston MA) equipped with two 500 μL syringes (Hamilton, Fisher Scientific), two pieces of ~ 40 cm long microbore tubing with an internal diameter of 50 μm and an outer diameter of 362 μm (Polymicro technologies, Phoenix, AZ). The RBCs or ATP standards loaded in one of the syringes are pumped through the tubing at a rate of 6.7 $\mu\text{L min}^{-1}$. As the RBCs traverse the tubing, ATP is released and it is combined with a luciferin/luciferase mixture that is loaded in the second syringe, at a tee (Upchurch Scientific, Oak Harbor, WA) in the system, and the resultant chemiluminescence is measured by a photomultiplier tube (PMT) built in house (Figure 9). The light intensity of the chemiluminescence is proportional to the amount of ATP present.⁷¹ A working curve was constructed using five ATP standards between 0 and 1.5 μM resulting in a slope of 0.092 and a y-intercept of 0.0039 ($r^2 = 0.9789$). The ATP standards were prepared from a stock 100 μM ATP in a buffered physiological salt solution (PSS). All solutions were prepared in the day of the experiment.

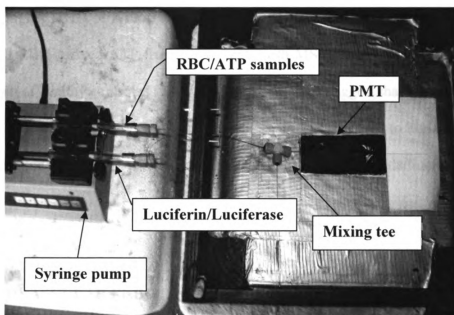


Figure 9. Instrumental setup employed to measure the RBC derived ATP release.

2.5.2 Results and Discussion

Quantitative evaluation of the MS RBC ATP release. Deformation-induced ATP release from RBCs obtained from control and MS patients was examined in order to determine if the MS RBCs release more ATP than control RBCs as a result of always being in a more “deformable” state. The data in Figure 10 provides evidence that MS-RBCs release higher levels of ATP compared to non-MS RBCs. The results demonstrate that the overall RBC-derived ATP from the patients with MS (375 +/- 51 nM) is 100% greater than that of healthy controls (138 +/- 21). These findings suggest that RBCs of MS patients may indeed be in a continuous “deformable” state that will lead to higher levels of ATP release and ultimately, to an increase in ATP-stimulated endothelium-derived NO.

2.6 CONSTITUTIVE PRODUCTION OF NITRIC OXIDE IN BRAIN MICROVASCULAR ENDOTHELIAL CELLS

It is well established that vascular endothelium constitutively generates NO in response to ATP stimulation and that endothelium-derived NO induces a relaxation of vascular smooth muscle cells. However, little is known about the production of NO in microvessels, where smooth muscle layers are thin or absent. Additionally, the mechanism by which mechanical stress induces NO synthesis in the microvessel endothelium is still controversial. There are contradicting reports in the literature regarding the constitutive production of NO in cerebral microvascular endothelium.

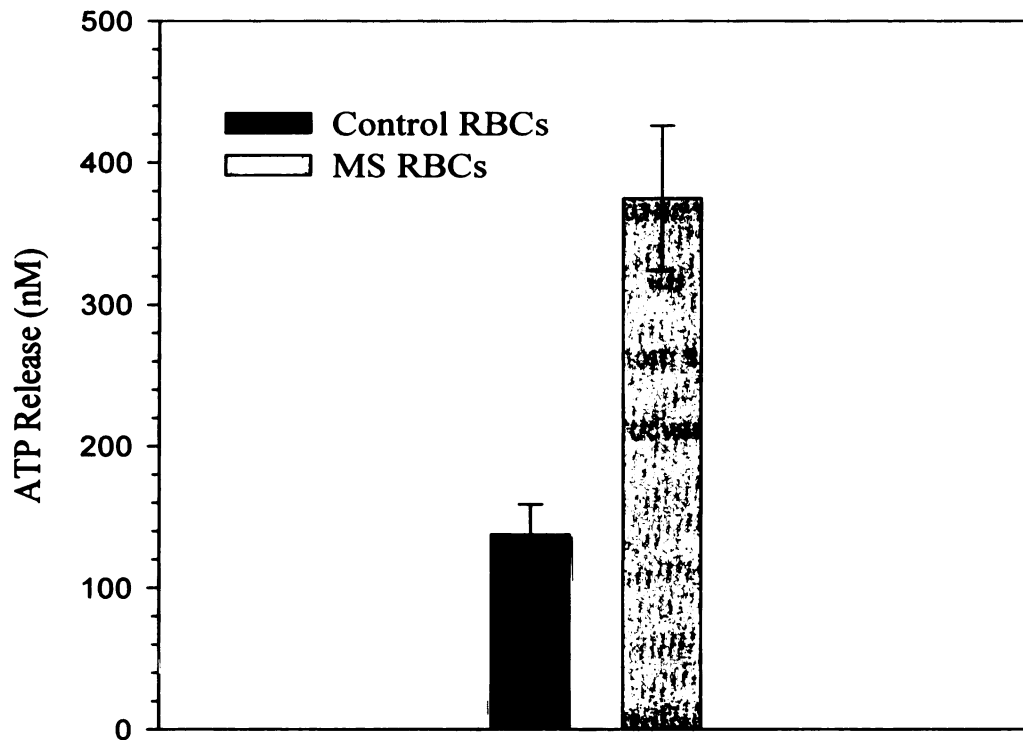


Figure 10. ATP released from RBCs subjected to shear-induced stress. The average ATP release from the RBCs obtained from healthy controls was 138 +/- 21 nM while the release from the RBCs obtained from people with MS was 375 +/- 51 nM. The error bars are reported as the SEM for 11 controls and 18 MS samples.

Kimura *et al.* reported that ATP and a calcium ionophore (A23187) induced Ca^{2+} transients in two types of endothelium, bovine brain microvascular endothelial cells (bBMVECs) and bovine aortic pulmonary endothelial cells (bPAEC), but they failed to induce NO production in bBMVEC, as measured with an NO-sensitive fluorescent dye, DAF-2.⁷² However, an observed increase in fluorescence was reportedly due to an increase in NO production in bPAECs. In contrast, Janigro *et al.* showed that ATP induces NO release in CNS endothelial cells due to an influx of Ca^{2+} into the cell through receptor-operated ion channels.⁷³ In this study, we demonstrated that NO is indeed constitutively generated in brain microvessels, more specifically in bBMVECs and that RBC-derived ATP is an *in vivo* stimulus of NO production in bovine brain endothelium.

2.7 EXPERIMENTAL

It has been previously shown that endothelium-derived NO production can be stimulated by ATP-binding to the P_{2y} purinergic receptors found on endothelial cells. Recently, our group has demonstrated the ability of measuring ATP stimulated endothelium-derived NO via dynamic fluorescence microscopy as an improvement over previous reports using amperometry as the detection scheme.⁷⁴ Different methods were reported for NO detection such as, chemiluminescence assays, bioassays, Griess reaction, oxy-hemoglobin assays, electron spin resonance, and electrochemical assays, each with its advantages and disadvantages.⁷⁵ Here we demonstrate that ATP induced, endothelium-derived NO production can be detected in real time using a commercially available cell-

permeable fluorescence probe, 4-amino-5-methylamino-2,7'-difluoroflorescein diacetate (DAF-FM DA).

2.7.1 Design and Methods

Preparation of cells. bBMVECs primary cultures (Cambrex, East Rutherford, NJ) were seeded on collagen-coated 25 mL tissue culture flasks at a density of 20,000 cells/cm². The cells were kept in humidified atmosphere, 37°C and 5% CO₂ and the media for confluent growth refreshed every 2-3 days. Generally, the cells reach confluence on day 7 or 8 and form a tight monolayer on ~ day 10 or 11. When the cells from primary culture reached confluence they were sub-cultured at a split ratio 1:2, and the harvested sub-cultured cells (divisions 3, 5, and 8) were used for the experiments. However, low passage is desirable for the cells to express cellular tight junctions and transport characteristics found in BBB.⁷⁶ In order to conduct the experiment, the cells were seeded in 2 inches Petri dishes and grown to confluence. All solutions were prepared in Hank's balanced salt solution (HBSS) and equilibrated for 20 min at 37°C and 5% CO₂.

Florescence determination of NO production. For the measurement of NO with DAF-FM, the confluent cells were incubated with 10 μM of the diacetylated form of DAF-FM (Molecular Probes, Eugene, OR) for 20 min. Subsequently, the cells were washed twice with equilibrated HBSS and stimulated with 10 μM or 100 μM ATP. DAF-FM fluoresces ($\lambda_{\text{ex}} = 494 \text{ nm}$; $\lambda_{\text{em}} = 515 \text{ nm}$) upon binding with NO, as measured by fluorescence microscopy. The fluorescence intensity (pixel intensity) was reported as an average of 4

pictures per dish taken every 5 min during a 30 min period. The images were captured by an Olympus IX71M inverted microscope (Olympus America, Melville, NY) equipped with an electrothermally-cooled CCD (Orca, Hamamatsu) and MicroSuite software (Olympus America). To confirm the ATP-stimulated NO production, cells were incubated with a competitive inhibitor of NO synthesis, L-nitro arginine methyl ester (L-NAME 100 μ M), for 15 min before loading them with the DAF-FM DA. Moreover, to ensure that the enzyme eNOS has excess substrate for NO production, the cells were incubated with L-arginine (100 μ M).

Control experiment. Basal levels of NO in bBMVECs were determined using DAF-FM DA as described above. Any increase in fluorescence intensity relative to the basal level was due to the stimulation of the NO production. The DAF-FM fluorescence was subtracted from the final value, thus the data represents the net gain in fluorescence due to NO production.

2.7.2 Results and Discussion

ATP constitutes an in vivo stimulus of NO production in bBMVECs. Figure 11 depicts the effect of ATP (100 μ M) and L-NAME (100 μ M) on bBMVEC NO production, assessed with DAF-FM DA. The results demonstrate the ability of bBMVECs to produce NO when ATP, a known stimulus of eNOS *in vivo*, is added to the cells. The bBMVEC were loaded with DAF-FM DA and the fluorescence intensity was assessed after 30 min. The black bar represents the fluorescence intensity of the adduct DAF-FM /NO.

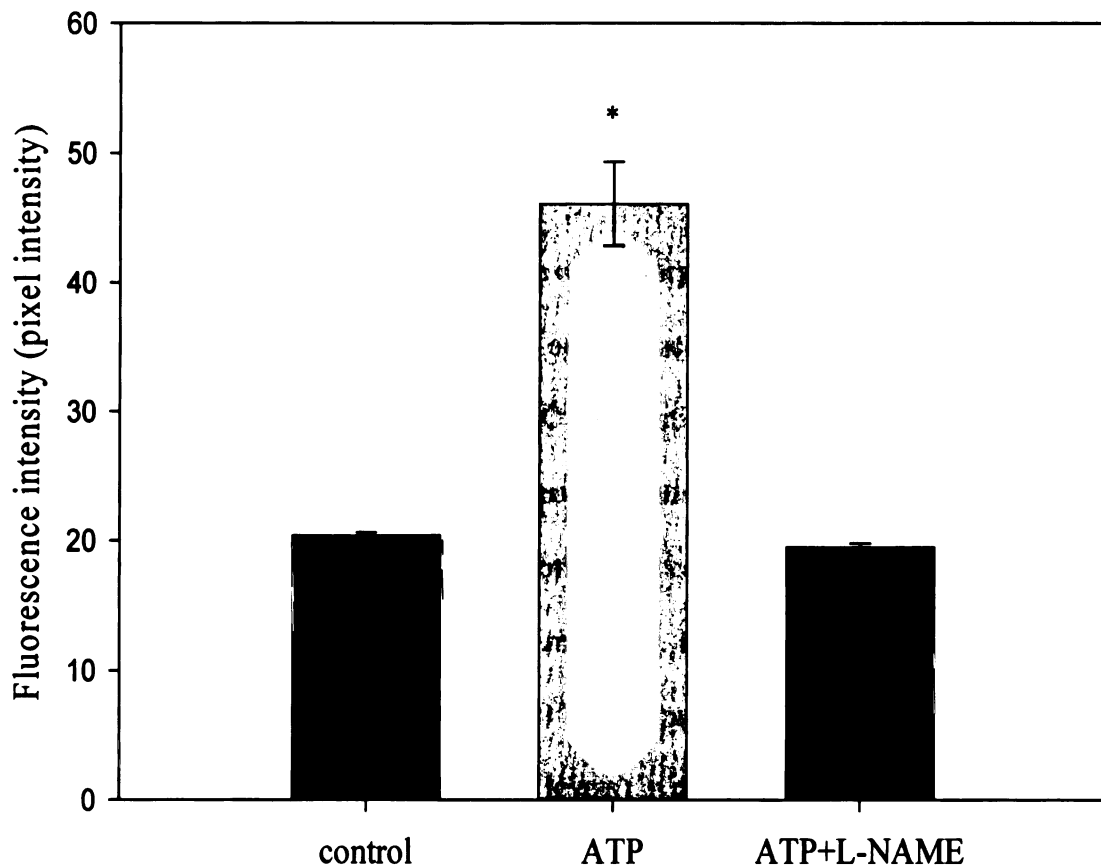


Figure 11. Effects of ATP (100 μ M) and L-NAME (100 μ M) on NO production in bBMVECs assessed with DAF-FM DA. L-MAME was used to demonstrate that the increase in DAF-FM DA fluorescence upon stimulation with ATP (100 μ M) was the result of NO production (* $p \leq 0.001$ vs. control).

The light gray bar represents the fluorescence intensity after the addition of 100 μ M ATP to the cells loaded with the probe. Darker gray bar shows that L-NAME (100 μ M) inhibited ATP-induced DAF-FM fluorescence, proving the endothelium NO production.

ATP-derived NO production with cells passage. It has been shown that primary or low passage brain capillary endothelial cultures retain many morphological and biochemical properties similar to the BBB *in vivo*.^{77,78} However, due to the high cost of the commercially available bBMVECs the use of primary cultures exclusively for our models is not financially practical. Therefore, in our protocols the cells were passaged and the ability of the endothelium to produce NO upon stimulation was investigated. Data in Figure 12 shows that with increasing the passage number, the ability of the bBMVEC to produce NO upon stimulation is significantly reduced. Black bars (control) represent the basal levels of NO production without stimulation. However upon stimulation with 100 μ M ATP, a significant increase (> 100%) in NO production is observed for division 3 compared with no increase (equal to basal levels) in divisions 5 or 8.

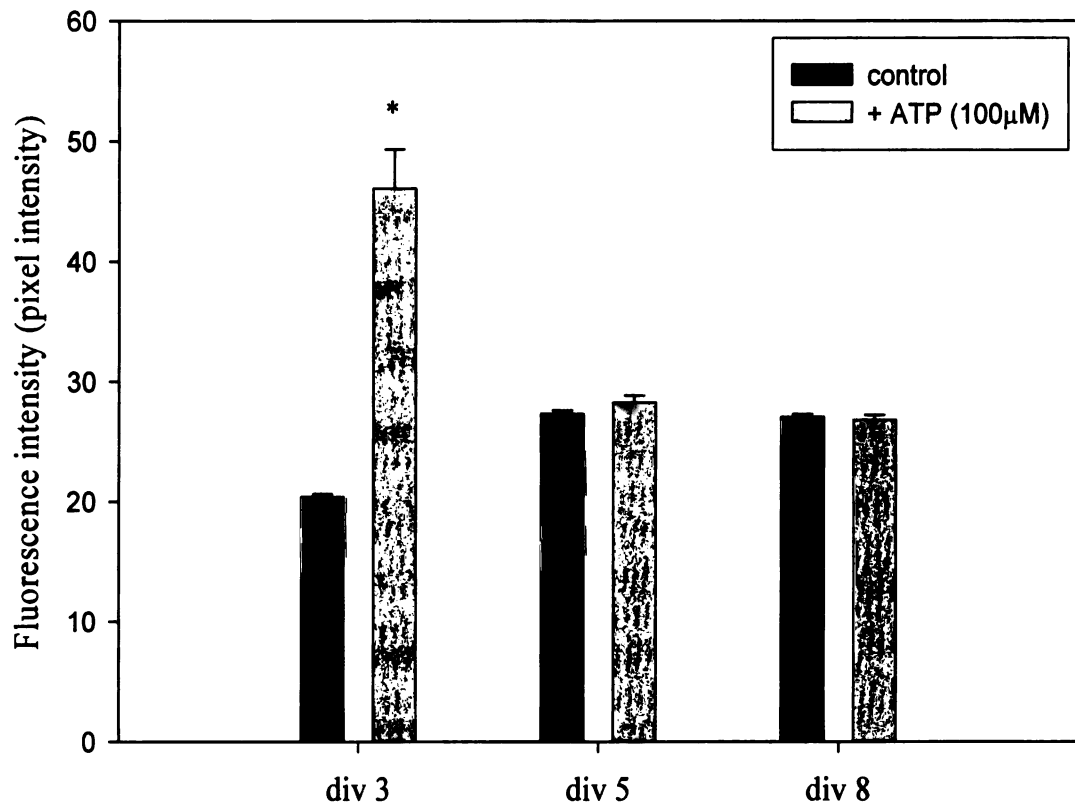


Figure 12. ATP-derived NO production is decreasing with increasing the passage of the cells. For cell division 3 there is a significant difference between the control (black bars) and the bBMVECs stimulated with 100 µM ATP (grey bars) (* $p \leq 0.001$ vs. control).

2.8 CONCLUSIONS

In this study we hypothesized that RBCs obtained from patients with MS are more deformable, therefore releasing more ATP, which in turn will lead to increased levels of NO production. For a more realistic depiction of the mechanism of endothelium-derived NO production *in vivo*, the RBCs obtained from MS patients were mechanically deformed by hydrodynamically pumping them through microbore capillary tubing. A continuous flow system is employed to create stress on the RBCs once they have entered the microbore tubing.⁷¹ It was found that MS-RBCs release higher levels of ATP compared to non-MS RBCs. These findings suggest that RBCs of MS patients may indeed be in a continuous “deformable” state that will lead to higher levels of ATP release and ultimately, to an increase in ATP-stimulated endothelium-derived NO. Additionally, it was shown that ATP acts as an agonist for NO production in bBMVECs and the increase in NO production is a function of cell division.

Based on these findings, we have constructed a theory that explains the overabundance of NO metabolites in the CSF of MS patients is actually blood-borne. In other words, it is possible that the NO levels are increased due to overstimulation by RBC-derived ATP.

LIST OF REFERENCES

- (1) Pryce, G.; Baker, D. *Trends in Neurosciences* **2005**, *28*, 272-276.
- (2) Noseworthy, J. H. *Nature* **1999**, *399*, A40-47.
- (3) Garren, H.; Steinman, L.; Lock, C. *Ann Neurol* **1998**, *43*, 4-6.
- (4) Parkinson, J. F.; Mitrobcvic, B.; Merrill, J. E. *J. Mol. Med. (Berlin)* **1997**, *75*, 174-186.
- (5) Grigoriadis, N.; Tselios, T.; Deraos, S.; Orologas, A.; Deraos, G.; Matsoukas, J.; Mavromatis, I.; Milonas, I. *Curr. Med. Chem.* **2005**, *12*, 1513-1519.
- (6) Barnett Michael, H.; Prineas John, W.; Institute of Clinical Neurosciences, Department of Medicine, University of Sydney, Australia: United States, 2004, pp 458-468.
- (7) Chaudhuri, A.; Behan Peter, O. *Arch Neurol* **2004**, *61*, 1610-1612.
- (8) Gilden, D. H. *Lancet Neurol.* **2005**, *4*, 195-202.
- (9) Gilden Donald, H. *Lancet Neurol* **2002**, *1*, 145.
- (10) Roach, E. S. *Arch Neurol* **2004**, *61*, 1615-1616.
- (11) Dymment, D. A.; Ebers, G. C.; Sadovnick, A. D. *Lancet Neurol.* **2004**, *3*, 104-110.
- (12) Coyle, P. K. *Adv Neuroimmunol* **1996**, *6*, 143-154.
- (13) Raine, C. S. *Ann Neurol* **1994**, *36 Suppl*, S61-72.
- (14) Thompson, A. J.; Polman, C. H.; Miller, D. H.; McDonald, W. I.; Brochet, B.; Filippi, M. M. X.; De Sa, J. *Brain* **1997**, *120 (Pt 6)*, 1085-1096.
- (15) Bagasra, O.; Michaels, F. H.; Zheng, Y. M.; Bobroski, L. E.; Spitsin, S. V.; Fu, Z. F.; Tawadros, R.; Koprowski, H. *Proc. Natl. Acad. Sci. U. S. A.* **1995**, *92*, 12041-12045.
- (16) Bo, L.; Dawson, T. M.; Wesselingh, S.; Mork, S.; Choi, S.; Kong, P. A.; Hanley, D.; Trapp, B. D. *Ann Neurol* **1994**, *36*, 778-786.

- (17) De Groot, C. J.; Ruuls, S. R.; Theeuwes, J. W.; Dijkstra, C. D.; Van der Valk, P. *J Neuropathol Exp Neurol* **1997**, *56*, 10-20.
- (18) Molina, J. A.; Jimenez-Jimenez, F. J.; Orti-Pareja, M.; Navarro, J. A. *Drugs Aging* **1998**, *12*, 251-259.
- (19) Brecht, D. S.; Snyder, S. H. *Annu Rev Biochem* **1994**, *63*, 175-195.
- (20) Dawson, T. M.; Dawson, V. L.; Snyder, S. H. *Ann. Neurol.* **1992**, *32*, 297-311.
- (21) Nathan, C.; Xie, Q.-W. *Cell (Cambridge, Mass.)* **1994**, *78*, 915-918.
- (22) Oset-Gasque, M. J.; Parramon, M.; Hortelano, S.; Bosca, L.; Gonzalez, M. P. *J Neurochem.* **1994**, *63*, 1693-1700.
- (23) Stamler, J. S.; Singel, D. J.; Loscalzo, J. *Science (Washington, D. C., 1883-)* **1992**, *258*, 1898-1902.
- (24) Giovannoni, G.; Heales, S. J. R.; Land, J. M.; Thompson, E. J. *Mult. Scler.* **1998**, *4*, 212-216.
- (25) Bagasra, O.; Michaels, F. H.; Zheng, Y. M.; Bobroski, L. E.; Spitsin, S. V.; Fu, Z. F.; Tawadros, R.; Koprowski, H. *Proc Natl Acad Sci U S A* **1995**, *92*, 12041-12045.
- (26) Smith, K. J.; Lassmann, H. *Lancet Neurology* **2002**, *1*, 232-241.
- (27) Cross, A. H.; Manning, P. T.; Stern, M. K.; Misko, T. P. *J Neuroimmunol.* **1997**, *80*, 121-130.
- (28) Koprowski, H.; Zheng, Y. M.; Heber-Katz, E.; Fraser, N.; Rorke, L.; Fu, Z. F.; Hanlon, C.; Dietzschold, B. *Proc. Natl. Acad. Sci. U. S. A.* **1993**, *90*, 5378.
- (29) Van Dam, A. M.; Bauer, J.; Man-A-Hing, W. K. H.; Marquette, C.; Tilders, F. J. H.; Berkenbosch, F. *J. Neurosci. Res.* **1995**, *40*, 251-260.
- (30) Bitsch, A.; Wegener, C.; da Costa, C.; Bunkowski, S.; Reimers, C. D.; Prange, H. W.; Bruck, W.; Department of Neurology, Georg-August-University, Gottingen, Germany; ENGLAND: United Kingdom, 1999, pp 138-146.
- (31) Zhao, W.; Tilton, R. G.; Corbett, J. A.; McDaniel, M. L.; Misko, T. P.; Williamson, J. R.; Cross, A. H.; Hickey, W. F. *J Neuroimmunol.* **1996**, *64*, 123-133.
- (32) Cowden, W. B.; Cullen, F. A.; Staykova, M. A.; Willenborg, D. O. *J Neuroimmunol.* **1998**, *88*, 1-8.

- (33) Okuda, Y.; Sakoda, S.; Fujimura, H.; Yanagihara, T. *J Neuroimmunol* **1998**, *81*, 201-210.
- (34) Sahrbacher, U. C.; Lechner, F.; Eugster, H. P.; Frei, K.; Lassmann, H.; Fontana, A. *Eur. J. Immunol.* **1998**, *28*, 1332-1338.
- (35) Thillaye-Goldenberg, B.; Goureau, O.; Naud, M. C.; de Kozak, Y. *J. Neuroimmunol.* **2000**, *110*, 31-44.
- (36) Zielasek, J.; Jung, S.; Gold, R.; Liew, F. Y.; Toyka, K. V.; Hartung, H. P. *J. Neuroimmunol.* **1995**, *58*, 81-88.
- (37) Willenborg, D. O.; Staykova, M. A.; Cowden, W. B. *J. Neuroimmunol.* **1999**, *100*, 21-35.
- (38) Singh, V. K.; Mehrotra, S.; Narayan, P.; Pandey, C. M.; Agarwal, S. S. *Immunol. Res.* **2000**, *22*, 1-19.
- (39) Rand, M. J. *Clin. Exp. Pharmacol. Physiol.* **1992**, *19*, 147-169.
- (40) Toda, N.; Tanaka, T.; Ayajiki, K.; Okamura, T. *Neuroscience (Oxford)* **2000**, *96*, 393-398.
- (41) Brian, J. E., Jr.; Faraci, F. M. *Stroke* **1998**, *29*, 509-515.
- (42) Faraci, F. M.; Breese, K. R. *Circ. Res.* **1993**, *72*, 476-480.
- (43) Kobari, M.; Fukuuchi, Y.; Tomita, M.; Tanahashi, N.; Yamawaki, T.; Takeda, H.; Matsuoka, S. *Brain Res. Bull.* **1993**, *31*, 443-448.
- (44) Giovannoni, G. *Multiple Sclerosis* **1998**, *4*, 27-30.
- (45) Mazzanti, L.; Faloia, E.; Rabini, R. A.; Staffolani, R.; Kantar, A.; Fiorini, R.; Swoboda, B.; De Pirro, R.; Bertoli, E. *Clin Biochem* **1992**, *25*, 41-46.
- (46) Blair, G. W.; Matchett, R. H. *J Neurol Neurosurg Psychiatry* **1972**, *35*, 730-731.
- (47) Karlov, V. A.; Savin, A. A.; Smertina, L. P.; Redchits, E. G.; Seleznev, A. N.; Svetailo, L. I.; Margosiuk, N. V.; Stulin, I. D.: USSR, 1990, pp 47-50.
- (48) Simpson, L. O.; Shand, B. I.; Olds, R. J.; Larking, P. W.; Arnott, M. J. *Pathology* **1987**, *19*, 51-55.
- (49) Ghigo, D.; Bosia, A.; Pagani, A.; Pescarmona, G. P.; Pagano, G.; Lenti, G. *Ric Clin Lab* **1983**, *13 Suppl 3*, 375-381.

- (50) Matkovics, B.; Kotorman, M.; Varga, I. S.; Hai, D. Q.; Roman, F.; Novak, Z. *Acta Physiol Hung* **1997**, *85*, 99-106.
- (51) Carroll, J.; Raththagala, M.; Subasinghe, W.; Baguzis, S.; Oblak, T. D. a.; Root, P.; Spence, D. *Mol. BioSyst.* **2006**, *2*, 305-311.
- (52) Sprague, R. S.; Stephenson, A. H.; Dimmitt, R. A.; Weintraub, N. A.; Branch, C. A.; McMurdo, L.; Lonigro, A. J. *American Journal of Physiology* **1995**, *269*, H1941-H1948.
- (53) Sprague, R. S.; Ellsworth, M. L.; Stephenson, A. H.; Lonigro, A. J. *American Journal of Physiology* **1996**, *271*, H2717-H2722.
- (54) Sprague, R. S.; Ellsworth, M. L.; Stephenson, A. H.; Kleinhenz, M. E.; Lonigro, A. J. *American Journal of Physiology* **1998**, *275*, H1726-H1732.
- (55) Collins, D. M.; McCullough, W. T.; Ellsworth, M. L. *Microvascular research* **1998**, *56*, 43-53.
- (56) Dietrich, H. H.; Ellsworth, M. L.; Sprague, R. S.; Dacey, R. G., Jr. *American Journal of Physiology* **2000**, *278*, H1294-H1298.
- (57) Dietrich, H. H.; Kajita, Y.; Dacey, R. G., Jr. *The American journal of physiology* **1996**, *271*, H1109-1116.
- (58) Ellsworth, M. L.; Forrester, T.; Ellis, C. G.; Dietrich, H. H. *Am J Physiol* **1995**, *269*, H2155-2161.
- (59) McCullough, W. T.; Collins, D. M.; Ellsworth, M. L. *American Journal of Physiology* **1997**, *272*, H1886-H1891.
- (60) Chien, S. *Annu Rev Physiol* **1987**, *49*, 177-192.
- (61) Albalak, A.; Streichman, S.; Marmur, A. *Chem. Eng. Commun.* **1996**, *152-153*, 5-15.
- (62) Evans, E.; Fung, Y. C. *Microvasc Res* **1972**, *4*, 335-347.
- (63) Suter, S. P.; Gardner, R. A.; Boylan, C. W.; Carroll, G. L.; Chang, K. C.; Marvel, J. S.; Kilo, C.; Gonen, B.; Williamson, J. R. *Blood* **1985**, *65*, 275-282.
- (64) Bessis, M.; Feo, C. *Actual Pharmacol (Paris)* **1981**, *33*, 39-55.
- (65) Stozicky, F.; Blazek, V.; Muzik, J. *J Biomech* **1980**, *13*, 417-421.

- (66) Riquelme, B.; Foresto, P.; D'Arrigo, M.; Filippini, F.; Valverde, J. *Clin Hemorheol Microcirc* **2006**, *35*, 277-281.
- (67) Ogura, E.; Abatti, P. J.; Moriizumi, T. *IEEE Trans Biomed Eng* **1991**, *38*, 721-726.
- (68) Koutsouris, D.; Hanss, M.; Skalak, R. *Biorheology* **1983**, *20*, 779-787.
- (69) Flieger, R.; Grebe, R. *Biorheology* **1997**, *34*, 223-234.
- (70) Edwards, J.; Sprung, R.; Spence, D.; Sprague, R. *Analyst (Cambridge, United Kingdom)* **2001**, *126*, 1257-1260.
- (71) Sprung, R.; Sprague, R.; Spence, D. *Analytical Chemistry* **2002**, *74*, 2274-2278.
- (72) Kimura, C.; Oike, M.; Ohnaka, K.; Nose, Y.; Ito, Y. *Journal of Physiology (Oxford, United Kingdom)* **2004**, *554*, 721-730.
- (73) Janigro, D.; Nguyen, T. S.; Gordon, E. L.; Winn, H. R. *American Journal of Physiology* **1996**, *270*, H1423-H1434.
- (74) Spence Dana, M.; Torrence Nicholas, J.; Kovarik Michelle, L.; Martin, R. S. *Analyst* **2004**, *129*, 995-1000.
- (75) Archer, S. *FASEB Journal* **1993**, *7*, 349-360.
- (76) Gumbleton, M.; Audus, K. L. *Journal of Pharmaceutical Sciences* **2001**, *90*, 1681-1698.
- (77) Audus, K. L.; Borhardt, R. T. *Annals of the New York Academy of Sciences* **1987**, *507*, 9-18.
- (78) Pal, D.; Audus, K. L.; Siahaan, T. J. *Brain Research* **1997**, *747*, 103-113.

CHAPTER 3

3.1 THE BLOOD BRAIN BARRIER

The existence of a separation between the blood circulation and the central nervous system (CNS) was first acknowledged by Paul Ehrlich in the 1880s in a trivial experiment using staining with certain dyes. He made the observation that when the dyes were injected into the circulatory system, all organs in the body were stained with the exception of brain and spinal cord.¹ Later on, Edwin Goldman, a student of Ehrlich discovered that the same dyes were able to stain the nervous system when injected into CNS and failed to stain the rest of the body.² It was not until 1967 when Reese and Karnovsky showed using electron-microscopic studies that the barrier is localized at the capillary endothelial cells within the brain.³

The blood brain barrier (BBB) (Figure 13)⁴ represents the wall of the capillaries that feed the brain and it is comprised of microvascular endothelial cells that present tight junctions with very high electrical resistance ($\sim 2000 \Omega \times \text{cm}^2$).⁵ The barrier restricts the passage of molecules between the systemic circulation and the central nervous system, thus blocking the entrance of unwanted cytotoxic agents or viruses circulating in the bloodstream. However, at the same time, the barrier prevents the entrance of a variety of drugs designed to target the CNS. The membranes of microvascular endothelial cells selectively express a specific transport system to mediate the direct transport of nutrients

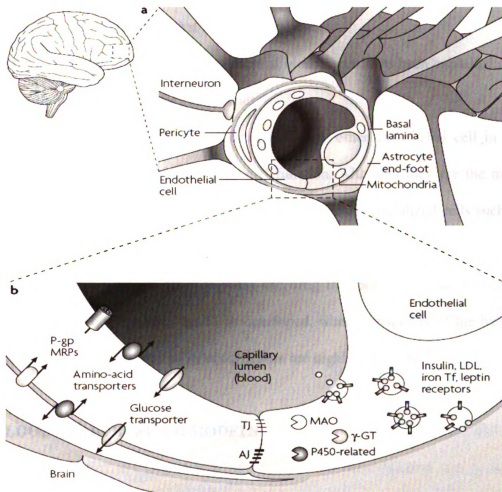


Figure 13. The Blood Brain Barrier. **a)** The BBB is formed by endothelial cells of the level of the cerebral capillaries. These endothelial cells interact with perivascular elements such as basal lamina and closely associated astrocytic end-feet processes, perivascular neurons and pericytes to form a functional BBB. **b)** Cerebral endothelial cells are unique in that they form complex tight junctions (TJ) produced by the interaction of several transmembrane proteins that effectively seal the paracellular pathway. These complex molecular junctions make the brain practically inaccessible for polar molecules, unless they are transferred by transport pathways of the BBB that regulate the microenvironment of the brain.⁴

into the CNS and of toxic metabolites out of the CNS.⁶ Currently, about 15 transporters are known, however it is estimated that at least 50 more exist.⁷

Recently, the transporter proteins in the endothelial membranes have been exploited as a real option of delivering drugs across the barrier.

Brain endothelial cells are very distinct from any other endothelial cell in the body due to their morphology, biochemistry and function. Although they are the main structural constituents of the barrier, their interaction with other specialized cells such as pericytes, perivascular macrophages and astrocytic end-feet is a prerequisite for the proper function of the BBB. In order to study the drug transport across the barrier, a suitable *in vitro* model of the BBB has to be developed, where the quality of the barrier and the differentiated morphology of its endothelium are highly preserved.⁸

3.2 BLOOD BRAIN BARRIER MODELS

In the last decade, an increasing effort to create *in vitro* models of the BBB was observed for studies of drug delivery to the CNS. Many drugs that showed promise in studies of CNS disorders are too large (tens or hundreds of kDa) for the passive diffusion through the brain-endothelium barrier. Therefore, a cell-based model that offers the potential of mimicking *in vivo* conditions, such as transcellular and paracellular drug diffusional processes, metabolism, and active transport processes is highly needed.⁹

Most of the BBB models exemplified in the literature are based on stationary cultures and co-culture of cells that take into account the complex environment of the brain. Early *in vitro* BBB models were described in terms of tight junction parameters

that have to be met, selective permeability properties for different standard sugar solutions and polarity. The first three prototypes of *in vitro* models consisted of either suspensions of isolated cerebral microvessels,¹⁰⁻¹³ isolated brain endothelial cells cultures,^{14,15} and co-culture of astrocytes and endothelial cell monolayers on plastic^{16,17} or on either side of filters.¹⁸⁻²²

Polycarbonate membranes with varying pore sizes were also utilized as support to grow endothelial cells,⁸ or co-culture of astrocytes and endothelial cells^{19,23} and to allow the passage of large drug molecules for transport studies. Typically, BBB models consisted of endothelial cells cultured on top of a polymeric membrane affixed to a cylindrical plastic insert. This culture insert was placed into a well of a standard culture plate, dividing the well into the luminal (blood) and abluminal (brain) chambers (Figure 14).⁴

Recently, Ma *et al.* reported an *in vitro* BBB model that utilizes membranes nanofabricated from low stress silicon nitride (SiN). They hypothesized that growing endothelial cells and astrocytes on the opposite sides of the membrane, therefore increasing the amount of direct contact between the two while still maintaining two distinct cell layers, will create a more differentiated and appropriate BBB model.²⁴

Some efforts have been made to develop BBB models with a three-dimensional architecture that will account for the blood flow differentiation of the cerebral endothelium.²⁵ Thus, endothelial cells have been culture inside hollow fiber tubes (the intraluminal side) and astrocytes were cultured extraluminally on the surface of the tubes. In this way, the endothelial cells were exposed to the flow conditions and allowed the investigation of signaling events in the BBB.

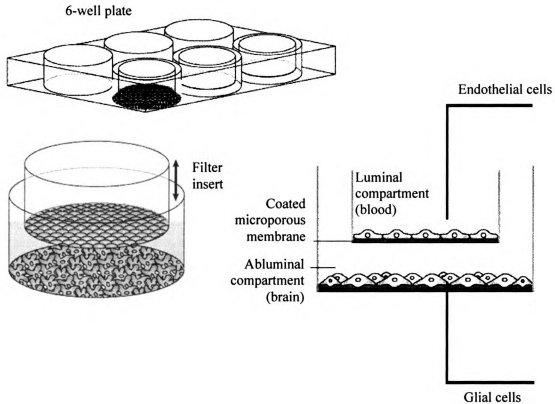


Figure 14. Typical *in vitro* model of the BBB. Brain endothelial cells are grown at the bottom of filter inserts together with glial cells grown at the bottom of 6-well plate. Soluble factors secreted from the glial cells induce the BBB phenotype in the brain capillary endothelium.⁴

However, technical demands of this model limit its use for drug screening. Very recently, Cucullo *et al.* utilized the aforementioned technique to develop a humanized dynamic *in vitro* model to study the BBB in epilepsy.²⁶ The model was based on the co-culture of human microvascular endothelial cells (HMVEC) from normal and drug-resistant epileptic brain tissue with human brain astrocytes (HA) from epilepsy patients or controls. Here, HMVEC and HA were co-cultured in polypropylene capillaries. However, for these studies, the dynamic *in vitro* blood brain barrier (DIV-BBB) setup was purchased from Spectrum (Spectrum Laboratories, Inc., Rancho Dominguez, CA).

These approaches of modeling the BBB for the pharmaceutical drug discovery and development process had to compromise between capacity, cost, time and how closely a model needs to resemble *in vivo* conditions. For successful use, any *in vitro* BBB model has to fulfill certain criteria such as reproducible permeability of reference compounds, good screening capacity, the display of complete tight junctions, adequate expression of BBB phenotypic transporters, to be reasonably robust and to display a physiologically relevant morphology.⁴ To date, the existing *in vitro* BBB models are labor intensive, expensive and have low throughput that makes them nearly impossible for testing the plethora of drugs designed to target the CNS.

3.3 MICROFLUIDIC TECHNOLOGY FOR THE DEVELOPMENT OF A BLOOD BRAIN BARRIER MIMIC

The use of a microfabricated device is a possible way to develop a complete BBB mimic. More specifically, using lithographically-derived microchips, it would be possible to monitor the fate of endothelium-derived NO that is stimulated by mechanically deformed RBCs. The concept of a micro total analysis system (μ TAS), also called a “lab on a chip”, miniaturized or microfluidic analysis systems, is a rapidly developing field. Microfluidic devices have found a broad area of applications, especially in the biological and life sciences, from cell handling and analysis, biomimetic and biopowered systems, clinical diagnosis, immunoassays, DNA, proteins and other bioassays to environmental concerns and gas analysis.²⁷

Typical dimensions of these microfluidic devices range from a few micrometers to several millimeters in length and width and from 100 nm to 100 μ m depth and height. These systems can be made in silicon,²⁸ glass,²⁸ and polymers such as polymethyl methacrylate (PMMA),²⁹ or poly(dimethylsiloxane) (PDMS).³⁰ Flow of sample or reagents through the chip is accomplished by either electrophoretic or hydrodynamic pumping.³¹⁻³³ Detecting the analytes directly in the micron-sized channels can be performed by a variety of mechanisms including optical (fluorescence, absorbance, chemiluminescence, refractive index), electrochemical (amperometry, potentiometry, conductivity), and mass spectrometry or NMR detection. The development of systems that combined surface engineering with layer-by-layer microfluidic technology to create 3D tissuelike structures, e.g., blood vessels have been reported.^{34,35} The utilization of an ultrathin nanofabricated silicon nitride membrane, where endothelial and astrocyte cells

were co-cultured on opposite sides of the membrane have also been reported.²⁴ This approach constitutes a potential starting point for development of a BBB mimic. Even though models of the BBB already exist, none incorporate actual blood flow. Here we report the development of a dynamic system that integrates blood flow and a barrier mimic.

3.4 EXPERIMENTAL

3.4.1 Design and Methods

Microchip fabrication. Microchips were fabricated using standard soft lithographic technology. Micrometer size channels were patterned in PDMS based on previous published methods.³⁰ Masters were made on a silicon wafer (Silicon, Inc., Boise, ID) using SU-8 photoresist (MicroChem Corp., Newton, MA) and photolithographic procedures employing masks in the form of negative films (Figure 15). The photoresist was prebaked at 95°C for 5 min prior to UV exposure with a near-UV flood source (Autoflood 1000, Optical Associates, Milpitas, CA) through a negative film (2400 dpi, Jostens, Topeka, KS), which contained the desired channel structures drawn in Freehand (PC version 10.0, Macromedia, Inc., San Francisco, CA). The masters were cast against a 20:1 mixture of Sylgard 184 elastomer and curing agent (Ellsworth Adhesives, Germantown, WI) and allowed to cure for ~ 2 hours at 75°C.

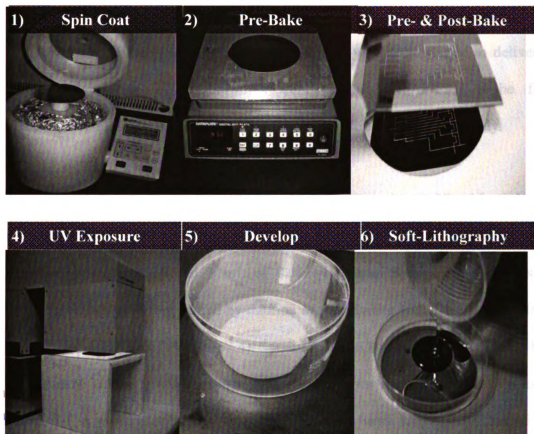


Figure 15. Photolithographic procedure for the fabrication of silicon master. **1)** Spin coat 4 mL of SU-8 50 photoresist at 1000 rpm for 20 s; **2)** Pre-bake for 5 min at 95°C to evaporate solvent and densify film; **3)** Post-bake for 5 min at 95°C to cross-link the exposed portions of the photoresist film; **4)** UV exposure, 350-450 nm, 50W for 60 s to polymerize and cross-link; **5)** Develop with propylene glycol monomethyl ether acetate (PGMEA); **6)** Soft-lithography to create microfluidic chip.

fabrication of the microfluidic device proposed to mimic the BBB. For the determination After the incubation period, the PDMS was peeled off the master to yield a pattern of negative relief channels. Chips containing channels of 100 μm depth x 100 μm width x 2cm length were used for the of NO and ATP flux through the polycarbonate membrane, a spiral shaped channel with a diameter of 150 μm was initially used to deliver the 4-amino-5-methylamino-2'7'-difluorofluorescein diacetate (DAF-FM) probe for NO detection and luciferin/luciferase mixture for the ATP detection, respectively.

Preparation of NO standards. Nitric oxide was prepared as a 38 mM stock solution from spermine NONOate (Cayman Chemical, Ann Arbor, MI) by dissolving 10 mg of spermine NONOate solid in 1 mL of 0.01 M sodium hydroxide (NaOH) solution. Working solutions were prepared by dilution of the alkaline NONOate solution in 0.1 M phosphate buffer saline (PBS, pH 7.4). Spermine NONOate is reported to have a half-life of 39 min at 37°C in 0.1 M phosphate buffer and follows first order kinetics for its rate of decay.³⁶ The working solutions were incubated in a water bath at 37°C for 15 min to ensure NO release from the donor. The NO samples were hydrodynamically pumped into the microfluidic channel at a flow rate of $1\mu\text{L min}^{-1}$ for 10 min.

Detection of NO. Methods based on fluorogenic probes for the measurement of the production of NO in cellular systems have been gaining increasing popularity due to their simplicity and sensitivity. The most successful indicator for NO reported in the literature has been 4,5-diaminofluorescein diacetate (DAF-2 diacetate) and 4-amino-5-methylamino-2'7'-difluorofluorescein diacetate (DAF-FM DA). These probes are

membrane permeable and they are deacetylated by intracellular esterases to DAF-2 and DAF-FM, respectively.³⁷ In all imaging studies DAF-FM or the diacetate form for cell membrane permeation was used for fluorescence determination. The reason for using DAF-FM versus DAF-2 is that DAF-FM is a more sensitive reagent for NO (NO detection limits for DAF-FM ~ 3 nM versus ~5 nM for DAF-2³⁸) and DAF-FM is independent of pH above pH 5.5. Moreover, the NO adduct of DAF-FM is known to be significantly more stable than that of DAF-2, enabling more time for image capture.

Detection of ATP flux through the polycarbonate membrane. ATP was measured by chemiluminescence using a luciferin/luciferase mixture as previously described in chapter 2, section 2.5.1. The reagents were delivered in a continuous flow setup using Tygon tubing (0.0200 mm ID x 0.0600 mm OD) fitted with 15 mm, 23 gauge hypodermic steel tubing bent at 90 degrees. This steel tubing was placed in the inlet access holes created in fabrication of the microfluidic device to deliver solutions directly into the channels. ATP standard solutions (0.0, 0.5, 1.0 and 1.5 μM) prepared in PSS buffer were added to aliquots of RBCs and delivered in the straight channel on the bottom of the device shown in Figure 16. The luciferin/luciferase mixture was hydrodynamically pumped for 10 min (or until the signal is stabilized) at a flow rate of 1.0 or 2.0 $\mu\text{L min}^{-1}$ into the spiral channel placed on the top of the membrane of the microchip device (Figure 16). The RBC/ATP samples loaded in one of the syringes were pumped through the tubing at a rate of 2.0 and 3.0 $\mu\text{L min}^{-1}$. Additionally, a solution of iloprost (a prostacyclin analogue known to induce ATP release) at 1 μM in PBS was incubated with a solution of RBC (final hematocrit 7%) for 15 min and hydrodynamically

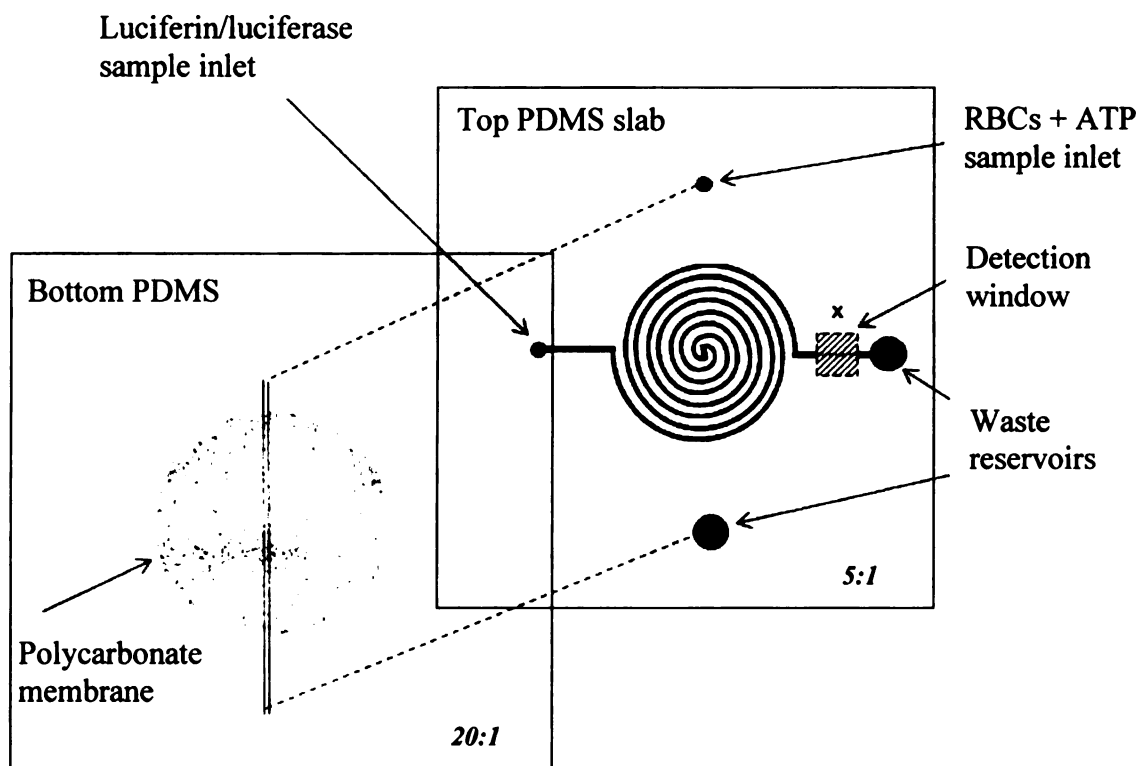


Figure 16. Detection of ATP flux through a polycarbonate membrane using a flow of luciferin/luciferase mixture hydrodynamically pumped into a spiral-shaped channel of a PDMS device. The set up is enclosed in a light excluding box over a PMT.

pumped through the bottom channel for 30 min. As the RBC/ATP or RBC/iloprost solutions traverse the microfluidic channel on the bottom of the device, ATP diffuses through the polycarbonate membrane into the spiral channel, reacts with the luciferin/luciferase mixture and the resulting chemiluminescence is detected at the end segment of this channel. The spiral channel intersects the linear channel underneath it in 17 locations, therefore creating a total contact surface area of $17 \times 150 \mu\text{m}$ (width of the spiral channel) $\times 100 \mu\text{m}$ (width of the linear channel). Chemiluminescence intensity was measured in a 1 mm long linear segment (x) situated at the end of the spiral-shaped channel using a photomultiplier tube (PMT) housed in a light-excluding box.

Fabrication of the microchip-based BBB. Figure 17 represents a schematic of the microfluidic device used to investigate the diffusion of NO through a polycarbonate membrane with pore size of $0.2 \mu\text{m}$ and a diameter of 13 mm. The proposed device is constructed of two PDMS slabs, each having patterned a 2 cm long, $100 \mu\text{m}$ wide channel and a polycarbonate membrane sandwiched in between the slabs. The membrane is tightly and reversibly sealed by the two pieces of PDMS, making the device amenable to cleaning and reuse.

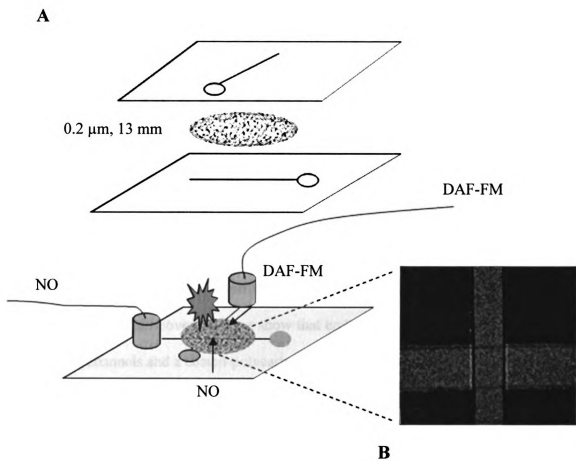


Figure 17. Proposed design for the microfluidic-based BBB mimic **A.** Assembly of a 3 dimensional fluidic device incorporating microchannels (100 μm diameter) for reagents delivery and a polycarbonate membrane sandwiched in between the PDMS layers. **B.** Micrograph of the channels junction with the polycarbonate membrane (13 mm diameter and 0.2 μm pore size).

3.4.2 Results and Discussion

In this work we described two approaches for the construction of a microfluidic-based BBB. The first approach consists of immobilization of bovine brain microvascular endothelial cells (bBMVECs) in the microfluidic channel underneath the membrane and monitoring of the NO production by the endothelial cells in the upper channel representing the CNS. A second approach is to culture the brain endothelial cells onto the polycarbonate membrane that will separate the two channels that pose as the microvascular system and CNS, respectively.

In the first approach, we are interested in optimizing the NO flux through the porous membrane in order to obtain the appropriate conditions for the detection of the analyte of interest. Moreover, here we show that endothelial cells can be immobilized on both PDMS channels and a coated-polycarbonate membrane.

For the second approach, the optimization of the ATP flux through the polycarbonate membrane is a prerequisite for the stimulation and detection of the NO production in bBMVECs cultured on the membrane. Ultimately, the ATP that is measured will be released by the RBCs obtained from patients with multiple sclerosis (MS).

NO flux through the polycarbonate membrane. In order to develop a realistic mimic of the BBB, the flux of NO across the polycarbonate membrane has to be determined. Therefore, a 3D microfluidic device was designed with one channel that ultimately

mimics the brain microvessels (cerebro-microvasculature), and is separated from a second channel that will pose as the CNS by a polycarbonate membrane.

One important step in the development of the device is the optimization of parameters such as flow rates, membrane pore sizes, channels lengths, and channel design in order to achieve high sensitivity and good limits of detection. These figures of merit are particularly important when investigating complex biological systems, such as the BBB and its periphery.

The first step in achieving this goal is the direct detection of NO that diffuses through the membrane with pore sizes 0.2, 0.4, and 0.6 μm . The fluorescent probe DAF-FM (10 μM) that flows through the second channel, above the membrane was used to create a highly fluorescent adduct with NO. Figure 18A schematically shows the diffusion of NO that is flowing in the channel S1, through the polycarbonate membrane into the upper channel S2 that contains the probe. The highly florescent DAF-FM/NO adduct is formed upon reaction between NO and DAF-FM and detected using a CCD camera mounted on an inverted microscope. The micrographs in Figure 18B show the diffusion of NO through the porous membrane and subsequent reaction with the probe at the channels junction.

The polycarbonate membrane experiences a uniform pressure drop across the entire length and width of the membrane at the channels junction (100 μm x 100 μm). A membrane pore size of 0.2 μm and flow rates of 1.0 $\mu\text{L min}^{-1}$ for both NO and DAF-FM streams were found to be optimal for the efficient diffusion of NO through the membrane. The bar graph in Figure 19 shows that with increasing NO concentration from

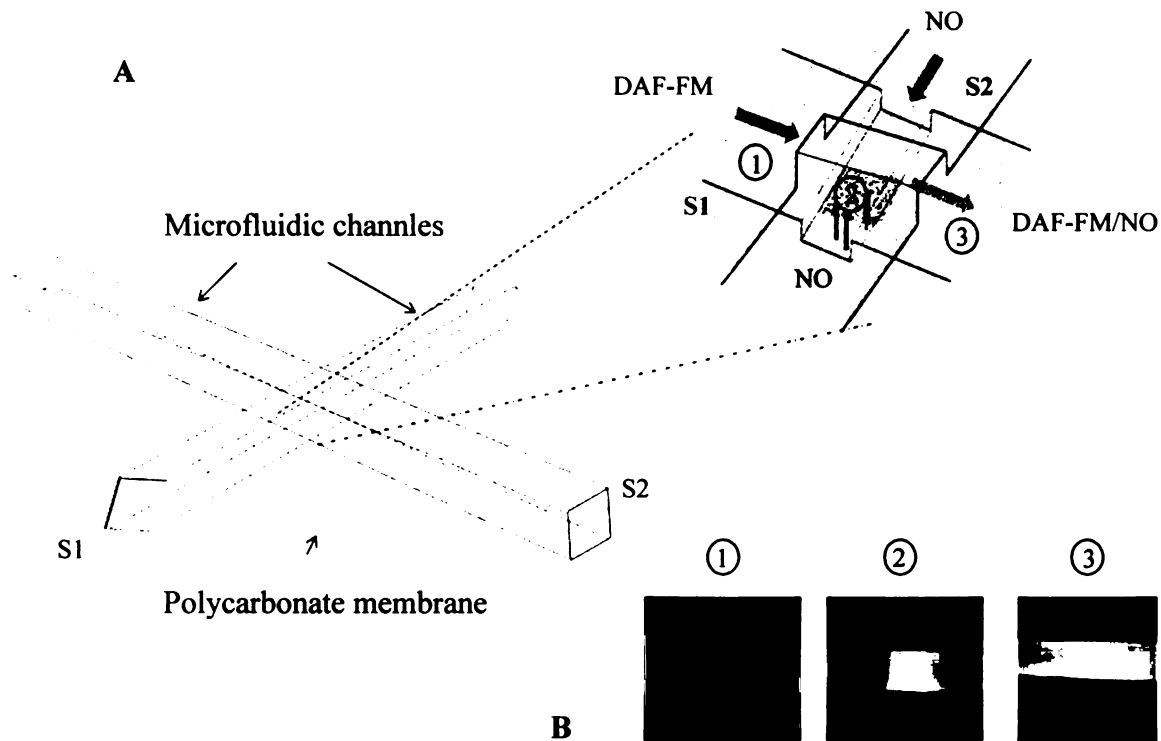


Figure 18. A. Detailed representation of the microfluidic channels junction with polycarbonate membrane in between. S1 represents the channel under the membrane, where NO ($3.8 \mu\text{M}$ stock solution in PBS) is being hydrodynamically pumped at a flow rate of $1 \mu\text{L min}^{-1}$. S2 represents the upper channel that poses as the CNS, where DAF-FM ($10 \mu\text{M}$) is being introduced. B. Micrographs of the upper channel before (1), at (2), and after (3) channels junction showing the formation of the highly fluorescent DAF-FM/NO adduct.

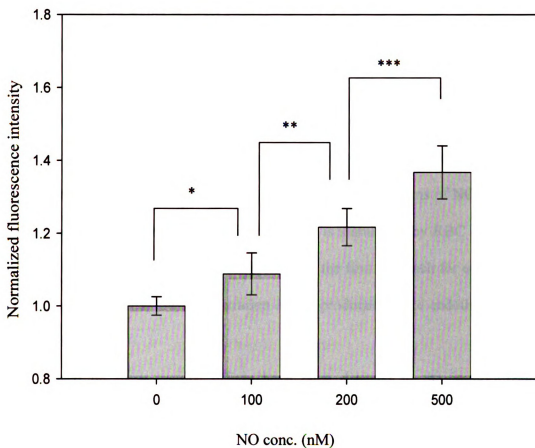


Figure 19. Detection of NO flux through the polycarbonate membrane with a pore size of $0.2 \mu\text{m}$ and at a flow rate of $1 \mu\text{L min}^{-1}$ as assessed by DAF-FM ($10 \mu\text{M}$). The control sample is PBS buffer. *, **, and *** represent the statistical significant differences versus control, 100, and 200 nM NO, respectively (* $p \leq 0.001$; ** and *** $p \leq 0.05$). The error bars represent the mean values \pm standard error ($n=4$).

0 (PBS only) to 500 nM, an increase in the fluorescence intensity is being detected across the membrane in the upper channel S2.

It was found that concentrations as low as 100 nM of NO can be detected using the proposed device. Moreover, significant statistical differences between 100 and 200 nM concentrations of NO were also reported. The data proves that the first approach for the microfluidic device described in this work in conjunction with the fluorescence detection could be utilized to investigate nanomolar concentrations of NO. However, the NO production in the brain endothelial cells that is stimulated by RBC derived ATP is one to two orders of magnitude lower. Therefore, the first approach for our device is not sensitive enough for the low concentration of NO produced by the endothelial cells, both *in vivo* and *in vitro*.

Based on these results, efforts have been directed to the immobilization of endothelial cells directly on the polycarbonate membrane, therefore the detection of intracellular NO production could be monitored in real time using fluorescence microscopy.

Cell immobilization on polycarbonate membrane/PDMS channels. Isolated bBMVECs have been previously successfully cultured as primary cultures on collagen-treated solid plastic surfaces (standard tissue culture flasks),^{14,15} polycarbonate membranes, or on commercial membrane inserts.⁸ At date, there are no reports in the literature describing bBMVEC immobilized onto PDMS substrates or channels as a part of a microfluidic device.

Despite the fact that bBMVECs are small ($< 10 \mu\text{m}$ in diameter), and that they generally need $\sim 10\text{-}12$ days to reach a confluent layer, we show here a successful attempt to immobilize these cells in a $100 \mu\text{g mL}^{-1}$ fibronectin-coated $100 \mu\text{m}$ diameter channel of a PDMS chip (Figure 20). However, the method of immobilizing the cells in the PDMS channels and the preservation of cell viability and morphology for the experimental period proved to be highly challenging. The lack of reproducibility and the high cost of the brain microvascular cell line were taken into consideration and a second approach was therefore envisioned.

Here, the cells were immobilized on a polycarbonate membrane in order to make the bBMVEC cell-coated membrane a part of a microfluidic device that will closely mimic the *in vivo* BBB and its proximal environment.

Detection of ATP flux through the polycarbonate membrane. RBCs 7% and ATP standard solutions (0, 0.5, 1.0 and $1.5 \mu\text{M}$) were prepared as previously described in chapter 2. RBC solutions were spiked with increasing concentrations of ATP and the flux of ATP through the polycarbonate membrane of the PDMS chip was detected as the chemiluminescence signal observed at the end portion of the spiral channel (distance x in Figure 15). The chemiluminescence signal is proportional to the amount of ATP reacted with the luciferin/luciferase mixture. In this case, a spiral-shaped channel ($150 \mu\text{m}$ diameter) was used to increase the time for ATP molecules to diffuse through the pores of the membrane.

The reason for using ATP-spiked RBC samples instead of ATP standard solutions in buffer was to account for the complexity of the RBC matrix and the possible

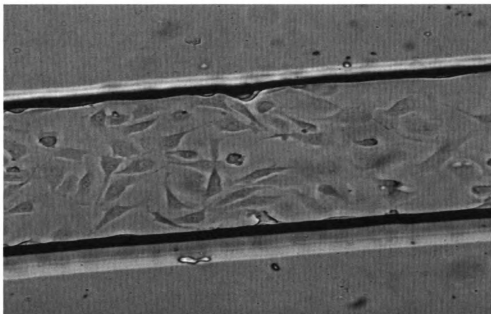


Figure 20. Micrograph of bBMVEC immobilized in a 100 μm PDMS channel. The channel was pre-coated with fibronectin ($100 \mu\text{g mL}^{-1}$) and incubated for 1 h at 37°C and 5% CO_2 to ensure cell adhesion.

interferences in the ATP detection that could occur when RBCs are present. Figure 21 shows that low micromolar ATP concentrations added to a continuous flow of RBCs can be detected on the other side of the polycarbonate membrane. These findings suggest that ATP diffusion through the membrane does not constitute a limiting factor in stimulating the NO production in endothelial cells cultured on the membrane. Polycarbonate membranes with pore sizes of 0.2, 0.6 and 1.0 μm were used in these studies. The optimum pore size diameter was found to be 1.0 μm . These data were found to be in good agreement with the literature. Recently, it has been reported that there is approximately four-fold smaller permeability of the 0.6 μm pore membranes than the 1.0 μm pore membranes ($k_{1\mu\text{m}}/k_{0.6\mu\text{m}} \sim 4$) for a standard solution of ADP.³⁹

The ATP flux was manipulated by varying parameters such as relative flow rate and concentration. The flow rates for both ATP and luciferin/luciferase streams were optimized to increase the sensitivity of the method. Therefore, we report here an optimum flow rate of 3.00 $\mu\text{L min}^{-1}$ for ATP flow, and of 1.00 $\mu\text{L min}^{-1}$ for luciferin/luciferase, respectively. Using this device we were able to detect as low as 500 nM concentration of ATP added to RBCs. Additionally, iloprost (a stable analogue of prostacyclin that is known to stimulate ATP release via a G-protein coupled receptor mechanism⁴⁰) was used to provoke ATP release. Data in Figure 20 shows that indeed, pharmacologically induced ATP release from RBC can diffuse through the polycarbonate membrane and be efficiently detected using chemiluminescence assay and a PMT housed in a light excluding box.

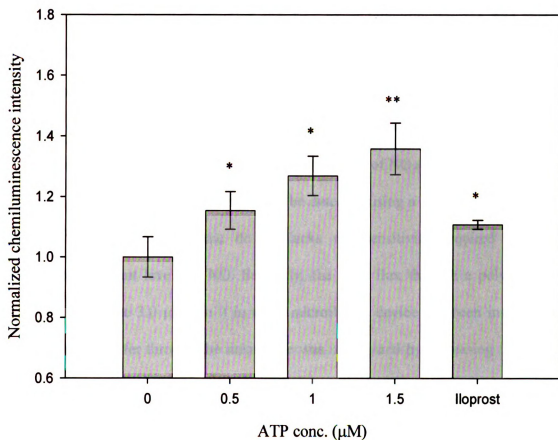


Figure 21. Detection of the ATP flux through a polycarbonate membrane with pore size of 1.0 μm and 13 mm diameter as assessed by chemiluminescence in a spiral-shaped channel, as part of a 3D microfluidic device. ATP and luciferin/luciferase flow rates are 3 $\mu\text{L min}^{-1}$ and 1 $\mu\text{L min}^{-1}$, respectively. Control represented by RBCs 7% (0 μM ATP). Iloprost is used as an ATP release stimulant of RBCs. * and ** represent the values statistically different from control and 0.5 μM ATP, respectively (* $p \leq 0.001$, ** $p \leq 0.05$) (n=4).

3.5 CONCLUSIONS AND OTHER CONSIDERATIONS

In this work we hypothesized that a complete BBB mimic can be developed on a microfluidic device that will monitor the fate of endothelium-derived NO that is stimulated by mechanically deformed RBCs. Key to investigating the NO production from the endothelium and its fate through the cell-coated polycarbonate membrane, that will constitute the BBB, is the ability to actually detect the NO after it crosses the barrier.

Primarily, we have demonstrated here that the flux of NO (flow rate $1.0 \mu\text{L min}^{-1}$) through a bare polycarbonate membrane can be detected using a specific probe for NO, DAF-FM ($10\mu\text{M}$). However, the device lacks the sensitivity required to detect physiological relevant levels of NO. Secondly, the ATP flux through a polycarbonate membrane (flow rate $3.0 \mu\text{L min}^{-1}$) in a 3D microfluidic device has been investigated. The molecular transfer through the membrane was maximized by increasing the area of contact between the two channels by designing the upper channel in a spiral shape that crosses the underneath linear channel in multiple points ($17 \times 150 \mu\text{m} \times 100 \mu\text{m}$). We showed here that the proposed device is sensitive enough for the detection of as low as 500 nM of ATP spiked into RBC samples and most importantly, is able to detect concentrations of ATP released by iloprost-treated RBCs.

Parameters such as membrane pore size, flow rates and probe concentrations have been optimized to increase the efficiency of the detection in the device. Although the results are promising, the inability to culture the cells on the membrane as part of the 3-D microfluidic BBB and the poor sensitivity for the physiological relevant NO concentrations constitute limiting factors.

Attempts have been made to culture the endothelial cells on isolated collagen-coated polycarbonate membranes and, after the cells have reached a confluent layer to integrate the membrane in the device. However, the two pieces of PDMS that make up the device would not seal together as a result of the membrane wetness from the cell culture media. As an alternative method, an attempt was made to culture the cells directly on the membrane by introducing the cell suspension in the upper channel, above the membrane. However, the lack of reproducibility and technical difficulties with the cell introduction made the device unsuitable for the purpose of our applications.

One way of avoiding these complications would be the integration of microvalves and multiple channels for the introduction of cells and DAF-FM, separately. Moreover, cell culture reactors on-chip where the viability of the cells can be sustained for days and the cell-cell signaling can be monitored in real time could also constitute an alternative option. In terms of using the polycarbonate membranes as support for endothelial cell culturing and proliferation, integration of transparent membranes for ease of optical cell imaging would be highly desirable.

The aforementioned microfluidic components, such as microvalves, microreactors or intricate designs are time consuming and prone to problems of engineering nature even before introducing the biological factor. A new, simpler and more amenable design has thus been constructed. Here, the high throughput capabilities of a microtitre plate technology was merged with the capabilities of microfluidic technology to create a device that mimics the BBB in a more realistic way by incorporating blood flow and having the capability of possible multi-drug screening simultaneously and in real time.

LIST OF REFERENCES

- (1) Ehrlich, P. *Berl. Klin. Wochenschr.* **1907**, *44*, 233-236.
- (2) Goldmann, E. E. *Lancet* **1913**, *172*, 1183-1188.
- (3) Reese, T. S.; Karnovsky, M. J. *J Cell Biol* **1967**, *34*, 207-217.
- (4) Cecchelli, R.; Berezowski, V.; Lundquist, S.; Culot, M.; Renftel, M.; Dehouck, M.-P.; Fenart, L. *Nat. Rev. Drug Discovery* **2007**, *6*, 650-661.
- (5) Crone, C.; Olesen, S. P. *Brain Res* **1982**, *241*, 49-55.
- (6) Engelhardt, B. *Cell Tissue Res.* **2003**, *314*, 119-129.
- (7) Miller, G. *Science (Washington, DC, United States)* **2002**, *297*, 1116-1118.
- (8) Guerin, J. L.; Bobilya, D. J. *Neurochem. Res.* **1997**, *22*, 321-326.
- (9) Gumbleton, M.; Audus, K. L. *Journal of Pharmaceutical Sciences* **2001**, *90*, 1681-1698.
- (10) Betz, A. L.; Goldstein, G. W. *Science* **1978**, *202*, 225-227.
- (11) Bowman, P. D.; Ennis, S. R.; Rarey, K. E.; Betz, A. L.; Goldstein, G. W. *Ann Neurol* **1983**, *14*, 396-402.
- (12) Matsumura, K.; Abe, I.; Fukuhara, M.; Tominaga, M.; Tsuchihashi, T.; Kobayashi, K.; Fujishima, M. *Am J Physiol* **1994**, *266*, R1403-1410.
- (13) Abbott, N. J.; Hughes, C. C.; Revest, P. A.; Greenwood, J. *J Cell Sci* **1992**, *103 (Pt 1)*, 23-37.
- (14) Audus, K. L.; Borchardt, R. T. *Ann NY Acad Sci* **1987**, *507*, 9-18.
- (15) Joo, F. *J Neurochem* **1992**, *58*, 1-17.
- (16) Arthur, F. E.; Shivers, R. R.; Bowman, P. D. *Brain Res* **1987**, *433*, 155-159.
- (17) Laterra, J.; Guerin, C.; Goldstein, G. W. *J Cell Physiol* **1990**, *144*, 204-215.

- (18) Beck, D. W.; Vinters, H. V.; Hart, M. N.; Cancilla, P. A. *J Neuropathol Exp Neurol* **1984**, *43*, 219-224.
- (19) Dehouck, M. P.; Meresse, S.; Delorme, P.; Fruchart, J. C.; Cecchelli, R. *J Neurochem* **1990**, *54*, 1798-1801.
- (20) Raub, T. J.; Kuentzel, S. L.; Sawada, G. A. *Exp Cell Res* **1992**, *199*, 330-340.
- (21) Biegel, D.; Pachter, J. S. *In Vitro Cell Dev Biol Anim* **1994**, *30A*, 581-588.
- (22) Deli, M. A.; Joo, F. *Keio J Med* **1996**, *45*, 183-198; discussion 198-189.
- (23) Wolburg, H.; Neuhaus, J.; Kniesel, U.; Krauss, B.; Schmid, E. M.; Ocalan, M.; Farrell, C.; Risau, W. *J Cell Sci* **1994**, *107 (Pt 5)*, 1347-1357.
- (24) Ma, S. H.; Lepak, L. A.; Hussain, R. J.; Shain, W.; Shuler, M. L. *Lab on a Chip* **2005**, *5*, 74-85.
- (25) Stanness, K. A.; Westrum, L. E.; Fornaciari, E.; Mascagni, P.; Nelson, J. A.; Stenglein, S. G.; Myers, T.; Janigro, D. *Brain Res* **1997**, *771*, 329-342.
- (26) Cucullo, L.; Hossain, M.; Rapp, E.; Manders, T.; Marchi, N.; Janigro, D. *Epilepsia* **2007**, *48*, 505-516.
- (27) Dittrich, P. S.; Tachikawa, K.; Manz, A. *Analytical Chemistry*, ACS ASAP.
- (28) Dolnik, V.; Liu, S.; Jovanovich, S. *Electrophoresis* **2000**, *21*, 41-54.
- (29) Becker, H.; Gartner, C. *Electrophoresis* **2000**, *21*, 12-26.
- (30) McDonald, J. C.; Duffy, D. C.; Anderson, J. R.; Chiu, D. T.; Wu, H.; Schueller, O. J. A.; Whitesides, G. M. *Electrophoresis* **2000**, *21*, 27-40.
- (31) Reyes, D. R.; Iossifidis, D.; Auroux, P.-A.; Manz, A. *Analytical Chemistry* **2002**, *74*, 2623-2636.
- (32) Polson, N. A.; Hayes, M. A. *Analytical Chemistry* **2001**, *73*, 312A-319A.
- (33) Seiler, K.; Fan, Z. H.; Fluri, K.; Harrison, D. J. *Analytical Chemistry* **1994**, *66*, 3485-3491.
- (34) Tan, W.; Desai, T. A. *Journal of Biomedical Materials Research, Part A* **2005**, *72A*, 146-160.
- (35) Tan, W.; Desai, T. *Encyclopedia of Biomaterials and Biomedical Engineering* **2004**, *2*, 1580-1593.

- (36) Maragos, C. M.; Morley, D.; Wink, D. A.; Dunams, T. M.; Saavedra, J. E.; Hoffman, A.; Bove, A. A.; Isaac, L.; Hrabie, J. A.; Keefer, L. K. *J Med Chem* **1991**, *34*, 3242-3247.
- (37) Balcerczyk, A.; Soszynski, M.; Bartosz, G. *Free Radical Biology & Medicine* **2005**, *39*, 327-335.
- (38) Kojima, H.; Nakatsubo, N.; Kikuchi, K.; Kawahara, S.; Kirino, Y.; Nagoshi, H.; Hirata, Y.; Nagano, T. *Analytical Chemistry* **1998**, *70*, 2446-2453.
- (39) Neeves, K. B.; Diamond, S. L. *Lab Chip* **2008**, *8*, 701-709.
- (40) Olearczyk Jeffrey, J.; Stephenson Alan, H.; Lonigro Andrew, J.; Sprague Randy, S. *Am J Physiol Heart Circ Physiol* **2004**, *286*, H940-945.

CHAPTER 4

4.1 ADDRESSING A VASCULAR ENDOTHELIUM ARRAY WITH BLOOD COMPONENTS USING UNDERLYING MICROFLUIDIC CHANNELS

Many technologies, such as those designed to perform adsorption, distribution, metabolism, excretion, and toxicity (ADMET) screening, are beginning to emerge as significant tools in drug discovery¹ and systems biology² and there exists a number of motivations for continued advancements in this area. A logical way to improve the drug discovery process at the preclinical stage is to create technologies that incorporate controlled, *in vitro* environments that closely mimic *in vivo* conditions and enable molecular-mediated communication between different cell types. Such technologies have been previously reported.^{3,4} Unfortunately, most systems fail to incorporate a major component of many *in vivo* processes, specifically, components of the circulation.

A quantitative understanding of molecule-mediated communication between different cell types in the circulation is challenging due to chemical and physical constraints. Chemically, the dynamic metabolic status of the cells dictates that measurements involving multiple cell types are made almost simultaneously as cellular events occur,² thus enabling the communication between the cell types.⁵ Physically, communication between two different cell types are often initiated by some type of stress placed upon one of the cell types. Hypoxia,⁶ shear stress,⁷⁻⁹ and oxidative stress^{10,11} are all types of stress that affect cell signaling. Measuring such *in vivo* events in real-time and in

a high throughput manner is difficult, especially if one of the cell types is in the complex matrix of the bloodstream.

There have been many reports involving microfluidics or lab-on-a-chip technology to create *in vivo* mimics using a controlled, *in vitro* platform with many of these devices incorporating cellular components.¹²⁻¹⁵ Stimulation has also been carried out on various cell types including the stimulation of a dopaminergic cell model (PC12 cells),¹⁶ endothelial cells,¹⁷ and islets¹⁸ contained within microfluidic devices.

Although previous reports have described the successful direct immobilization of endothelial cells in the channels of a microfluidic device, the device described here utilized a polycarbonate membrane to separate the flow of red blood cells (RBCs) from the endothelial cells. First, the use of the membrane in the device enables already available technologies associated with microtitre plate technology. Furthermore, the use of the membrane will allow other cell types to be immobilized on or near the endothelium, thus creating a working mimic of the blood brain barrier in a three dimensional device.

Such a device has the potential to examine communication between the circulation (in particular, RBCs) and the nervous system. Here, we report a method that combines microfluidic technologies in an array setup to elucidate the communication skills between RBCs and bovine pulmonary artery endothelial cells (bPAECs). This array-type device represents an improvement from the previous design with two single channels patterned onto PDMS chips (representing the circulatory system and the CNS) and a sandwiched polycarbonate membrane in between.

4.2 EXPERIMENTAL

4.2.1 Material and methods

Preparation of RBCs. RBCs were obtained from male New Zealand White rabbits as previously described. RBC samples were prepared as a 7% hematocrit with and without 1 μM iloprost (Cayman Chemical, Ann Arbor, MI) which, when added, was incubated off-chip for approximately 15 min. Iloprost was also added to a sample containing 7% RBCs incubated with 250 nM glybenclamide for approximately 10 min (Sigma Chemical, St. Louis MO) to demonstrate that the additional ATP release due to iloprost was not a result of cell lysis. ATP standards ranging from 0 -1.5 μM were prepared in a physiological saline solution (PSS) by diluting a 100 μM stock solution made up in distilled and deionized water (DDW) to allow for the quantitation of ATP release.

Measurement of ATP via chemiluminescence. Each sample or standard solution was individually mixed at the T-junction within the device with a luciferin/luciferase solution to examine the iloprost stimulated, RBC-derived ATP. The sensitivity of the assay was increased by adding 2 mg of luciferin (Sigma Chemical, St. Louis, MO) to a vial of luciferase and luciferin (FLE-50, Sigma Chemical, St. Louis, MO). The chemiluminescence for all samples as well as ATP standards were measured in real time by a photomultiplier tube (PMT) at 10 Hz for 30 seconds as previously described. These chemiluminescence measurements were performed by placing the downstream portion of the chip over the PMT using software written in house.

Measurement of bPAEC-derived NO. NO production in bBPAECs was determined by fluorescence imaging using the fluorescent nitric oxide probe DAF-FM (Molecular Probes, Eugene, OR). Cells were loaded with 10 μM of the membrane permeable diacetate form of the probe (DAF-FM DA). After loading, the cells were incubated for 20 min at 37°C to ensure intracellular probe distribution. The DAF-FM DA and all the other solutions were prepared in PBS 1X (Phosphate-Buffered Saline, Mediatech Inc., Herndon, VA) which had been previously equilibrated for 20 min at 37°C and 5% CO_2 . Samples containing RBCs at 7% hematocrit, RBCs incubated with 1 μM iloprost, RBCs incubated with 1 mM glybenclamide, RBCs incubated with 1 mM glybenclamide and 1 μM iloprost, and two controls (buffer and 1 μM iloprost) were pumped at a flow rate of 1.0 $\mu\text{L min}^{-1}$ at room temperature. After 30 min, the fluorescence images corresponding to each well were taken and the increase in intensity (corresponding to the NO production by bPAECs) was analyzed. The probe-loaded cells were visualized using an electrothermally-cooled CCD digital camera (Orca; Hamamatsu, Hamamatsu City, Japan) attached to an Olympus IX71M inverted microscope (Olympus America, Melville, NY). Time-lapse images were acquired using MicroSuite software (Olympus America).

Preparation of glybenclamide solution. Glibenclamide (Sigma; St. Louis, MO) was prepared as a 0.01M stock solution by adding 49 mg of glibenclamide to a solution containing 2 mL NaOH and 7.94 mL of dextrose in distilled water (50 mg mL^{-1}) and heating it slowly to 52°C. Washed RBCs were incubated with glibenclamide at a final concentration of either 250 nM or 1 mM for 15 min.

Preparation of the microfluidic devices. In all subsequent experiments, an irreversibly sealed PDMS microfluidic device was fabricated from a master that has been previously described in chapter 3. Briefly, 4 mL of SU-8 50 negative photoresist (MicroChem Corp., Newton, MA) was spin coated (Laurell Technologies Corp., North Wales, PA) onto a 4 inch silicon wafer (Silicon, Inc., Boise, ID) for 20 s. at 2000 rpm. The coated substrate was prebaked at 95°C for 5 min. prior to UV exposure through a negative film (Pageworks, Cambridge, MA) with a near-UV flood source (Spectra-Physics, Stratford, CT). The negatives were patterned using Freehand software (PC Version 10.0, Micromedia, Inc. San Francisco, CA) and taped to 2.5 by 4 inch glass slides to ensure proper alignment and exposure. The exposed wafer was then postbaked again at 95°C for an additional 5 min before developing with propylene glycol monomethyl ether acetate (Sigma-Aldrich Inc). The master was then rinsed with acetone and isopropyl alcohol to dissolve any remaining excess photoresist and dried with compressed nitrogen. The dimensions of the T-channel, corresponding to the raised photoresist dimensions of the master, were measured using a profilometer (Alpha Step-200, Tencor Instruments, Mountain View, CA) to be 150.0 μm wide by 118.6 μm deep.

Studies involving the measurement of ATP release from RBCs required the fabrication of two individual PDMS molds irreversibly sealed together, one absent of any features and the other a mold of a T-channel master. The T-channel chip was created by pouring a degassed 5:1 mixture of Sylgard 184 elastomer and curing agent (Ellsworth Adhesives, Germantown, WI) onto the silicon master and curing at 75°C for ~ 20 min. This chip was removed from the wafer and inlet holes were punctured through the chip using a 20 gage luer stub adapter (Becton Dickinson and Co., Sparks, MD) as well as 1/8

inch exit holes. This chip was then placed channel-side down onto a blank chip that was created by pouring a degassed 20:1 PDMS mixture onto a blank wafer and curing at 75°C for ~ 30 min before removing it from the silicon wafer. The device was completed by irreversibly curing both chips together at 75°C for an additional hour. A displacement syringe pump (Harvard Apparatus Inc., Holliston, MA) was used to introduce samples through Tygon tubing (Thermo Fisher Scientific Inc., Waltham, MA) that was fitted with 15 mm 23 gage hypodermic steel tubing bent at 90 degrees (New England Small Tube, Linchfield, NH). This steel tubing was simply placed in the inlet access holes created in fabrication to deliver solutions directly into the channels.

The SU-8 mold masters with the respective designs were obtained as described in chapter 3 using soft lithography. PDMS prepolymer was mixed with curing agent with a 20:1 mass ratio, degassed in a vacuum chamber for 5 min and spread on the 6 channel (100 μm diameter) mold master. PDMS was then partially cured by heating for 10 min at 75°C. A second layer of a 5:1 mixture was poured onto the chip and baked in the oven for additional 20 to 30 min. A PDMS layer with a soft side (20:1) and a more rigid side (5:1) was obtained by peeling off from the master. Subsequently, holes were punched on the PDMS layer as the inlets and outlets using a 23 gage RW hypodermic full hard tube, internal diameter 0.33 mm (New England Small Tube, Litchfield, NH) and a 1/8 inch puncher respectively.

A non patterned, 20:1 ratio PDMS slab was obtained similarly, by baking for 30 min and cell reservoir holes are punched using 1/8 inch puncher. The two PDMS layers, one with 6 straight channels and one with 6 x 3 holes are semi-irreversibly sealed together with the polycarbonate membrane (13 mm diameter, 1.0 μm pore size) in

between by baking at 75°C for additional 20 min. The connections between the microdevice and the external syringe pumps (Hamilton, Fisher Scientific) were achieved using Tygon flexible plastic tubing (Fisher) (0.020" ID x 0.060" OD) through small hard pins (0.025" OD x 0.013" ID) (New England Small Tube, Litchfield, NH).

Immobilization of the bPAECs on the membrane array. Bovine pulmonary aortic endothelial cells (bPAECs) primary cultures were purchased (Cambrex, East Rutherford, NJ) and they were fed with fresh medium every 2-3 days. After they reached confluence the cells were enzymatically detached with trypsin (0.25%), pelleted (220 x g for 5 min) and resuspended in culture medium until ready to use. Cells from divisions 3, 4 and 5 were used to run the experiments and seeded on collagen-coated 25 cm² tissue culture flasks (Corning Inc., NY) at a density of 20,000 cells / cm². The cells were kept in a humidified atmosphere at 37°C and 5% CO₂.

After the device was fully assembled, 20 µL of 100 µg mL⁻¹ fibronectin was added to each reservoir, on the membrane side, followed by incubation at 37°C for one hour. The concentration and incubation time for fibronectin were optimized such as to insure the best adhesion of the endothelial cells to the polycarbonate membrane. After fibronectin addition, the device was exposed to UV light for 30 min to crosslink the fibers and sterilize the device. bPAECs division 3 were harvested from the T-25 flasks and pelleted by centrifugation at 220 x g for 5 min and 37°C. Then, they were resuspended in 5 mM L-Arginine (Sigma) (the substrate for eNOS) at a density of 3.1 x 10⁶ cells mL⁻¹. The suspension was homogenized by vortex for a couple of seconds. Subsequently, 20 µL of the cell suspension was added to each well and incubated at 37°C

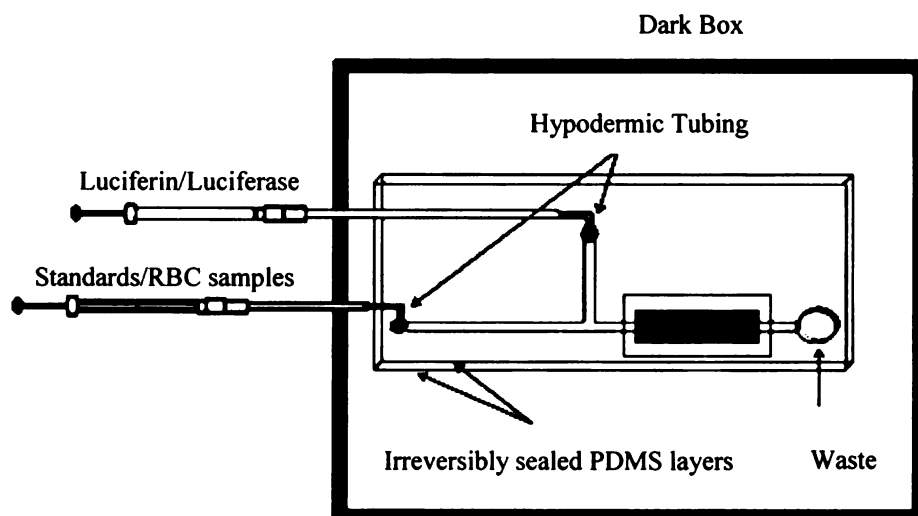
for one hour. One hour was found to be the optimum time for the cells to adhere to the membrane in the wells.

4.2.2 Results and Discussion

Here, we report a method that combines microfluidic technologies in an array setup to elucidate the communication skills between RBCs and endothelial cells obtained from bovine pulmonary artery (bPAECs). RBCs, obtained from healthy rabbits, were pumped through the channels of a microfluidic device. These channels were fabricated such that the internal diameter closely approximates those of resistance vessels in vivo. Moreover, the RBCs that were hydrodynamically pushed through the channels were incubated in the presence or absence of iloprost, a stable analogue of prostacyclin that is known to stimulate ATP release via a G-protein coupled receptor mechanism.

Figure 22 provides information on the experimental setup (a) as well as the obtained data (b). The summary of results from the RBCs of $n = 5$ rabbits are shown in Figure 23. Figure 22a describes the system used to obtain the data; briefly, a syringe pump is connected to the device via hypodermic stainless steel tubing. The syringes deliver RBCs (in the presence or absence of ATP release stimulant, such as iloprost, or inhibitors such as glybenclamide) to the channels of the microfluidic device. The device, made from PDMS is then placed over a photomultiplier tube (PMT) contained in a light

a)



b)

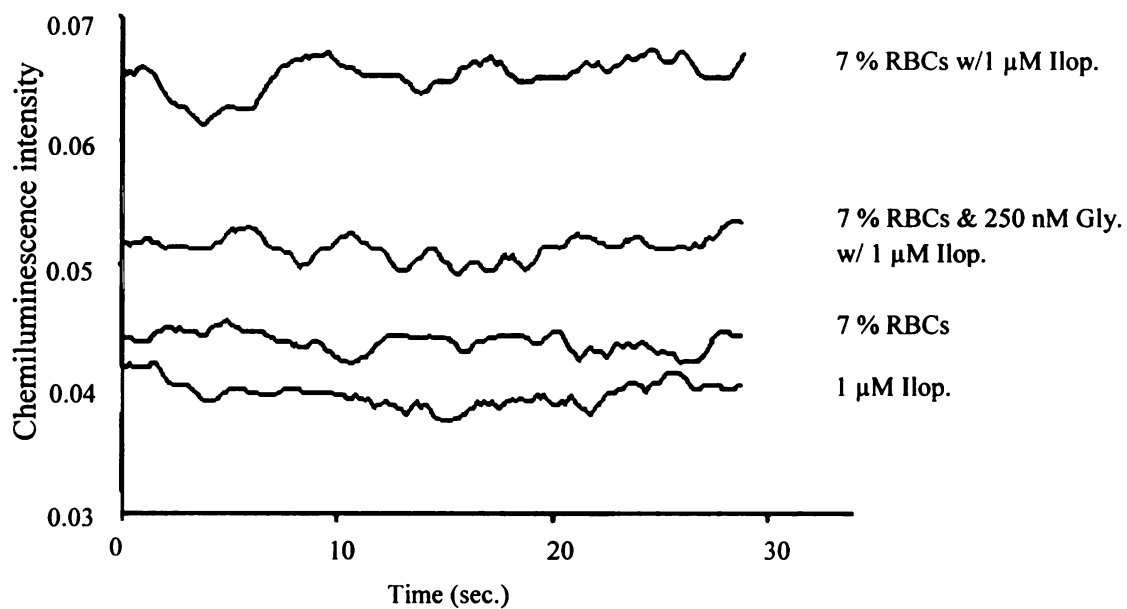


Figure 22. (a) Schematic of experimental set up for chemiluminescence measurements taken to determine the iloprost-stimulated ATP release from RBCs in real time shown in **(b)**

excluding box. The ATP released from the RBCs is then combined at an intersection of channels on the microfluidic device with a solution of luciferase containing luciferin (which is pushed through via the syringe pump). The chemiluminescence product that is formed results in the emission of light that is measured by the PMT. The amount of chemiluminescence is proportional with the ATP present.

A representation of the data is shown in Figure 22b and, as shown, the amount of ATP released from the RBCs increases in the presence of the iloprost. To verify that the increased chemiluminescence is not due to cellular lysis, the RBCs were also incubated in the presence of iloprost and glybenclamide, an inhibitor of ATP release from the RBC.¹⁹ As shown, incubation of the RBCs with glybenclamide present reduces the ATP release from these cells, thus providing evidence the measured signal is due to ATP and, importantly, that the signal is not due to cellular lysis but rather a release from intact cells. If the signal was due to lysis, glybenclamide would have no affect on the signal. Figure 23 summarizes the results from the RBCs obtained from n = 5 rabbits. The data in Figure 24 verifies that iloprost is capable of inducing ATP release in the channels of the microfluidic device and that this ATP release can be controlled using the appropriate inhibitors.

In an attempt to classify a possible role for this ATP release *in vivo*, a device was prepared that contained a polycarbonate membrane that separated the channels containing RBCs from a layered endothelium. The schematic of such a device is shown in Figure 23a. The top of the membrane, the side away from the RBC stream, was pre-treated with fibronectin prior to introducing bPAECs to the membrane. After the bPAECs were immobilized to the membrane (as verified through microscopy), the RBCs were.

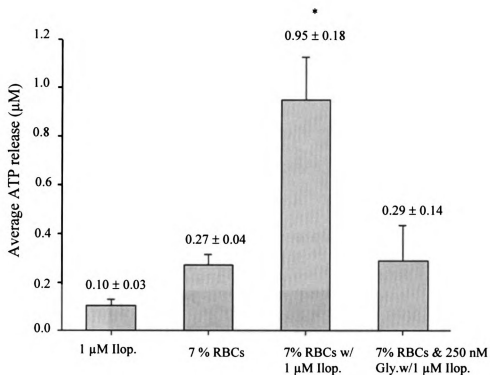
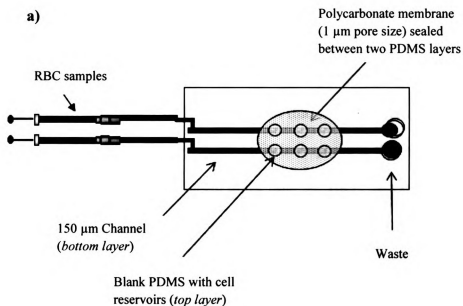


Figure 23. Comparison to the controls of iloprost (1 µM) and RBCs alone as well as the inhibition of ATP release when iloprost-stimulated RBCs were incubated with glybenclamide (250 nM) (* $p \leq 0.005$).



b)

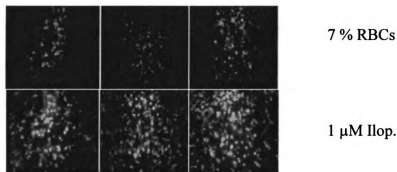


Figure 24. Iloprost-derived ATP release from RBCs stimulates NO production in a microfluidic device-containing an endothelium immobilized to a polycarbonate membrane. In **(a)**, the microfluidic device contains a polycarbonate membrane sealed between two PDMS layers that separates a channel containing RBCs (bottom layer) from a layered endothelium (top layer). In **(b)**, fluorescence microscopy images are shown for pre- (images on the top) and post- (images on the bottom) addition of iloprost.

introduced to the microfluidic device. First, an aliquot of RBCs in the absence of iloprost were introduced to the system and, as shown in images 1-3 in Figure 24b, the level of fluorescence intensity is minimal. However, upon addition of an aliquot of RBCs that had been incubated in the presence of iloprost, the fluorescence intensity of the bPAECs increased by 67% (Figure 25). This increase in fluorescence intensity can be attributed to an increase in NO production by the bPAECs in response to the increase in ATP derived from those RBCs that were incubated in the iloprost. These data suggest that the efficacy of iloprost in improving blood flow in the intact circulation may be due, in part, to its ability to stimulate the release of a known stimulus of nitric oxide synthase, namely, ATP. In addition to creating a controlled *in vitro* platform that simulates *in vivo* conditions, it is also necessary to have a system that will enable high throughput measurements that include calibration, drug-dose response data, and proper controls for verification of measurements. In an extension of the data shown in Figures 24 and 25, data from a device that incorporates multiple wells, all addressable by a microfluidic channel, is shown in Figure 26. Here, 18 wells were prepared in the absence (column C) and presence (columns A and B) of bPAECs; all of the wells were addressable with the RBC flow stream. The bPAECs in column A were also loaded with DAF-FM DA, an intracellular fluorescence probe for NO.

In this system, the wells were subjected to buffer alone (row 1), iloprost (row 2), RBCs in the absence (row 3) and presence (row 4) of iloprost, RBCs with glibenclamide (row 5) or RBCs and iloprost combined in the presence of glibenclamide (row 6). The data shown is summarized in Figure 25b. Note the significant increase in fluorescence intensity due to endothelium-derived NO in the presence of the RBCs and the RBCs.

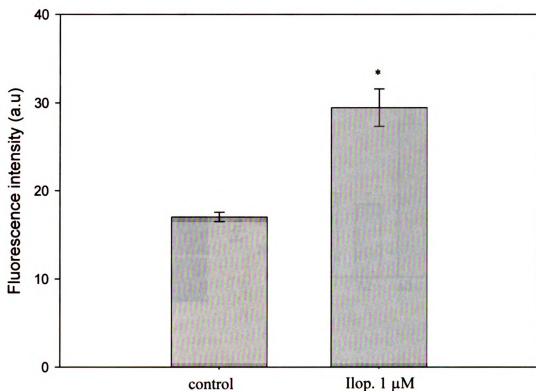
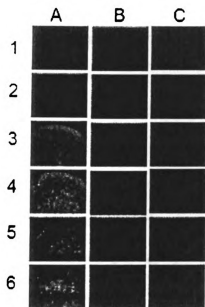


Figure 25. The increase in fluorescence intensity due to endothelium-derived NO production when a sample of RBCs incubated with iloprost (23.0 ± 3.5) vs. a sample of RBCs alone (16.5 ± 1.0) is pumped through the channel. The values reported are the average intensity and standard deviation ($n = 3$ wells for each sample). The difference in fluorescence intensity between samples incubated in the presence and absence of iloprost are statistically different ($p \leq 0.005$).

a)



b)

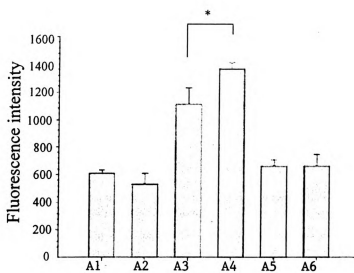


Figure 26. Micrographs of a vascular endothelium array with blood components are shown in (a). The wells in columns A and B contain bPAECs cultured on a polycarbonate membrane. Column C contains cell free wells. The rows represent the wells of the array that are addressable by the underlying microchannel network, each delivering a different reagent to the wells as described in the text. The quantitative representation of the data is shown in (b). The difference in fluorescence intensity between samples containing the RBCs in the absence (row 3) and presence (row 4) of iloprost are statistically different from the other rows. There is also a difference in the intensities of rows 3 and 4 ($*p \leq 0.005$).

4.3 CONCLUSIONS

In addition to interacting with an appropriate molecule, there are many characteristics required of a drug candidate throughout the testing process. Drug adsorption properties, its ability to be distributed *in vivo*, its effects on metabolism, excretion characteristics and its toxicity are often monitored.

Here, we showed that an array of endothelial cells, addressable by an underlying microfluidic network of channels containing RBCs, can be employed as an *in vitro* model of the *in vivo* circulation to monitor cellular communication between different cell types. Results obtained from this array suggest that the ability of iloprost, a stable analogue of prostacyclin, to stimulate nitric oxide production in endothelial cells, may be due to its ability to stimulate ATP release from the red cell. These results provide evidence that the described device may serve as a controlled, *in vitro* platform for performing *in vivo*-type measurements.

LIST OF REFERENCES

- (1) Dittrich Petra, S.; Manz, A. *Nat Rev Drug Discov* **2006**, *5*, 210-218.
- (2) Breslauer David, N.; Lee Philip, J.; Lee Luke, P. *Mol Biosyst* **2006**, *2*, 97-112.
- (3) Pardridge, W. M. *Introduction to the Blood-Brain Barrier: Methodology, Biology and Pathology*, 1998.
- (4) Shah, M. V.; Audus, K. L.; Borchardt, R. T. *Pharm Res* **1989**, *6*, 624-627.
- (5) Carroll, J. S.; Ku, C.-J.; Karunaratne, W.; Spence, D. M. *Anal. Chem. (Washington, DC, U. S.)* **2007**, *79*, 5133-5138.
- (6) Ellsworth, M. L.; Forrester, T.; Ellis, C. G.; Dietrich, H. H. *American Journal of Physiology* **1995**, *269*, H2155-H2161.
- (7) Sprague, R. S.; Ellsworth, M. L.; Stephenson, A. H.; Kleinhenz, M. E.; Lonigro, A. J. *American Journal of Physiology* **1998**, *275*, H1726-H1732.
- (8) Sprague, R. S.; Stephenson, A. H.; Ellsworth, M. L.; Keller, C.; Lonigro, A. J. *Exp Biol Med (Maywood)* **2001**, *226*, 434-439.
- (9) Sprung, R.; Sprague, R.; Spence, D. *Analytical Chemistry* **2002**, *74*, 2274-2278.
- (10) Carroll, J.; Raththagala, M.; Subasinghe, W.; Baguzis, S.; Oblak, T. D. a.; Root, P.; Spence, D. *Mol. BioSyst.* **2006**, *2*, 305-311.
- (11) Evans Joseph, L.; Goldfine Ira, D.; Maddux Betty, A.; Grodsky Gerold, M. *Diabetes* **2003**, *52*, 1-8.
- (12) Khademhosseini, A.; Langer, R.; Borenstein, J.; Vacanti, J. P. *Proc. Natl. Acad. Sci. U. S. A.* **2006**, *103*, 2480-2487.
- (13) Shin, M.; Matsuda, K.; Ishii, O.; Terai, H.; Kaazempur-Mofrad, M.; Borenstein, J.; Detmar, M.; Vacanti, J. P. *Biomed. Microdevices* **2004**, *6*, 269-278.
- (14) Takayama, S.; Ostuni, E.; LeDuc, P.; Naruse, K.; Ingber, D. E.; Whitesides, G. M. *Nature* **2001**, *411*, 1016.
- (15) Sin, A.; Chin Katherine, C.; Jamil Muhammad, F.; Kostov, Y.; Rao, G.; Shuler Michael, L. *Biotechnol Prog* **2004**, *20*, 338-345.

- (16) Li, M. W.; Spence, D. M.; Martin, R. S. *Electroanalysis* **2005**, *17*, 1171-1180.
- (17) Spence Dana, M.; Torrence Nicholas, J.; Kovarik Michelle, L.; Martin, R. S. *Analyst* **2004**, *129*, 995-1000.
- (18) Roper, M. G.; Shackman, J. G.; Dahlgren, G. M.; Kennedy, R. T. *Anal. Chem.* **2003**, *75*, 4711-4717.
- (19) Sprague, R. S.; Olearczyk, J. J.; Spence, D. M.; Stephenson, A. H.; Sprung, R. W.; Lonigro, A. J. *Am. J. Physiol.* **2003**, *285*, H693-H700.

CHAPTER 5

5.1. A PROPOSED MECHANISM FOR THE INVOLVEMENT OF PROLACTIN-RELEASING PEPTIDE (PrRP) IN THE REGULATION OF VASCULAR TONE

In 1998 Hinuma *et al.*¹ reported the identification of two novel peptides, PrRP-20 and PrRP-31 that stimulated the release of prolactin from the pituitary gland. The peptides were identified in the bovine hypothalamus as the endogenous ligands of the orphan seven-transmembrane-domain receptor (GPR10/hGPR3). Initial studies revealed that the role of PrRP was associated with weak prolactin release *in vivo*¹ and *in vitro*.^{2,3} Other roles of this peptide have been reported, for example regulation of energy balance,⁴ suggesting that PrRP is involved in food regulation and body weight. Lawrence *et al.* have shown that intracerebralventricular (i.c.v.) administration of PrRP reduced the food intake significantly in male rats, but did not affect the water intake.⁵ However, PrRP not only regulates the energy homeostasis, but also is a potent mediator of stress responses in the brain.^{2,3,6-15}

Subsequent work by Samson *et al.*¹⁶ and Jarry *et al.*¹⁷ questioned the capacity of the PrRP to serve as physiological regulator of prolactin (PRL), and other functions for this peptide have been explored. Samson *et al.* reported that microinjections of PrRP in the ventrolateral medulla (VM) resulted in a specific dose dependent increase in mean arterial pressure, heart rate, and sympathetic activity. It was shown that PrRP acts as a modulator of blood pressure in areas with little or no receptor expression and contrary,

has no effect in areas of high receptor expression, such as the area postrema (AP).¹⁸ It became clear that although PrRP and its receptor may be acting to release prolactin in some tissues, it may have some independent functions of its own.⁸ To date, the physiological function of PrRP is not yet completely understood.

Prolactin-releasing peptide has two molecular forms, one with a C-terminal 20-residue peptide (PrRP20) and one with a 31-residue peptide (PrRP31), both known to be derived from a single precursor molecule. Their amino acid sequences, TPDINPAWYAGRGIRPVGRF-amide and SRAHQHSMEIRTPDINPAWYAGRGIRPVGRF-amide respectively, are highly conserved among several species, such as human, bovine, and rat.³

Roland *et al.*⁸ reported that the fragment PrRP(12-31) was the minimum agonist fragment, with a receptor affinity of $K_i = 1$ nM. Moreover, an alanine scan of the segment PrRP(25-31) showed the importance of the three arginine residues. Boyle *et al.*¹⁹ found that the functionally important residues are located within the carboxyl-terminal heptapeptide segment Ile²⁵-Arg²⁶-Pro²⁷-Val²⁸-Gly²⁹-Arg³⁰-Phe³¹-NH₂. He also acknowledged that the only essential amino acid residue in PrRP is the Arg,³⁰ which donates both a critical basic side chain in the L-configuration and is also reported to contribute an essential backbone NH. The five Arg and two His residues of PrRP31 impart a very basic character to the peptide at physiological pH, and therefore high tendency to bind negatively charged molecules. Because of its basic character and because only the carboxyl-terminal heptapeptide segment is involved in the receptor binding with the Arg³⁰ residue being the essential amino acid, PrRP could adapt its “body structure” to other functions of physiological importance.

In this study we propose a mechanism for the previously reported cardiovascular/blood pressure regulatory properties of the PrRP, that is PrRP binding to the red blood cell (RBC)-derived adenosine triphosphate (ATP) that is released under various stimuli. It has been previously reported that RBC-derived ATP contributes to the control of vascular resistance in both the pulmonary²⁰⁻²² and the systemic circulation.²³ RBCs, when traversing microvascular beds, are subjected to mechanical deformation and as a response they release ATP. Moreover, it is well established that vascular endothelium constitutively generates nitric oxide (NO) in response to ATP stimulation and that endothelium-derived NO induces a relaxation of vascular smooth muscle cells. If PrRP binds ATP, this will lower the extracellular ATP pool available for the stimulation of the endothelial NO synthesis and subsequently, a decrease in the vascular relaxation/increase in the blood pressure might be possible.

This proposed mechanism seems very plausible in the construct of Samson's findings, that significant elevations in the mean arterial pressure were observed in response to i.c.v. administration of low nanomolar concentrations of PrRP31. Also, he reported that the mean blood pressures returned to pre-injection control levels in approximately 15 to 25 min from the peptide administration. Moreover, he showed that effective doses of PrRP failed to alter the thirst and also, affect the salt appetite in rat models, therefore attesting the specificity of the blood pressure elevated actions of the PrRP. All these findings led us to investigating in more depth the alternative physiological function proposed for the PrRP as well as the mechanism by which the peptide exerts this function.

In this work, different techniques, such as mass spectrometry, chemiluminescence and fluorescence microscopy were utilized to show, directly or indirectly, the PrRP binding to ATP. Moreover, by using an *in vitro* microfluidic-based mimic of an *in vivo* microcirculation that we previously reported,²⁴ we constructed a system where the direct involvement of the PrRP in the regulation of the blood pressure and/or vascular tone could be monitored in real time.

5.2 EXPERIMENTAL

5.2.1 Materials and Methods

Collection of RBCs. All procedures involving the collection of blood samples from animals were approved by the appropriate Animal Investigation Committee. For studies involving rabbit RBCs, male New Zealand white rabbits (2.0–2.5 kg) were anesthetized with ketamine (8 mL kg⁻¹, intramuscular injection) and xylazine (1 mg kg⁻¹, i.m.) followed by pentobarbital sodium (15 mg kg⁻¹, intravenous injection). A cannula was placed in the trachea and the animals were ventilated with room air at 20 breaths min⁻¹ and a tidal volume of 20 mL kg⁻¹. A catheter was placed into a carotid artery for administration of heparin and for phlebotomy. After heparin (500 units, i.v.) animals were exsanguinated. Blood was centrifuged at 500 × g at 4°C for 10 min. The plasma and buffy coat were removed for other experiments. RBCs were then resuspended and washed three times in a physiological salt solution (PSS). The PSS was made by combining 25 mL of TRIS buffer [prepared by mixing 50.9 g of TRIS in 1 L of distilled

and deionized water (DDW)] and 25 mL of Ringer's solution (164.2 g NaCl, 7.0 g KCl, 5.9 g CaCl₂ · 2H₂O, and 2.83 g MgSO₄ in 1 L of DDW). After the addition of 0.50 g of dextrose and 2.50 g of albumin bovine fraction V (fatty acid-free) to the TRIS–Ringer's mixture, the entire solution was diluted to 500 mL with DDW and the pH was adjusted to 7.35–7.45. The PSS was then filtered three times using a 0.45 µm filter (Corning, Fisher Scientific).

Measurement of the ATP release. All reagents were from Sigma Chemical (St. Louis, MO) unless otherwise noted. A 100 µM stock solution of ATP was prepared by adding 0.0551 g of ATP to 1000 mL of DDW. ATP standards with concentrations ranging between 0 and 1.5 µM were then prepared in PSS from the stock. To prepare the luciferin–luciferase mixture used to measure the ATP by chemiluminescence, 5 mL of DDW were added to a vial containing luciferase and luciferin (FLE-50, Sigma). In order to enhance the sensitivity of the assay, 2 mg of luciferin were added to the vial. For ATP measurements involving RBCs, all RBC samples were diluted to a 7% hematocrit. To stimulate the ATP release from the RBCs, cells were treated with iloprost (Cayman Chemicals, Ann Arbor, MI), and Zn(II) activated-C-peptide (American Peptide, Sunnyvale, CA, USA). Detection of ATP release from the RBCs was performed using the luciferase assay and chemiluminescence measurement by a photomultiplier tube. The resultant current from the photomultiplier tube, which is proportional to the ATP induced chemiluminescence, was measured as a potential by a data acquisition board controlled by a program written with LabView (National Instruments, Austin, TX, USA).

Mass spectrometry analysis. All experiments were performed using a Thermo model LTQ linear ion trap mass spectrometer (Thermo, San Jose, CA, USA). Samples were prepared by dissolving synthetic human PrRP in purified water at a concentration of $6.6 \mu\text{mol L}^{-1}$. For ATP binding studies, a $20 \mu\text{mol L}^{-1}$ solution of ATP prepared in purified water was added to a PrRP solution then introduced to the mass spectrometer at a flow rate of $0.5 \mu\text{L min}^{-1}$ by nanoelectrospray ionization. The spray voltage was maintained at 2.0 kV. The heated capillary temperature was 250°C .

Fabrication of the microfluidic array. Fabrication of the poly(dimethylsiloxane) (PDMS)-based microchips involves well established soft lithography methods.²⁵ The fabrication relied on two individual PDMS molds irreversibly sealed together, one absent of any features and the other a mold of a 6 channels master. The 6 channels chip was created by pouring a degassed 20: 1 mixture of Sylgard 184 elastomer (Ellsworth Adhesives, Germantown, WI, USA) and curing agent onto a 4 inch silicon master (Silicon Inc., Boise, ID, USA) and curing at 75°C for 30 min. An additional layer of a 5:1 mixture was poured on top of the 20:1 mixture to give the chip enough surface brittleness for ease of puncturing the inlet holes. After additional 30 min bake at 75°C , the chip was removed from the wafer and inlet holes were punctured through the chip (using a 20 gauge luer stub adapter) as well as $1/8$ inch exit holes. A non-patterned, 20:1 ratio PDMS slab was obtained as before, by curing for 30 min followed by the creation of cell reservoir holes using a $1/8$ inch hole punch. The two PDMS layers, one with 6 straight channels and one with 18 holes (6 rows x 3 columns) were irreversibly sealed together with the transparent polycarbonate membrane (13 mm diameter, $0.03 \mu\text{m}$ pore size) in

between by curing at 75°C for an additional 30 min. The connections between the microdevice and the external syringe pumps were achieved using the Tygon plastic tubing (0.02" ID x 0.06" OD) that were fitted with 15 mm, 23 gauge hypodermic steel tubing bent at 90 degrees. This steel tubing was simply placed in the inlet access holes created in fabrication to deliver solutions directly into the channels. All channels used in the studies reported here had a width of 200 μm and a depth of 100 μm . After the bPAECs were immobilized to the membrane and loaded with the NO probe, the RBCs were introduced to the microfluidic device through the underlying channels on the bottom layer of PDMS. These 18 wells in the presence of bPAECs were addressed with the RBC flow stream.

Cell immobilization. The design of the microfluidic device allows the easy introduction of the cells to the wells. The top of the membrane, the side away from the RBCs, serves as a support for the bPAECs. The membrane was pre-treated with 100 $\mu\text{g mL}^{-1}$ fibronectin (Sigma Chemical Co., St. Louis, MO) and incubated for 1 h at 37°C. The fibronectin treatment ensures the adhesion of the cells to the membrane. bPAECs, low passage, were harvested by trypsinization and introduced to the 18 wells of the array and incubated at 37°C and 5% CO_2 for 3 h or until the cells had attached to the fibronectin layer. Once the endothelial cells had adhered to the membrane, fluorescence microscopy was used to monitor the NO production brought about the RBC-derived ATP in the underlying microfluidic channels.

Measurement of Nitric Oxide. NO derived from bPAECS cultured on the membrane of the microfluidic array was monitored using the fluorescence probe 4-amino-5-methylamino-2',7'-difluorofluorescein diacetate (DAF-FM DA) (Molecular Probes, Eugene, OR).^{26,27} Next 10 μL of a 10 μM solution of DAF-FM in Hank's Balanced Salt Solution (HBSS, Sigma) were added to the cells in each well of the microfluidic array and incubated for 30 min at 37°C and 5% CO_2 to ensure a sufficient amount of dye had accumulated in the endothelial cells. After probe incubation, the wells were rinsed twice with equilibrated HBSS to eliminate any extracellular DAF-FM that might result in an increased background fluorescence.

To measure the NO production in the cells, RBC samples of 7% hematocrit in PSS were incubated in the presence or absence of iloprost (a stable analogue of prostacyclin), or metal-activated C-peptide,²⁸ both known to stimulate/increase the ATP release from RBCs. Contrary, for the samples incubated with the aforementioned solutions followed by incubation with PrRP, a decrease in ATP release, as result of PrRP binding to ATP, would translate into a decrease in NO production. All solutions are pumped for 30 min at a flow rate of 1 $\mu\text{L min}^{-1}$ in the microfluidic channels underlying the array of wells. The ATP within each sample diffuses through the polycarbonate membrane into the wells and stimulates the NO production in bPAECS.

Fluorescence images for each well were taken using an Olympus IX71M microscope (Olympus America, Melville, NY) with an electrothermally cooled CCD (Orca, Hamamatsu) and MicroSuite software (Olympus America). The microscope incorporated a FITC filter cube (Chroma Technology Corp) containing the excitation (460-500 nm) and emission (505-560 nm) filters. The results were reported as gray value

mean per well, where the gray-level intensity refers to the amount of light energy actually reflected from or transmitted through the physical specimen.

5.2.2 Results and Discussion

It has been well established that RBCs participate in vascular regulation and the property of these RBCs responsible for the stimulation of NO synthesis was their ability to release ATP in response to mechanical deformation.²¹ ATP is an *in vivo* stimulus of endothelial NO production,^{29,30} it is present in millimolar concentrations in the RBCs,^{31,32} and it is released in response to physiological stimuli, such as hypoxia and hypercapnia.^{33,34} When RBCs are traversing the resistant vessels *in vivo*, they are increasingly deformed by increments in the velocity of the blood flow through a vessel and/or by reduction in vascular caliber,³⁵ and as a result they release ATP through a mechanism involving the cystic fibrosis transmembrane regulator (CFTR). This RBC-derived ATP can then act on the endothelial cells to stimulate endogenous NO synthesis and enable RBCs to participate in local regulation of vascular caliber.^{21-23, 34,36-38}

However, depending on the type of purinergic receptor ATP binds, it can induce antagonistic effects on the vasculature. Thus, ATP binding to the P2x receptor, which is primarily found on the vascular smooth muscle cells, results in contraction of the cells,³⁹ whereas ATP binding to the P2y receptor found primarily on the endothelium, results in NO synthesis and/or vasodilatation.^{29,30} Thus, ATP applied to the luminal side of a vessel, that released from the RBCs within the circulation, would be expected to produce

endothelium-dependent relaxation through an interaction with the endothelial P2y purinergic receptor (Figure 27.)

ATP binding to PrRP. In this work we show the possible role that PrRP could play in the regulation of the mean arterial pressure through a mechanism involving intraluminal ATP depletion. Mass spectrometry data, obtained in collaboration with Dr. Gavin Reid at Michigan State University, showed the ability of the peptide to bind ATP. Based on these findings, additional experiments involving the luciferin/luciferase assay and chemiluminescence detection were performed. Standard ATP samples were prepared as described in the methods section. Data in Figure 28 provides further evidence that PrRP binds to ATP. Here, upon the addition of 10 nM PrRP, the chemiluminescence signal from the samples containing ATP standard solutions decreased in a time dependent fashion. After the immediate introduction of the peptide, a decrease of approximately 30% of the chemiluminescence signal was observed for the ATP concentrations of 0.75, 1, and 1.5 μ M. Moreover, about 50% of the initial ATP signal was inhibited by the 60 min incubation with PrRP. This signifies that free ATP in solution decreases either by binding to another species present and/or by degradation. However, in this case, based on the mass spectral data and the structural information, PrRP is found to bind ATP.

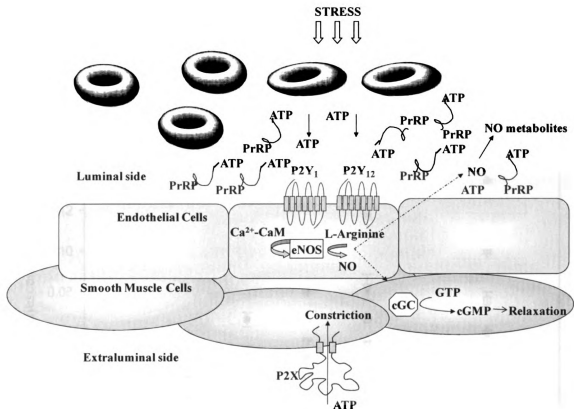


Figure 27. Representation of the mechanism of RBC-mediated regulation of the vascular tone and the possible involvement of prolactin-releasing peptide (PrRP) in scavenging the RBC-derived ATP. ATP binds to the P2y purinergic receptors found on the endothelial cells that line up the luminal side of the blood vessel and through a Ca²⁺-dependent mechanism triggers the activation of the eNOS, and therefore production of NO. NO activates the guanylate cyclase signaling cascade that ultimately results in vasodilation.

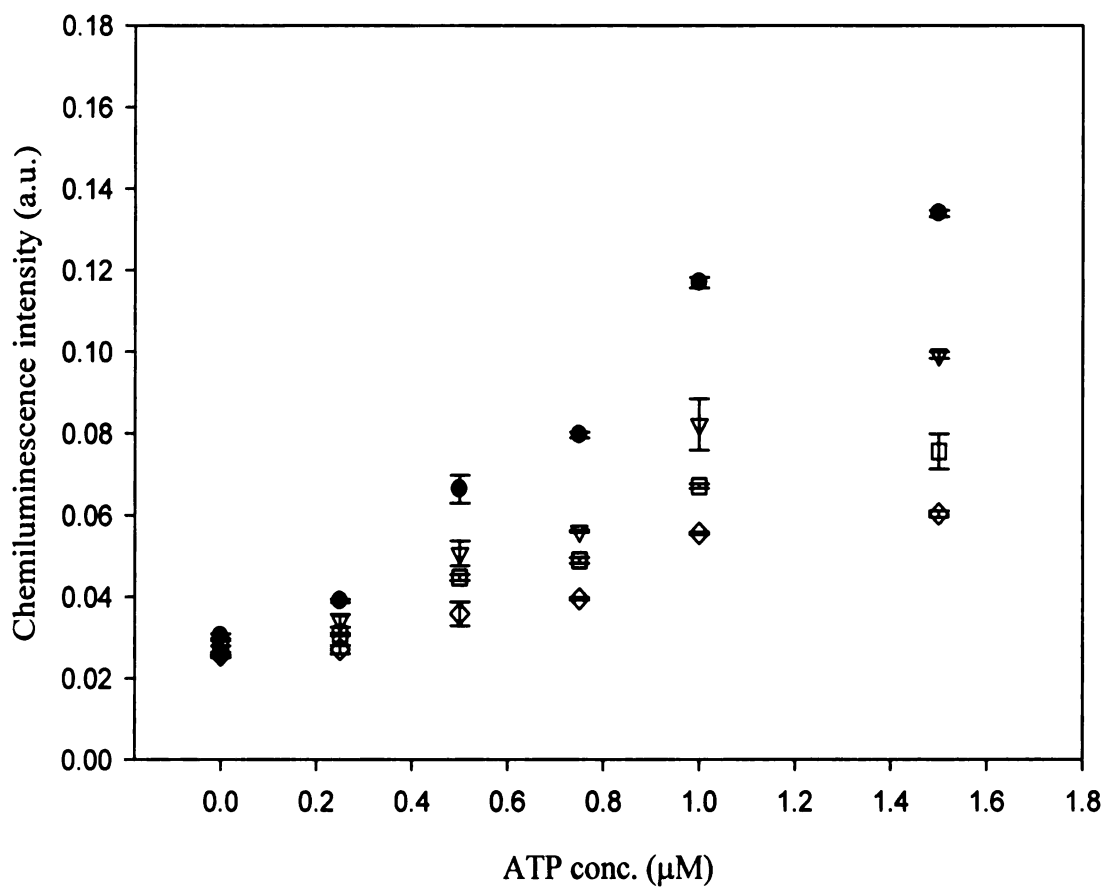


Figure 28. PrRP binding to ATP. Filled circles (●) represent the ATP standards (0-1.5 μM) without the peptide. Open triangles (▽), squares (□) and rhomboids (◇) show the decrease in ATP signal after the incubation with PrRP (10 nM) for 0, 30, and 60 min, respectively (n=3). The decrease in chemiluminescence signal suggests that PrRP binds to ATP ($p \leq 0.005$).

Antagonistic effect of PrRP on the ATP release from C-peptide/iloprost treated RBCs.

We hypothesized that PrRP binds to physiological ATP and reduces the pool of ATP needed for stimulation of the endothelium-derived NO. In order to prove this hypothesis, RBCs were treated with different agents known to have the ability to increase the ATP release, specifically C-peptide and iloprost. We have previously demonstrated that the ability of the C-peptide to increase the RBC-derived ATP depends on the activation with metal ions, such as Fe^{2+} and Cr^{3+} .²⁸ Moreover, the ATP release was dependent upon the ability of the C-peptide to increase glycolysis within the RBCs via increased cellular glucose transport through GLUT1. However, in this work we used Zn^{2+} to stimulate the activity of C-peptide before incubation with RBCs. Figure 29 shows a significant ATP release from the RBCs treated with the Zn^{2+} activated C-peptide compared to control (RBC 7%), which is in very good agreement with our previously published data.²⁸

Moreover, the data in Figure 28 demonstrates that PrRP (10 nM) induces a significant decrease in the RBC-derived ATP release and the decrease is higher after 90 min (n=5) incubation compared to 6 h (n=8). This is because the PrRP is being consumed and ATP release is being partially restored after the 6 h incubation period. We have to note here that all reagents have been added at the same time and have been incubated for

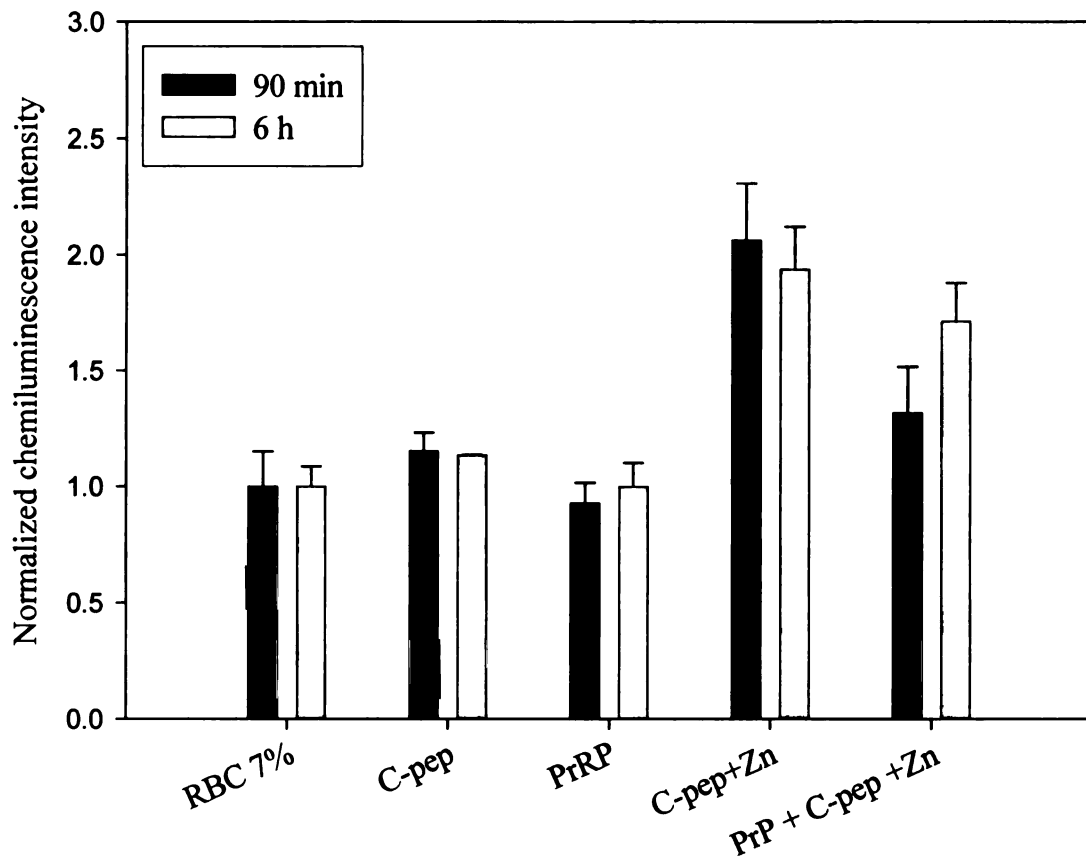


Figure 29. Effect of PrRP (10 nM) on the ATP release from RBCs treated with Zn²⁺-activated C-peptide. The decrease in chemiluminescence intensity corresponds to a decrease in the measured ATP released from the RBCs when PrRP was added to the metal activated C-peptide. Filled bars correspond to the 90 min incubation with PrRP (n=5) and the open bars correspond to 6 hrs incubation (n=8). The results are reported as the average \pm standard error of the mean. The differences in chemiluminescence intensity between the samples incubated in the presence and absence of PrRP are statistically significant (* $p \leq 0.005$).

90 min or 6 h. However, for the C-peptide samples, pre-activation of the peptide with the metal in water followed by the addition of this cocktail in PSS to the RBCs was required. In order to prove whether the PrRP is actively binding to the ATP released from the RBCs or it is involved in some mechanism of C-peptide-dependent membrane deformability, we incubated the RBCs with iloprost. Iloprost is a stable analogue of prostacyclin that is known to stimulate ATP release via a G-protein coupled receptor mechanism. Data in Figure 30 provides further evidence that PrRP decreases the pool of that ATP released from RBCs rather than having a direct effect on the RBCs membrane.

In an attempt to classify the possible role of PrRP in regulating the vascular tone by decreasing the endothelium-derived NO production through a decrease in ATP, a device was constructed that closely mimics *in vivo* microcirculation by using a transparent polycarbonate membrane to separate a flow of RBCs from a layered endothelium. This device was previously described and successfully used as a controlled, *in vitro* platform for performing *in vivo*-type measurements.²⁴ This device has the potential of performing high throughput measurements that include calibration, drug-dose response data and proper controls.

In this study, all 18 wells contained a layer of confluent bPAECs and were addressable by a flowing stream of RBCs. The bPAECs were loaded with DAF-FM DA and the NO production was monitored as ATP diffused from different samples containing RBC, (row **a**), Zn(II)-activated C-peptide-treated RBCs incubated with and without PrRP (rows **d** and **c**, respectively), and iloprost treated RBCs incubated with and without PrRP (rows **f** and **e**, respectively). The data shown is summarized in Figure 31I. The quantitative representation of the normalized data from 4 different experiments is shown

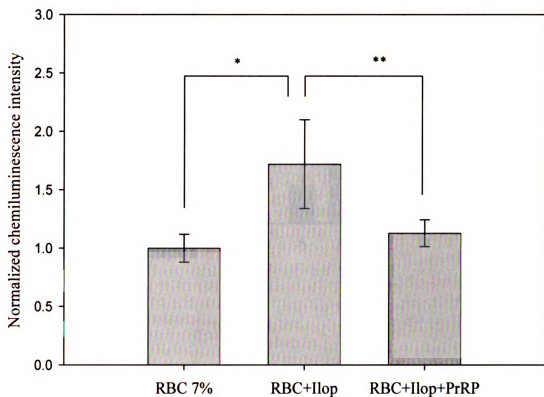


Figure 30. The effect of the PrRP (10 nM) on the measured ATP release from the RBCs treated with iloprost (10 μ M) (n=3). All samples contain RBC (final hematocrit 7%). Control sample is represented by RBC 7%. The iloprost-treated RBCs samples incubated with or without PrRP are significantly different (* $p < 0.005$; ** $p \leq 0.05$).

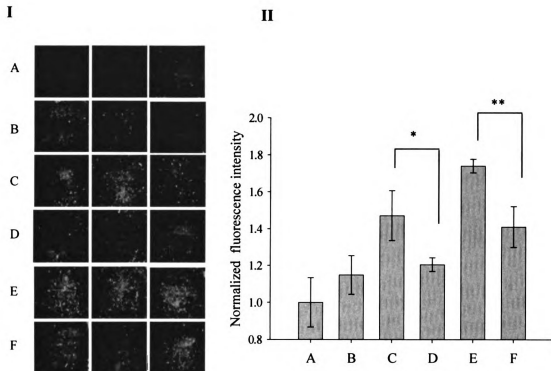


Figure 31. Antagonistic effect of PrRP on the endothelium-derived NO production in the bovine pulmonary artery endothelial cells (bPAECs) Picture I shows micrographs of vascular endothelium array with blood components. The rows a-f represent the wells of the array that are addressable by the underlying microchannel network each delivering a different reagent to the wells as described in the text. The quantitative representation of the normalized data from 4 different experiments is shown in II. The difference in fluorescence intensity between samples containing RBC + C-pep + Zn(II) incubated in the absence (bar C) and presence (bar D) of the PrRP is statistically significant ($*p < 0.05$) There is also significant difference in the intensities of rows (bars E and F), where the RBCs + Iloprost samples were incubated in the absence and the presence of PrRP ($**p < 0.001$), respectively. Errors bars are the mean \pm standard error A: RBC7%; B: RBC + PrRP; C: RBC + C-pep + Zn; D: RBC + C-pep + Zn + PrRP; E: RBC + Iloprost; F: RBC + Iloprost + PrRP.

in Figure 31III. A significant decrease in fluorescence intensity between samples containing activated C-peptide-treated RBCs or iloprost-treated RBCs and the same samples incubated with PrRP was observed. This decrease in fluorescence translates to a decrease in NO production as result of depletion of ATP pools available for endothelium stimulation. Herein we showed that PrRP has the ability to decrease the NO production and therefore, constitute a possible alternative mechanism for regulation of the blood flow by exerting vascular smooth muscle constriction.

LIST OF REFERENCES

- (1) Hinuma, S.; Habata, Y.; Fujii, R.; Kawamata, Y.; Hosoya, M.; Fukusumi, S.; Kitada, C.; Masuo, Y.; Asano, T.; Matsumoto, H.; Sekiguchi, M.; Kurokawa, T.; Nishimura, O.; Onda, H.; Fujino, M. *Nature* 1998, 393, 272-276.
- (2) Minami, S.; Nakata, T.; Tokita, R.; Onodera, H.; Imaki, J. *Neurosci. Lett.* 1999, 266, 73-75.
- (3) Maruyama, M.; Matsumoto, H.; Fujiwara, K.; Kitada, C.; Hinuma, S.; Onda, H.; Fujino, M.; Inoue, K. *Endocrinology* 1999, 140, 2326-2333.
- (4) Bray, G. A. *Int J Obes* 1984, 8 Suppl 1, 119-137.
- (5) Lawrence, C. B.; Celsi, F.; Brennand, J.; Luckman, S. M. *Nat. Neurosci.* 2000, 3, 645-646.
- (6) Zhu, L. L.; Onaka, T. *Neuroscience (Oxford, U. K.)* 2003, 118, 1045-1053.
- (7) Yamakawa, K.; Kudo, K.; Kanba, S.; Arita, J. *Neurosci. Lett.* 1999, 267, 113-116.
- (8) Roland, B. L.; Sutton, S. W.; Wilson, S. J.; Luo, L.; Pyati, J.; Huvar, R.; Erlander, M. G.; Lovenberg, T. W. *Endocrinology* 1999, 140, 5736-5745.
- (9) Morales, T.; Sawchenko, P. E. *Neuroscience (Oxford, U. K.)* 2003, 121, 771-778.
- (10) Morales, T.; Hinuma, S.; Sawchenko, P. E. *J. Neuroendocrinol.* 2000, 12, 131-140.
- (11) Mera, T.; Fujihara, H.; Kawasaki, M.; Hashimoto, H.; Saito, T.; Shibata, M.; Saito, J.; Oka, T.; Tsuji, S.; Onaka, T.; Ueta, Y. *Neuroscience (San Diego, CA, U. S.)* 2006, 141, 1069-1086.
- (12) Maruyama, M.; Matsumoto, H.; Fujiwara, K.; Noguchi, J.; Kitada, C.; Fujino, M.; Inoue, K. *Endocrinology* 2001, 142, 2032-2038.
- (13) Lee, Y.; Yang, S. P.; Soares, M. J.; Voogt, J. L. *Brain Res. Bull.* 2000, 51, 171-176.
- (14) Iijima, N.; Kataoka, Y.; Kakihara, K.; Bamba, H.; Tamada, Y.; Hayashi, S.; Matsuda, T.; Tanaka, M.; Honjyo, H.; Hosoya, M.; Hinuma, S.; Ibata, Y. *NeuroReport* 1999, 10, 1713-1716.

- (15) Chen, C. T.; Dun, S. L.; Dun, N. J.; Chang, J. K. *Brain Res.* 1999, 822, 276-279.
- (16) Samson, W. K.; Resch, Z. T.; Murphy, T. C. *Brain Res.* 2000, 858, 19-25.
- (17) Jarry, H.; Heuer, H.; Schomburg, L.; Bauer, K. *Neuroendocrinology* 2000, 71, 262-267.
- (18) Horiuchi, J.; Saigusa, T.; Sugiyama, N.; Kanba, S.; Nishida, Y.; Sato, Y.; Hinuma, S.; Arita, J. *Brain Res.* 2002, 958, 201-209.
- (19) Boyle, R. G.; Downham, R.; Ganguly, T.; Humphries, J.; Smith, J.; Travers, S. J. *Pept. Sci.* 2005, 11, 161-165.
- (20) Sprague, R. S.; Ellsworth, M. L.; Stephenson, A. H.; Kleinhenz, M. E.; Lonigro, A. J. *American Journal of Physiology* 1998, 275, H1726-H1732.
- (21) Sprague, R. S.; Ellsworth, M. L.; Stephenson, A. H.; Lonigro, A. J. *American Journal of Physiology* 1996, 271, H2717-H2722.
- (22) Sprague, R. S.; Stephenson, A. H.; Dimmitt, R. A.; Weintraub, N. A.; Branch, C. A.; McMurdo, L.; Lonigro, A. J. *American Journal of Physiology* 1995, 269, H1941-H1948.
- (23) Collins, D. M.; McCullough, W. T.; Ellsworth, M. L. *Microvascular research* 1998, 56, 43-53.
- (24) Genes, L. I.; Tolan, N. V.; Hulvey, M. K.; Martin, R. S.; Spence, D. M. *Lab Chip FIELD Full Journal Title: Lab on a Chip* 2007, 7, 1256-1259.
- (25) McDonald, J. C.; Duffy, D. C.; Anderson, J. R.; Chiu, D. T.; Wu, H.; Schueller, O. J.; Whitesides, G. M. *Electrophoresis* 2000, 21, 27-40.
- (26) Kojima, H.; Nakatsubo, N.; Kikuchi, K.; Kawahara, S.; Kirino, Y.; Nagoshi, H.; Hirata, Y.; Nagano, T. *Analytical Chemistry* 1998, 70, 2446-2453.
- (27) Kojima, H.; Urano, Y.; Kikuchi, K.; Higuchi, T.; Hirata, Y.; Nagano, T. *Angew. Chem., Int. Ed.* 1999, 38, 3209-3212.
- (28) Meyer, J. A.; Froelich, J. M.; Reid, G. E.; Karunarathne, W. K. A.; Spence, D. M. *Diabetologia* 2008, 51, 175-182.
- (29) Busse, R.; Ogilvie, A.; Pohl, U. *Am J Physiol* 1988, 254, H828-832.
- (30) Bogle, R. G.; Coade, S. B.; Moncada, S.; Pearson, J. D.; Mann, G. E. *Biochem Biophys Res Commun* 1991, 180, 926-932.

- (31) Dean, B. M.; Perrett, D. *Biochim Biophys Acta* 1976, 437, 1-5.
- (32) Miseta, A.; Bogner, P.; Berenyi, E.; Kellermayer, M.; Galambos, C.; Wheatley, D. N.; Cameron, I. L. *Biochim Biophys Acta* 1993, 1175, 133-139.
- (33) Bergfeld, G. R.; Forrester, T. *Cardiovasc. Res.* 1992, 26, 40-47.
- (34) Ellsworth, M. L.; Forrester, T.; Ellis, C. G.; Dietrich, H. H. *American Journal of Physiology* 1995, 269, H2155-H2161.
- (35) Goldsmith, H. L. *J Gen Physiol* 1968, 52, 5Suppl-28s.
- (36) Dietrich, H. H.; Ellsworth, M. L.; Sprague, R. S.; Dacey, R. G., Jr. *American Journal of Physiology* 2000, 278, H1294-H1298.
- (37) Dietrich, H. H.; Kajita, Y.; Dacey, R. G., Jr. *The American journal of physiology* 1996, 271, H1109-1116.
- (38) McCullough, W. T.; Collins, D. M.; Ellsworth, M. L. *American Journal of Physiology* 1997, 272, H1886-H1891.
- (39) Houston, D. A.; Burnstock, G.; Vanhoutte, P. M. *J Pharmacol Exp Ther* 1987, 241, 501-506.

CHAPTER 6

6.1 OVERALL CONCLUSIONS

At the dawn of the 21st century, with the accelerated pace of the pharmaceutical and chemical industries, microfluidic technologies are emerging as powerful tools in many stages of the drug discovery process. Microfluidic technologies have the potential to radically transform the medicinal chemistry and biology interface.

In this work, we applied the recent developments in microfabrication technology to create an *in vitro* model that will closely mimic an *in vivo* system. More specifically, this work describes the development of a blood brain barrier (BBB) mimic with blood components using lithographically-derived microchips in order to monitor the fate of endothelium-derived nitric oxide (NO) that is stimulated by mechanically deformed red blood cells (RBCs). The microchip-based BBB mimic was developed by addressing an array of cell reservoirs, which pose as the central nervous system (CNS), with a network of underlying channels that represent the circulatory system. The cells were cultured on a polycarbonate membrane, integrated in the device that separates the “so called” CNS from the “so called” blood stream. The diameters of the patterned channels in the fabricated chips will ultimately approximate those of brain capillaries *in vivo*.

Because a molecular level understanding of the mechanisms by which RBCs deformability properties relate to the occurrence of multiple sclerosis (MS) is lacking, to gain insight into these mechanisms would be ideal to employ such a model system. In this

study we hypothesized that RBCs obtained from patients with MS are more deformable, therefore releasing more ATP, which in turn will lead to increased levels of NO production. For a more realistic depiction of the mechanism of endothelium-derived NO production *in vivo*, the RBCs obtained from MS patients were mechanically deformed by hydrodynamically pumping them through microbore capillary tubing. A continuous flow system is employed to create stress on the RBCs once they have entered the microbore tubing. It was found that MS-RBCs release higher levels of ATP compared to non-MS RBCs. These findings suggest that RBCs of MS patients may indeed be in a continuous “deformable “state that will lead to higher levels of ATP release and ultimately, to an increase in ATP-stimulated endothelium-derived NO. Additionally, it was shown that ATP acts as an agonist for NO production in bovine brain microvascular endothelial cells (bbMVECs) and the increase in NO production is a function of cell division.

Based on these findings, we have constructed a theory that the overabundance of NO metabolites in the CSF of MS patients is actually blood-borne. In other words, it is possible that the NO levels are increased due to overstimulation by RBC-derived ATP. Using chip technology, we were able to investigate the flux of NO across the BBB brought about by changes in ATP concentrations, both in the form of ATP standards and RBC-derived ATP. As the detection scheme, fluorescence microscopy was employed to enable the qualitative and quantitative identification of endothelium derived-NO after it diffuses through the membrane of the microchip device.

Key to investigating the NO production from the endothelium and its fate through the cell-coated polycarbonate membrane, that will constitute the BBB, is the ability to actually detect the NO after it crosses the barrier. Primarily, we have demonstrated here

that the flux of NO through a bare polycarbonate membrane can be detected using a specific probe for NO, DAF-FM. However, the device lacks the sensitivity required to detect physiological relevant levels of NO. Secondly, the ATP flux through a polycarbonate membrane in a 3D microfluidic device has been investigated. The molecular transfer through the membrane was maximized by increasing the area of contact between the two channels by designing the upper channel in a spiral shape that crosses the underneath linear channel in multiple points. We showed here that the proposed device is sensitive enough for the detection of as low as 500 nM of ATP spiked into RBC samples and most importantly, is able to detect concentrations of ATP released by iloprost-treated RBCs.

Parameters such as membrane pore size, flow rates and probe concentrations have been optimized to increase the efficiency of the detection in the device. Although the results are promising, the inability to culture the cells on the membrane as part of the 3-D microfluidic BBB and the poor sensitivity for the physiological relevant NO concentrations constitute limiting factors.

Attempts have been made to culture the endothelial cells on isolated collagen-coated polycarbonate membranes and, after the cells have reached a confluent layer, to integrate the membrane in the device. However, the two pieces of PDMS that make up the device would not seal together as a result of the membrane wetness from the cell culture media. As an alternative method, an attempt was made to culture the cells directly on the membrane by introducing the cell suspension in the upper channel, above the membrane. However, the lack of reproducibility and technical difficulties with the cell introduction made the device unsuitable for the purpose of our applications.

One way of avoiding these complications would be the integration of microvalves and multiple channels for the introduction of cells and DAF-FM, separately. Moreover, cell culture reactors on-chip, where the viability of the cells can be sustained for days and the cell-cell signaling can be monitored in real time, could also constitute an alternative option. In terms of using the polycarbonate membranes as support for endothelial cell culturing and proliferation, integration of transparent membranes for ease of optical cell imaging would be highly desirable.

The aforementioned microfluidic components, such as microvalves, microreactors or intricate designs are time consuming and prone to problems of engineering nature even before introducing the biological factor. A new, simpler and more amenable design has thus been constructed. Here, the high throughput capabilities of a microtitre plate technology was merged with the capabilities of microfluidic technology to create a device that mimics the BBB in a more realistic way by incorporating blood flow and having the capability of possible multi-drug screening simultaneously and in real time.

In addition to interacting with an appropriate molecule, there are many characteristics required of a drug candidate throughout the testing process. Drug adsorption properties, its ability to be distributed *in vivo*, its effects on metabolism, excretion characteristics and its toxicity are often monitored. Here, we showed that an array of endothelial cells, addressable by an underlying microfluidic network of channels containing RBCs, can be employed as an *in vitro* model of the *in vivo* circulation to monitor cellular communication between different cell types. Results obtained from this array suggest that the ability of iloprost, a stable analogue of prostacyclin, to stimulate NO production in endothelial cells, may be due to its ability to stimulate ATP release

from the red cell. These results provide evidence that the described device may serve as a controlled, *in vitro* platform for performing *in vivo*-type measurements.

Moreover, this device was successfully used in a study that attempts to classify the possible role of prolactin releasing peptide (PrRP) (a peptide that stimulate the release of prolactin from the pituitary gland) in regulating the vascular tone by decreasing the endothelium-derived NO production through a decrease in ATP.

In this study we propose a mechanism for the previously reported cardiovascular/blood pressure regulatory properties of the PrRP, that is PrRP binding to RBC-derived ATP that is released under various stimuli. If PrRP binds ATP, this will lower the extracellular ATP pool available for the stimulation of the endothelial NO synthesis and subsequently, a decrease in the vascular relaxation/increase in the blood pressure might be possible. Herein, different techniques, such as mass spectrometry, chemiluminescence and fluorescence microscopy were utilized to show, directly or indirectly, the PrRP binding to ATP. Moreover, by using an *in vitro* microfluidic-based mimic of an *in vivo* microcirculation we constructed a system where the direct involvement of the PrRP in the regulation of the blood pressure and/or vascular tone could be monitored in real time.

6.2 FUTURE DIRECTIONS

The ultimate goal of the present work is to determine endothelium-derived NO, using the microfluidic array device and high throughput fluorescence detection, where the NO is stimulated by ATP from deformed RBCs obtained from people with MS. In this sense, the microfluidic device presented here will enable a comparison to be made between the ability of RBCs from different patient groups to stimulate endothelium-derived NO. This endothelium-derived NO and its fate through the BBB is important in establishing the source of the elevated levels of nitrites and nitrates in the CSF of patients with MS.

Based on our previous results involving the determination of RBC-derived ATP from people with MS (Figure 10, chapter 2), it is anticipated that a higher level of ATP release from those RBCs obtained from the MS patients will be measured in comparison to the RBCs obtained from healthy controls. In our previous studies, the MS patient pool was not subdivided into stage of disease; therefore, it will be interesting to determine if there is a further correlation of ATP release with stage of disease.

Another important direction of the project would be to investigate more closely the relationship between the RBC-derived ATP release from MS patients and factors, such as cholesterol and zinc, that have been reported to affect the erythrocytes membrane fluidity. One such report of lower cholesterol levels in the membranes of erythrocytes obtained from people with MS suggests that the RBCs of patients with MS may be more “deformable” because, typically, a decrease in cholesterol leads to an increase in deformability.

In a series of papers nearly two decades ago, an analysis of erythrocyte membranes obtained from controls and people with MS was performed. The data in these manuscripts provided evidence that the levels of zinc in the membranes from the RBCs of people with MS were significantly higher than the RBCs obtained from controls.^{1, 2} Moreover, in the work by Dore-Duffy, the zinc levels found to be significantly different were compartmentalized to the red cell membrane. No significant differences between MS patients and controls were found when examining the cell as a whole, serum, or plasma.²

It is known that zinc exerts physiological and biochemical roles as a component of the known zinc metalloenzymes and also, plays an important role in the maintenance of membrane structure and function.³ Therefore, it would be very interesting to try to correlate the ATP release from RBCs of patients with different stages of MS and the RBC membrane zinc content. This information would be critical in establishing the relationship between RBC deformability, ATP release, endothelium-derived NO production and elevated levels of NO metabolites found in CSF and other fluids of MS patients.

Another approach in trying to correlate ATP and MS has the basis in recent reports in the literature, that inhibition of the P2X7 receptors, which are receptors for ATP, found on oligodendrocytes prevented ATP triggering of these cells excitotoxicity.⁴ Moreover, a recent report by Feinstein⁵ has shown that P2X7 deficient mice showed a reduction in onset of experimental autoimmune encephalomyelitis (EAE), an autoimmune mouse model of MS. Similar to the work by Feinstein, Voskuhl work showed a reduction in EAE onset when the mice were administered estrogen analogues.⁶

Voskuhl's results are key to the work that will be proposed here because preliminary studies (not shown here) have found that estradiol has the ability to significantly reduce ATP release from RBCs. Thus, one future aim would be to determine the ability of estradiol to attenuate shear-induced release of ATP from the erythrocytes of people with MS.

Collectively, the preliminary data involving ATP release from the RBCs of MS patients and reports in the literature indicating novel roles for ATP in a mouse model of MS (EAE), suggest that events in the bloodstream may play a role in MS. As shown in Figure 10 chapter 2, we propose that abnormally high levels of ATP release from the RBC may be a determinant in the high levels of NO metabolites that have been reportedly found in people with MS. High concentrations of NO production have been reported to inhibit collagen production, the substrate for the endothelium, *in vivo*. Upon inhibition of collagen production, the BBB is compromised and constituents in the bloodstream (leukocytes, erythrocytes, bacteria, etc.) are able to penetrate through to the CNS resulting in the hallmark features of MS (demyelination, oligodendrocyte toxicity, iron deposits, bacterial infections, etc.). Unfortunately, investigating such a complex event would be difficult with current technology. Therefore, herein, we propose to expand our current microchip based blood/endothelium model to include a collagen-coated membrane and to determine the extent of NO mediated damage of the collagen base and breakdown of the endothelium barrier. Subsequently, it would be worth examining the integrity of the collagen-supported microchip-based BBB through a separation and detection of cells and molecules breaking through the BBB when using whole blood obtained from people with MS in the presence and absence of estradiol.

LIST OF REFERENCES

- (1) Cunnane, S. C.; Ho, S. Y.; Dore-Duffy, P.; Ells, K. R.; Horrobin, D. F. *Am J Clin Nutr* **1989**, *50*, 801-806.
- (2) Dore-Duffy, P.; Catalanotto, F.; Donaldson, J. O.; Ostrom, K. M.; Testa, M. A. *Ann Neurol* **1983**, *14*, 450-454.
- (3) Bettger, W. J.; O'Dell, B. L. *Life Sci*. **1981**, *28*, 1425-1438.
- (4) Matute, C.; Torre, I.; Perez-Cerda, F.; Perez-Samartin, A.; Alberdi, E.; Etxebarria, E.; Arranz, A. M.; Ravid, R.; Rodriguez-Antiguedad, A.; Sanchez-Gomez, M. V.; Domercq, M. *J. Neurosci*. **2007**, *27*, 9525-9533.
- (5) Sharp, A. J.; Polak, P. E.; Simonini, V.; Lin, S. X.; Richardson, J. C.; Bongarzone, E. R.; Feinstein, D. L. *J. Neuroinflammation* **2008**, *5*, No pp given.
- (6) Kim, S.; Liva, S. M.; Dalal, M. A.; Verity, M. A.; Voskuhl, R. R. *Neurology* **1999**, *52*, 1230-1238.

MICHIGAN STATE UNIVERSITY LIBRARIES



3 1293 02956 9526